HHS Public Access

Author manuscript

Nat Cancer. Author manuscript; available in PMC 2022 April 22.

Published in final edited form as:

Nat Cancer. 2021 October ; 2(10): 1018–1038. doi:10.1038/s43018-021-00263-z.

RNF2 ablation reprograms the tumor-immune microenvironment and stimulates durable NK and CD4+ T-cell-dependent antitumor immunity

Zhuo Zhang[1,2,*], **Lin Luo**[2,3,4,5], **Chuan Xing**[1,2], **Yu Chen**[6,7], **Peng Xu**[6,7], **Mao Li**[8], **Ling Zeng**[1,2], **Chao Li**[9], **Sadashib Ghosh**[2,3,4], **Deborah Della Manna**[1,2], **Tim Townes**[9], **William J. Britt**[8], **Narendra Wajapeyee**[2,9], **Barry P. Sleckman**[2], **Zechen Chong**[6,7], **Jianmei Wu Leavenworth**[2,3,4,*], **Eddy S Yang**[1,2,10,*]

[1]Department of Radiation Oncology, University of Alabama at Birmingham, Hazelrig Salter Radiation Oncology Center, 1700 6th Avenue South, Birmingham, AL 35233

[2]The O'Neal Comprehensive Cancer Center, University of Alabama at Birmingham, 1824 6th Avenue South, Wallace Tumor Institute, Birmingham, AL 35233

[3]Department of Neurosurgery, University of Alabama at Birmingham, 1600 6th Avenue South, Children's Harbor Building, Birmingham, AL 35233

[4]Department of Microbiology, University of Alabama at Birmingham, 1600 6th Avenue South, Children's Harbor Building, Birmingham, AL 35233

[5]School of Pharmacy, Nantong University, Nantong, Jiangsu 226001, China

[6]Department of Genetics, University of Alabama at Birmingham, Tinsley Harrison Tower, Suite 134, 1900 University Boulevard, Birmingham, Alabama 35294

[7]Informatics Institute, University of Alabama at Birmingham, Tinsley Harrison Tower, Suite 134, 1900 University Boulevard, Birmingham, Alabama 35294

[8]Department of Pediatrics, University of Alabama at Birmingham, Children's Harbor Building, Birmingham, AL 35294

[9]Department of Biochemistry and Molecular Genetics, University of Alabama at Birmingham, Kaul Human Genetics Building, 720 20th Street South, Birmingham, AL 35294

[*]To whom correspondence should be addressed: Eddy S Yang, MD, PhD; Phone: 205-996-0780; eyang@uab.edu; Jianmei Wu Leavenworth, MD, PhD; Phone: 205-996-7880; jleavenworth@uabmc.edu; Zhuo Zhang, MD, PhD; Phone: 205-975-2881; zhuophar@uab.edu.

Author Contributions Statement

Z.Z., J.W.L. and E.S.Y. conceived the concept. Z.Z., J.W.L., E.S.Y., and L.L. designed studies, interpreted data and wrote the manuscript. Z.Z., L.L., J.W.L., X.C., M.L., L.Z., C.L. and S.G. performed experiments with assistance from D.D.M. P.X., Y.C., Z.C. and Z.Z. performed bioinformatic analyses. N.W. T.T., W.J.B., and B.P.S. contributed to data interpretation and study design. J.W.L. and E.S.Y. collected funding supports. E.S.Y. critically reviewed manuscript and supervised whole study.

These authors contributed equally: Z. Zhang, L. Luo

Competing Interests Statement

Eddy S Yang is the consultant for AstraZeneca Plc, Eli Lilly and Company and is on the Advisory Board for Bayer Pharmaceuticals, AstraZeneca Plc, Clovis Oncology, and Strata Oncology. The research in Eddy S Yang's laboratory is also supported by the funding from Novartis International AG, Eli Lilly and Company, Clovis Oncology and American Society of Clinical Oncology. The remaining authors declare no competing interests.

[10]Hugh Kaul Precision Medicine Institute, Kaul Human Genetics Building, 720 20th Street South, Birmingham, AL 35294

Abstract

Expanding the utility of immune-based cancer treatments is a clinical challenge due to tumor-intrinsic factors that suppress the immune response. Here we report the identification of tumoral Ring Finger Protein 2 (RNF2), the core subunit of the Polycomb Repressor Complex 1 (PRC1), as a negative regulator of antitumor immunity in various human cancers, including breast cancer. In syngeneic murine models of triple negative breast cancer, we found that deleting genes encoding PRC1 subunits Rnf2 or BMI1 proto-oncogene, polycomb ring finger (Bmi1), or the downstream effector of Rnf2, Remodeling and Spacing Factor 1 (Rsf1), was sufficient by itself to induce durable tumor rejection and establish immune memory by enhancing infiltration and activation of NK and $CD4^+$ T-cells, but not $CD8^+$ T-cells, into the tumor and enabled their cooperativity. These findings uncover an epigenetic reprogramming of the tumor-immune microenvironment which fosters durable antitumor immunity and memory.

Keywords

RNF2; Polycomb Repressive Complex 1 (PRC1); Cancer Immunity; Immune Evasion; Major Histocompatibility Complex Class II (MHCII)

Tumor growth and progression are normally restrained by cytotoxic innate and adaptive immune cells, but cancer cells have developed mechanisms to evade their immune attack[1,2]. One of the major means of immune escape is to exclude and/or inactivate cytotoxic immune cells in the tumor, which often results from low tumor immunogenicity[1,2]. The delicate cellular interaction within the tumor microenvironment (TME), particularly tumor-immune crosstalk, helps to determine tumor response to therapy[3-8]. Uncovering the factors that regulate this crosstalk may facilitate the understanding of the mechanisms for tumor immune evasion and lead to the development of different immunotherapeutic approaches from current immunotherapies that have faced much resistance[9]. However, such regulators that shape the tumor-immune landscape and hence tumor immunogenicity remain poorly defined[7].

Several epigenetic regulators are reported to shape the TME and modulate the tumor-immune interaction to impact tumor growth and response to therapy[8,10-17]. The plastic nature of epigenetic changes makes them attractive targets to enhance anti-tumor response. Unfortunately, the outcomes of clinical trials testing inhibitors for histone deacetylase and DNA methyltransferases are not satisfactory[18], and the clinical efficacy of other regimens targeting recently identified epigenetic regulators is still unclear.

To identify the tumor-intrinsic factor(s) that may aid immune evasion, we adopted a data driven approach and analyzed published single cell RNA sequencing (RNAseq) datasets from human cancer patients[19]. This initial data-screen identified multiple epigenetic pathways associated with tumor immune evasion, including Polycomb repressive complex 1 (PRC1), PRC2 and SWI/SNF related, matrix associated, actin dependent regulator

of chromatin, subfamily b, member 1 (SMARCB1) (also known as SNF5). Subsequent analysis of a published list including 524 genes encoding epigenetic regulators[13] confirmed *Ring Finger Protein 2 (RNF2)*, the enzymatic component of the PRC1 complex, to be one of the top genes significantly correlated to immune cold niches within human tumors. Additional results showed that *RNF2* expression was correlated with reduced cytotoxicity of tumor-infiltrating immune cells. These results consistently implicated a general immunosuppressive role of PRC1 complex/RNF2 in human cancers.

Recently, RNF2 is implicated in tumorigenesis[20-23] and is a poor prognostic factor in patients with various types of tumors that have high RNF2 expression or *RNF2* amplification[21,22,24,25]. However, the immune-mediated mechanisms by which RNF2 promotes tumorigenesis remain elusive. The identification of PRC1 complex/RNF2 as a suppressor of cancer immunity prompted us to further investigate its role in immune control of tumors. Using syngeneic models of triple negative breast cancer (TNBC) that are inherently refractory to immunotherapy[26], we found that deletion of genes encoding PRC1 subunits *Rnf2 or Bmi1*, or *Rsf1* (a downstream executor of Rnf2)[27], was sufficient to reject tumors by enhancing the recruitment, activation, and cooperation of NK and $CD4^+$ T-cells, but minimally affected $CD8^+$ T-cells. This coordination between innate (NK cells) and adaptive immunity ($CD4^+$ T-cells) was mediated largely by IFNγ and resulted in a sustained anti-tumor response as well as establishment of immune memory. These effects were not dependent on Rnf2 E3 ligase activity as *Rnf2* catalytic-inactive mutant knock-in tumors grew robustly in immunocompetent mice. Mechanistically, ablation of *Rnf2* or *Rsf1* in *in vivo* tumors de-repressed multiple tumoral genes related to immune response including those involved in the MHCII-mediated antigen processing/presentation pathway. Subsequent ATACseq analysis of these tumor cells isolated from corresponding tumors implanted in mice demonstrated that immune-related genes, including genes in the MHCII restricted antigen processing/presentation pathway, were significantly more accessible upon deletion of *Rnf2/Rsf1*, but these genes remained largely inaccessible in *Rnf2* catalytic-inactive mutant knock-in tumors. Consistently, these immune-related genes significantly overlapped with Rnf2 bound genes determined by CHIPseq. These findings uncover an epigenetic reprogramming from depleting tumor-expressed *RNF2*, which reshapes the TME favorably for the immune response and leads to long term immune memory and rejection of tumor.

Results

RNF2 marks the signature of immunologically cold tumors

We first leveraged large human cancer datasets to analyze malignant cell states that facilitate immune evasion. Gene Set Enrichment Analysis (GSEA)[28] of a single cell RNAseq dataset interrogating the transcriptome of tumor cells[19] revealed significant overlaps of the gene signature of cold tumors with multiple GO terms of PRC1 complex or of its target gene, *homeobox A9 (HOXA9)* (Extended Data Fig. 1a). We also found that tumoral *RNF2* was ranked as the 4^{th} top gene among the total of 248 genes encoding epigenetic writers, erasers and readers associated with the cold tumor gene signature (Extended Data Fig. 1b). This finding was confirmed (*RNF2* ranked as the 3^{rd} top gene) by analyzing another list including 524 epigenetic regulators[13] (Extended Data Fig. 1c). Additionally, the genes

encoding subunits of PRC1 complex, including *RNF2*, *CBX2*, *CBX4* and *CBX8*, were among the top-listed epigenetic genes that were inversely correlated with a published tumor-infiltrating immune cell cytotoxicity gene signature[29] in multiple human cancers, including breast cancer (BRCA) (Extended Data Fig. 1d-f). Further TCGA analysis revealed that both invasive BRCA, including its deadly subtype, triple negative breast cancer (TNBC), and metastatic BRCA, displayed gene amplification and expressed significantly higher levels of *RNF2* and *RSF1*, which are overexpressed and associated with poor patient prognosis in various other types of cancers[30], compared to normal controls at both transcriptional and protein levels (Extended Data Fig. 2a-e). These data are consistent with recent findings of overexpression and amplification of *RNF2* in BRCA[22,23,31]. The overexpression[31]/amplification of *RNF2*, *CBX2*, *CBX8* and *RSF1* were unfavorable prognostic factors for overall survival in invasive BRCA patients (Extended Data Fig. 2f-i), in addition to the recently reported negative correlation of *RNF2* amplification to the survival in patients with the basal subtype of BRCA[22].

Deleting *Rnf2*/*Bmi1*/*Rsf1* induces durable tumor rejection

Based on the above analyses, we hypothesized that ablating tumoral *RNF2* may enhance tumor immunogenicity and promote immune activation. To test this hypothesis, we first knocked down the expression of *Rnf2* using two sequence-independent short-hairpin RNAs (shRNAs) in the 4T1 cell line, a murine model of TNBC with poor immunogenicity (Extended Data Fig. 3a). Notably, targeting *Rnf2* with shRNAs inhibited tumor growth with an almost complete tumor rejection that was correlated with the extent of *Rnf2* knockdown (Extended Data Fig. 3b-c). To validate these findings, we next deleted *Rnf2* in 4T1 cells using two independent single-guide RNAs (sgRNAs) through CRISPR-Cas9 system (Fig. 1a). Strikingly, tumors with *Rnf2* deletion started to shrink at day 5-7 after implantation and were completely cleared within two weeks after injection. Importantly, mice remained tumor free for more than one year (Fig. 1b-g). In contrast, mice injected with the control 4T1 cells had to be euthanized at 40-50 days after injection due to the large tumor burden. We also observed a similar durable tumor rejection when we deleted tumor *Rnf2* in another murine TNBC model EMT6 (Fig. 1h-i, Extended Data Fig. 3d). To further validate these results, we established a doxycycline (DOX)-inducible *Rnf2* KO 4T1 cell line (Fig. 1j) by introducing a lentiviral-based vector TLCV2[32], which is an all-in-one dox inducible system and integrates with sgRNA targeting murine *Rnf2*, and treated mice harboring this inducible 4T1 tumors with DOX 1 day prior to implantation. As shown in Fig. 1k-l, 3 out of 5 DOX-treated mice, exhibited complete rejection of tumor, while 5 out of 5 mice treated with vehicle had robust growth of tumors. Similar anti-tumor activities were observed when DOX was given after the tumors were established to induce *Rnf2* KO (Extended Data Fig. 3e-h).

PRC1 complex has been biochemically characterized as canonical or non-canonical[20,22]. Co-immunoprecipitation using anti-Rnf2 antibody coupled with immunoblotting of chromatin bound proteins (chromatin fractionation) isolated from 4T1 cells revealed that Rnf2 interacted with Cbx2, Cbx4, Bmi1, the subunits of canonical PRC1 complex[22] (Extended Data Fig. 3i). In contrast, minimal interaction with non-canonical PRC1 complex subunits Pcgf1, Pcgf3, Pcgf5[22] was observed (Extended Data Fig. 3i). Meanwhile, co-immunoprecipitation using anti-CBX4 antibody pulled-down Rnf2 (Extended Data Fig. 3j).

These results suggested that Rnf2 was associated with the canonical PRC1 complex in chromatin. Subsequent targeting of *Bmi1* (Fig. 1m) or *Rsf1*[27] (Extended Data Fig. 3k) similarly resulted in complete and durable rejection of 4T1 tumors (Fig. 1n-p, Extended Data Fig. 3l-q). These data pointed to the role of the canonical PRC1 complex in mediating tumor growth. Of note, deletion of *Rnf2* or *Rsf1* did not suppress *in vitro* cell growth (Extended Data Fig. 3r), and the growth of *Rnf2* KO 4T1 tumors in immunodeficient NOD-Prkdc^{em26Cd52}Il2rg^{em26Cd22}/NjuCrl (NCG) mice (Extended Data Fig. 3s) was at a significantly greater rate than that of control tumors implanted in immunocompetent BALB/c mice (Extended Data Fig. 3t-u), further supporting the importance of the immune system in the phenotypes we observed.

Rnf2/*Rsf1* KO mobilizes both NK and CD4$^+$ T-cells

We next explored the tumor-immune microenvironment in *Rnf2* KO and *Rsf1* KO 4T1 tumors 7 days post implantation before they were cleared. Compared to control tumors, both *Rnf2* KO and *Rsf1* KO tumors had significantly higher frequencies of infiltrated NK cells and FoxP3$^-$ CD4$^+$ effector T-cells (including CD44$^+$ subsets), but not CD8$^+$ T-cells (Fig. 2a). As *Rnf2* KO and *Rsf1* KO tumors started to shrink before day 7, these KO tumors were much smaller and had fewer total number of cells compared to control tumors when collected for analysis (day 7) (Extended Data Fig. 3v). Although there were no significant differences for the absolute numbers of NK cells, CD4$^+$ T-cells, and FoxP3$^-$CD4$^+$ effector T-cells (including CD44$^+$ subsets) in *Rnf2* KO and *Rsf1* KO tumors compared to those of control tumors (Extended Data Fig. 3v), their frequencies relative to tumor-infiltrating CD45$^+$ cells in the KO tumors were significantly higher (Fig. 2a). We also noted that NK cells in KO tumors expressed higher levels of activating receptor NKG2D than NK cells from control tumors (Fig. 2b), indicating their increased activation status in KO tumors. Indeed, both NK and CD4$^+$ T-cells in *Rnf2* KO and *Rsf1* KO tumors expressed increased levels of interferon γ (IFNγ), tumor necrosis factor α (TNFα) and granzyme B (GZMB) (Fig. 2c-d). The immune profile of *Rnf2* KO tumors was also confirmed in another TNBC model EMT6 in immunocompetent mice (Fig. 2e). All these differences were observed only in tumor locally but not the spleens and draining lymph nodes, suggesting that deletion of *Rnf2* or *Rsf1* induced immune activation mainly in the tumor and had minimal systemic impact. Therefore, it is not surprising that *Rnf2* KO tumors did not display “abscopal” like effects[33] (Extended Data Fig. 4a-b). These findings suggested that deletion of *Rnf2* or *Rsf1* in tumor cells preferentially recruited NK and CD4$^+$ T-cell subsets with enhanced effector activity.

We then performed RNAseq analysis of FACS-sorted NK cells from *Rnf2* KO or *Rsf1* KO tumors, which revealed their augmented effector activity as evidenced by the increased expression of multiple granzymes and mast cell proteases (Extended Data Fig. 4c-d). To further validate the importance of NK cells in mediating tumor clearance, we depleted NK cells in mice and assessed tumor growth. Although depletion of NK cells did not significantly alter the growth of control tumors (Extended Data Fig. 4e), *Rnf2* KO and *Rsf1* KO tumors were rescued in mice treated with the NK neutralizing antibody (5 out of 5 mice) (Fig. 2f-i). Importantly, analysis of the human TCGA datasets showed that the high expression of NKG2D that was increased on infiltrated NK cells in *Rnf2* KO/*Rsf1*

KO 4T1 tumors (Fig. 2b) was a significant favorable prognostic factor for invasive BRCA (Extended Data Fig. 4f). Furthermore, *RNF2* expression was significantly and negatively correlated with NK cell signature[19] in TNBC and multiple other cancer types, including BRCA (Extended Data Fig. 4g-j). Thus, these results established a critical role of tumoral RNF2 in the regulation of NK cell infiltration and activation in the tumor.

Similar to NK cells, we also found increased infiltration of $CD4^+$ T-cells into the *Rnf2* KO tumors. Indeed, depletion of $CD4^+$ T-cells using a neutralization antibody rescued the growth of *Rnf2* KO tumors (5 out of 5 mice) (Fig. 2j-k). Although depletion of $CD4^+$ T-cells increased the growth rates of control tumors, the extent of this increase did not achieve statistical significance (Extended Data Fig. 4k). CD4 was also a significant predictor of favorable survival for invasive BRCA and was inversely correlated with *RNF2* in multiple cancer types, including both BRCA and TNBC (Extended Data Fig. 4l-p).

$CD8^+$ T-cells are considered as the primary cytotoxic immune cells mediating anti-tumor immunity[8,34]. As expected, depletion of $CD8^+$ T-cells (Extended Data Fig. 4q) in BALB/c mice significantly promoted control tumor growth (Figures 2l-m). However, depletion of $CD8^+$ T-cells failed to rescue the growth of *Rnf2* KO tumor in these immunocompetent BALB/c mice (Fig. 2l-m). These results suggested that $CD8^+$ T-cells likely did not contribute significantly to *Rnf2* KO induced tumor rejection. Taken together, the above findings demonstrated that NK and $CD4^+$ T-cells but not $CD8^+$ T-cells were essential for the rejection of *Rnf2* KO and *Rsf1* KO tumors.

NK and $CD4^+$ T-cells in *Rnf2* KO tumor activate mutually

The above depletion studies showed that depletion of NK cells in mice harboring *Rnf2* KO tumors resulted in significantly reduced infiltration of effector $CD4^+$ T-cells (but not Tregs), diminished $CD4^+$ T-cell activation, and reduced effector activity (IFNγ and TNFα secretion) (Fig. 3a). On the other hand, depletion of $CD4^+$ T-cells attenuated the infiltration, proliferation ($Ki67^+$), activation, and effector function (expressing NKG2D and granzyme B) of NK cells (Fig. 3b). These results suggested that ablating tumoral *Rnf2* not only enhanced the effector activity of NK and $CD4^+$ T-cells but also their mutual activation *in vivo*.

Next, we elucidated the mechanisms by which deletion of tumoral *Rnf2* activated $CD4^+$ T-cells or NK cells and enhanced their cooperativity using *in vitro* co-culture assays. Control or *Rnf2* KO 4T1 tumor cells ($CD45^-$) were isolated and enriched from corresponding tumors implanted in mouse mammary pads (at time before KO tumors were cleared), followed by co-culture with NK cells or $CD4^+$ T-cells isolated from spleens of mice bearing control tumors in the presence of IL-2 and soluble CD28 (for $CD4^+$ T-cells). Quantitation of the frequency of NK or $CD4^+$ T-cells expressing IFNγ, a factor indicative of their activation status, revealed that there were more $IFN\gamma^+$NK or $IFN\gamma^+CD4^+$ T-cells in the co-cultures with *Rnf2* KO than control tumor cells (Fig. 3c-d, Left panels, compare group #6 to #2). These increases of $IFN\gamma^+$NK or $IFN\gamma^+CD4^+$ T-cells were largely abrogated by blockade of either NKG2D or MHCII (Fig. 3c-d, Left panels, compare group #3 to #2 and compare group #7 to #6), which are involved in the direct activation of NK or $CD4^+$ T-cells, respectively'. We also noted that NKG2D ligand (NKG2DL) levels trended higher

(p<0.01 for 4T1 *Rnf2* KO tumor, p=0.07 for *Rsf1* KO 4T1 tumor and *Rnf2* KO EMT6 tumors) in *Rnf2* KO and *Rsf1* KO tumor cells of both 4T1 and EMT6 tumors implanted into the BALB/c mice (Extended Data Fig. 5a). Blockade of NKG2DL in the *in vitro* co-culture study consistently abolished the activation of NK cells (Extended Data Fig. 5b, Left Panel, compare group #7 to #6). The NKG2D or NKG2DL blocking assays suggested that NKG2D-NKG2DL interaction was involved in NK cell activation.

NKG2D is reported to be expressed on $CD4^+$ T-cells and the engagement of this $CD4^+$ T-cell-expressed NKG2D is capable of stimulating $CD4^+$ T-cells[35]. However, NKG2D was expressed on infiltrated $CD4^+$ T-cells at similarly low levels among all of groups of control, *Rnf2* KO and *Rsf1* KO tumors (Extended Data Fig. 5c). Additionally, pre-blocking NKG2D on $CD4^+$ T-cells failed to significantly change the frequencies of IFNγ-expressing $CD4^+$ T-cells or NK cells when co-cultured with either control or *Rnf2* KO tumor cells (Extended Data Fig. 5d, Left panel, compare groups #3, 5, 7, 9 to groups #2, 4, 6, 8 respectively, Right panel, compare groups #3, 5 to groups #2, 4 respectively). Therefore, the observed NKG2D and NKG2DL blocking effects in the co-culture system with *Rnf2* KO tumors appeared independent of NKG2D expression on $CD4^+$ T-cells.

Notably, the increases in IFNγ^+NK or IFNγ^+CD4^+ T-cells induced by *Rnf2* KO tumor cells were significantly enhanced by the presence of the other type of immune cell ($CD4^+$ T-cells or NK cells) in the co-culture, respectively (Fig. 3c-d, Left panels, compare group #8 to groups #4 and #6), suggesting a mutual activation of NK and $CD4^+$ T-cells by *Rnf2* KO tumor cells. Interestingly, increased IFNγ^+NK cells in the co-culture with $CD4^+$ T-cells and *Rnf2* KO tumor cells were largely diminished in the presence of anti-NKG2D neutralization antibody that blocked NK cell activation (Fig. 3c, Left Panel, compare group #9 to #8), or anti-MHCII antibody that blocked $CD4^+$ T-cell activation (Fig. 3d, Right Panel, compare group #5 to #4). Similarly, the proportion of IFNγ^+CD4^+ T-cells in the co-culture with NK cells and *Rnf2* KO tumor cells was decreased by adding anti-MHCII antibody (Fig. 3d, Left Panel, compare group #9 to #8) or anti-NKG2D neutralization antibody (Fig. 3c, Right Panel, compare group #5 to #4). In support of the mutual activation between NK and $CD4^+$ T-cells, blocking NKG2DL also significantly abrogated the activation of $CD4^+$ T-cells (Extended Data Fig. 5b, Right Panel, comparing group #5 to #4), in addition to inhibiting the activation of NK cells in the co-culture of NK, $CD4^+$ T-cells and *Rnf2* KO tumor cells (Extended Data Fig. 5b, Left Panel, compare group #9 to #8). The NK/$CD4^+$ T-cell cooperativity in the presence of *Rnf2* KO tumor cells was confirmed by using GFP-labeled 4T1 cells (both control and *Rnf2* KO) that were enriched by FACS sorting GFP^+ populations from corresponding tumors implanted in immunocompetent mice (Extended Data Fig. 5e, both panels, compare group #5 to others). All these results supported a cooperative activation of NK and $CD4^+$ T-cells induced by *Rnf2* KO tumor cells.

Finally, we examined whether the cooperation between NK and $CD4^+$ T-cells could directly impact on tumor cells by comparing the *in vitro* tumoricidal activity of pre-activated NK plus $CD4^+$ T-cells to that of NK or $CD4^+$ T-cells alone. Although $CD4^+$ T-cells displayed tumoricidal activity (Figure 3e, compare column #6 to #1), NK cells appeared to play a dominant role in killing tumor cells (Fig. 3e, compare group #2 to #1, and #7 to #6). This cytolytic function of NK cells was dramatically enhanced by co-cultured *Rnf2* KO tumor

cells and $CD4^+$ T-cells (Fig. 3e, compare group #9 to groups #2, 4, 7). This enhancement was largely abrogated by NKG2D blockade (Fig. 3e, compare groups #3, 5, 8, 10 to groups #2, 4, 7, 9, respectively), but not by pre-blockade of NKG2D expressed on $CD4^+$ T-cells (Extended Data Fig. 5f, compare groups #3, 7 to groups #4, 8 respectively), suggesting an NKG2D-dependent killing of *Rnf2* KO tumor cells by NK cells.

A significant reduction in the expression of MHCI molecules in 4T1 KO tumors was also observed (Extended Data Fig. 5g), which may contribute to increased NK cell activation and cytotoxicity induced by these KO tumors due to "missing" self. This downregulation may also help to explain why $CD8^+$ T-cells were not affected by KO tumors given the critical role of MHCI in activating $CD8^+$ T-cells. Interestingly, the level of MHCI in *Rnf2* KO EMT6 tumors was not different from that of control EMT6 tumors (Extended Data Fig. 5h), suggesting that $CD8^+$ T-cells might not also be involved in *Rnf2* KO-induced anticancer immunity in the EMT6 model. This discrepancy of MHCI expression could be contextual/tumoral dependent.

IFNγ drives mutual activation of NK-$CD4^+$ T in *Rnf2* KO tumor

We next defined potential factor(s) mediating the mutual activation of NK and $CD4^+$ T-cells induced by *Rnf2* KO tumors. The increased expression of IFNγ by both NK and $CD4^+$ T-cells in *Rnf2* KO or *Rsf1* KO tumors (Fig. 2c-d) implicated IFNγ as such a factor, given the positive roles of IFNγ in regulating both NK and $CD4^+$ T-cells[36,37]. Indeed, neutralization of IFNγ by the addition of anti-IFNγ antibody dramatically reduced $IFN\gamma^+CD4^+$ T-cells or $IFN\gamma^+$NK cells when NK and $CD4^+$ T-cells were co-cultured with *Rnf2* KO tumors (Fig. 3f-g, compare group #9 to #8 in both figures). Pre-blocking IFNγ receptor (IFNγR) on $CD4^+$ T-cells using an anti-IFNγR antibody abrogated both the increases of $IFN\gamma^+CD4^+$ T-cells (Extended Data Fig. 5i, Left panel, compare group #9 to #8) and $IFN\gamma^+$NK cells (Extended Data Fig. 5i, Right panel, compare group #7 to #6) when these cells were co-cultured with *Rnf2* KO tumor cells. Similarly, pre-blocking IFNγR on NK cells abolished the increases of $IFN\gamma^+$NK cells (Extended Data Fig. 5j, Left panel, compare group #9 to #8) and $IFN\gamma^+CD4^+$ T-cells (Extended Data Fig. 5j, Right panel, compare group #7 to #6) in the co-culture with *Rnf2* KO tumor cells.

Because cancer cells also express IFNγR and IFNγ signaling in cancer cells affects cancer immunity[4,37], we also examined the potential role of IFNγR on tumor cells. To this end, we deleted *IFNγR1* or *IFNγR2* or both in *Rnf2* KO 4T1 tumor cells to establish double KO (DKO) (*IFNγR1* KO-*Rnf2* KO or *IFNγR2* KO-*Rnf2* KO) (Extended Data Fig. 5k-l) or triple KO (TKO) (*IFNγR1* KO-*IFNγR2* KO-*Rnf2* KO) (Extended Data Fig. 5m) 4T1 cells. Interestingly, these DKO and TKO tumors were still efficiently rejected by BALB/c mice (Extended Data Fig. 5n-o), with similar kinetics as *Rnf2* KO tumors. TKO tumor cells isolated from these *in vivo* tumors also activated $CD4^+$ T-cells and NK cells to express IFNγ to similar extents as *Rnf2* KO tumors in the co-culture (Extended Data Fig. 5p, compare group #6 to #4 and group #7 to #5 in both panels). These results suggested that *Rnf2* KO-induced tumor rejection largely required IFNγ signaling acting in the immune cells.

Given that IFNγ can promote cancer immune surveillance[36] and its proposed role in mediating the mutual activation between innate and adaptive immunity[38], we reasoned that

it might contribute to the enhanced *in vivo* anti-tumor effects induced by *Rnf2* KO or *Rsf1* KO. As expected, IFNγ blockade with a neutralization antibody fully rescued growth of both *Rnf2* KO and *Rsf1* KO 4T1 tumors in immunocompetent mice (5 out of 5 mice in both experiments) (Fig. 3h-k). Although neutralization of IFNγ did promote the growth of control tumors (Extended Data Fig. 5q), the relative ratio of fold change in tumor volumes between anti-IFNγ group and control antibody group (=fold change in mean tumor volumes of group treated with anti-IFNγ antibody divided by fold change in mean tumor volumes of group treated with control antibody) in control tumors is much smaller than that of *Rnf2* KO tumors at the end of this experiment (3.73-fold in control tumor vs 46.08-fold in *Rnf2* KO tumor) (Extended Data Fig. 5r). Taken together, these results suggested that IFNγ was at least one of the cytokines contributing to tumor rejection of *Rnf2* KO tumors via mutual activation of NK and $CD4^+$ T-cells independent of its direct effects on tumor cells.

Activated $CD4^+$ T-cells produce IL-2, which may stimulate NK cells, and IL-2 from NK cells may in turn influence the functional status of $CD4^+$ T-cells[39]. We also tested whether IL-2 was involved in the mutual activation of NK and $CD4^+$ T-cells induced by *Rnf2* KO tumors by including an anti-IL-2 antibody in the *in vitro* co-culture experiment. However, neutralization of IL-2 did not significantly reduce the increased amount of $IFN\gamma^+$NK or $IFN\gamma^+CD4^+$ T-cells induced by *Rnf2* KO tumor cells (Extended Data Fig. 5s, compare group #5, 7, 9 to group # 4, 6, 8 respectively, in both Left and Right panels). Therefore, IL-2 did not appear to be significantly involved in this crosstalk between NK and $CD4^+$ T-cells in the context of *Rnf2* KO.

Rnf2/Rsf1 KO upregulates immune-related genes

We further explored the molecular mechanism by which deletion of tumoral *Rnf2* or *Rsf1* elicited both NK and $CD4^+$ T-cell-mediated anticancer immune response. We first profiled the transcriptomes of tumor cells isolated and sorted from *Rnf2* KO or *Rsf1* KO tumors and compared them to those from control tumors. Notably, multiple immune-related genes were induced in 4T1 tumor cells upon *Rnf2* deletion (Extended Data Fig. 6a). Further analysis using NetworkAnalyst[40] showed that both *Rnf2* KO and *Rsf1* KO tumor cells had significantly upregulated genes enriched in both adaptive and innate immune processes, including IFNγ response, antigen processing/presentation, and MHCII (Extended Data Fig. 6b-e). These results suggested a reprogramming of tumor cells upon *Rnf2/Rsf1* KO by de-repressing these immune-related genes, leading to increased immune activation. An independent GSEA analysis of the whole transcriptome of tumor cells by clustering the whole gene expression dataset confirmed these findings (Fig. 4a, Extended Data Fig. 6f-g, 7a). Analysis of published transcriptomic data in the human TNBC cell line MDA-MB-231[22] also demonstrated significant enrichment in both innate and adaptive immune responses with *Rnf2* KO (Extended Data Fig. 7b). Thus, the epigenetic program driven by RNF2 that regulated the immune response appeared to be conserved in human TNBC.

We also noted that the differentially expressed genes (DEGs) in *Rnf2* KO tumors overlapped significantly with those in *Rsf1* KO tumors (Extended Data Fig. 7c), and 98.5% (132 out of 134 DEGs) of these overlapping DEGs exhibited changes of expression in the same direction (Extended Data Fig. 7d). Furthermore, these overlapping DEGs were enriched

in immune-activation pathways, including MHCII and antigen processing/presentation (Extended Data Fig. 7e), as well as several genes encoding chemokines (Extended Data Fig. 7f). Consistently, there were inverse associations of expression of *RNF2/RSF1*, but not *EZH2*, with the expression of chemokines in human invasive BRCA TCGA dataset (Extended Data Fig. 7g). Among these chemokines, *CCL5* and *CXCL10*, were significant favorable prognostic factors in invasive BRCA (Extended Data Fig. 7h).

Consistent with previous reports[41,42], the downregulated DEGs in both *Rnf2* or *Rsf1* KO tumors were also enriched in cell cycle (Fig. 4a, Extended Data Fig. 6f-g, 7a), Myc and E2F targets, as well as ribosome biogenesis indicative of cold tumors[19] (Fig. 4a, Extended Data Fig. 6f-g, 7a), supporting our initial screening of clinical datasets that identified *RNF2* as a negative regulator of tumor immunogenicity. In contrast, among those upregulated DEGs in both *RNF2* KO and *RSF1* KO tumors were multiple gene signatures of the MHCII-mediated antigen processing/presentation pathway (Fig. 4a, Extended Data Fig. 6f). Notably, multiple isoforms of *MHCII* and *Cd74* (also known as HLA class II histocompatibility antigen gamma chain that facilitates MHCII-mediated antigen presentation) that are capable of and essential for activating $CD4^+$ T-cells were significantly upregulated in both *Rnf2* KO and *Rsf1* KO tumors (Fig. 4b). These increases were confirmed in *ex vivo*-isolated tumor cells at the protein levels (Fig. 4c). Further analysis of human invasive BRCA TCGA revealed that *RNF2* and *RSF1* were significantly and negatively correlated with most of the known *MHCII* isoforms and *CD74*, both of which were significant favorable prognostic factors for overall survival of invasive BRCA patients (Fig. 4d-e). This is consistent with the previous report that tumoral MHCII is a favorable prognosis factor for TNBC[43]. Knockout of both *H2-Ab1* (encoding the class II antigen A beta 1) and *H2-Eb1* (encoding the class II antigen E beta) (Fig. 4f) in *Rnf2* KO 4T1 cells at least partially rescued tumor growth in 3 out of 5 mice (Fig. 4g-i). Deletion of *H2-Ab1* and *H2-Eb1* also failed to increase the frequencies of $IFN\gamma^+CD4^+$ T-cells or $IFN\gamma^+$ NK cells (Fig. 4j-k, compare group #6 to #4 and group #7 to #5 in both figures), when the double KO tumor cells isolated from *in vivo* tumors were co-cultured with NK and $CD4^+$ T-cells together. Moreover, these double KO cells displayed significantly reduced capacity to induce $CD4^+$ T-cell cytotoxicity compared to *Rnf2* KO and control tumor cells (Fig. 4l). These findings supported the role of tumor-expressed MHCII in promoting anti-tumor responses elicited by tumor-specific deletion of *Rnf2*.

RNF2 regulates the transcription of multiple immune genes

One of the means by which RNF2 regulates the transcription[22,44] is to orchestrate chromatin accessibility[22,23], alterations of which in immune related genes are relevant for the sensitivity of cancer cells to immune attack[11,15]. To investigate whether the chromatin accessibility of immune related genes were altered due to *Rnf2* KO, we performed ATACseq analysis of *Rnf2* KO (n=2) and control 4T1 tumor cells (n=2) sorted from *in vivo* tumors by FACS. ATACseq showed that compared to control tumors, *Rnf2* KO tumors had thousands of genes with either significantly more or less accessible chromatin sites (Fig. 5a), consistent with the recent reports that PRC1 complex/RNF2 plays a dual role (both opens and closes) in regulating chromatin accessibility and thus transcription[22,23,27,45]. These more open genes were related to immunity, including antigen presentation via MHCII (Fig. 5b). Other enriched gene signatures were related to development, transcription by RNA polymerase

II (RNAPII), and mammary gland development, consistent with the reported functions of PRC1 complex/RNF2[20,22,23,45]. Moreover, the genes with more/less accessible chromatin sites significantly overlapped with up-/down-regulated DEGs in *Rnf2* KO tumors revealed by RNAseq (Fig. 5c), including antigen presentation via MHCII (Fig. 5b, 5d).

We next analyzed the profile of Rnf2 target genes in cultured 4T1 cells by CHIPseq. As expected, the Rnf2 target genes significantly overlapped with genes having more/less accessible chromatin sites identified by ATACseq (Extended Data Fig. 8a) and DEGs determined by RNAseq (Extended Data Fig. 8b) in control and *Rnf2* KO tumor cells that were isolated from tumors implanted in immunocompetent mice. Correspondingly, these overlapping genes were also both more accessible/upregulated and less accessible/downregulated upon *Rnf2* KO (Fig. 5e-f, Extended Data Fig. 8a-b), consistent with the dual roles (both opens and closes) of Rnf2 in regulating chromatin accessibility and thus transcription[22,23,27,45,46]. Importantly, the overlapping genes with more open chromatin sites/upregulated were significantly and highly enriched with gene signatures of immunity (Fig. 5e-f). Other enriched gene signatures were development, transcription by RNAPII, and mammary gland development, which are related to the well-established functions[20] and the recently reported activity of PRC1 complex/RNF2 in estradiol signaling[22,23].

The screenshots of RNAseq and ATACseq of MHCII genes *H2-Ab1* and *H2-Eb1* showed that they were significantly open and upregulated upon *Rnf2* KO (Extended Data Fig. 8c). The occupancy by Rnf2 was determined by Cut&RUN-qPCR (Figure 5g). Further evidence obtained from reanalyzing published datasets of Rnf2/RING1B CHIPseq in mouse embryonic stem cells (mES)[45] (Extended Data Fig. 8d) and human triple negative breast cancer cell MDA-MB-231[22] (Extended Data Fig. 8g, shown below) all demonstrated the occupancy of Rnf2/RING1B on these MHCII genes. Furthermore, upon *Rnf2* KO, *H2-Ab1* expression was also increased in mES cells demonstrated by analyzing published RNA microarray dataset[45,47] (Extended Data Fig. 8e).

We next examine the potential correlation of RNF2 to immune-related genes in human cancers by analyzing published RNF2 CHIPseq dataset for the human TNBC cell line MDA-MB-231[22]. RNF2 was shown to bind to multiple genes involved in immune processes (11.48%, 164 genes out of total 1428 RNF2 bound genes), including MHCII genes-*HLA-DPA1*, and *HLA-DPB1* (Extended Data Fig. 8f-g). GSEA analysis confirmed the association of these genes with immunity (Extended Data Fig. 8h). We then analyzed the correlation of the expression of the above RNF2 bound genes identified in MDA-MB-231 cells[22] (Extended Data Fig. 8i) to *RNF2* expression using the RNAseq dataset of TCGA human invasive BRCA patients. This analysis showed that 34.9% of RNF2 bound immune-related genes (58 out of 166) (Fig. 5h) and 17.2% of all RNF2 bound genes (246 out of 1428) (Extended Data Fig. 8h) were significantly and negatively correlated with *RNF2* expression levels, consistent with the putative role of PRC1/RNF2 in repressing transcription of target genes[20,48]. Notably, these genes included those related to immune activation and high tumor immunogenicity, such as *HLA-DPB1*, *CCL20* and *SLAMF7* (Fig. 5h). Consistent with the possible role of PRC1/RNF2 in transcriptional activation[22,23,27,45,46], a subset of RNF2 bound genes, including immune-suppressive genes (e.g., *FLRT3*[49], *IGFR1*[50], *FOXP1* and *SOCS5*[51]), were positively associated with *RNF2* (Fig. 5h), supporting the notion that

the PRC1 complex/RNF2 mediated immune suppression. Taken together, RNF2 repressed immunogenicity by controlling the accessibility of the immune genes, and knockout of *Rnf2* resulted in de-repression of genes that mediated immune activation.

We also performed ATACseq analysis of *Rsf1* KO tumor cells (n=2), which revealed that the more/less accessible chromatin genes (Fig. 6a) were significantly overlapped with those of *Rnf2* KO tumors (Fig. 6b). Interestingly, these overlapped genes that were more accessible were also enriched in the signatures related to immunity, including antigen presentation through MHCII (Fig. 6c). Moreover, up-/down-regulated DEGs shared by *in vivo Rnf2* KO and *Rsf1* KO tumors revealed by RNAseq (Extended Data Fig. 7c-e) largely overlapped with shared genes with more/less accessible chromatin sites between *Rnf2* KO and *Rsf1* KO tumors, respectively (Fig. 6d). These overlapping genes with more accessible chromatin sites and upregulated in *Rnf2* KO/*Rsf1* KO tumors were also significantly enriched in gene signatures of immunity, including MHCII restricted antigen presentation (Fig. 6e). Taken together, *Rsf1* KO and *Rnf2* KO tumors displayed enhanced immuno-eliciting characteristics due to the direct changes of gene transcription by *Rnf2/Rsf1*.

Catalytic dead mutant Rnf2 does not elicit immune response

We investigated the role of the E3 ubiquitin ligase activity of Rnf2 in its transcriptional regulation and suppression of tumor immunity. We used CRISPR/Cas9 technology to generate a catalytic dead mutant of *Rnf2* (*Rnf2*$^{I53A/I53A}$)[21,23] knock-in 4T1 cell line (Fig. 7a). This amino acid change (I to A) disrupts the interaction of Rnf2 with the E2 UBCH5C and ablates the ability of Rnf2 to act as an E3 ligase[23], without affecting the incorporation of Rnf2 into canonical and variant PRC1 complexes. Although the level of endogenous H2aK119ub1 that is catalyzed by the Rnf2 E3 ligase was largely reduced (Fig. 7b), this tumor cell line was able to grow robustly in syngeneic BALB/c mice at similar rates as control tumors (Fig. 7c-d). Similar immune profiles within the microenvironment of *Rnf2*$^{I53A/I53A}$ tumor and the tumoral MHCII level were also observed to those of control 4T1 tumors (Fig. 7e). All these data suggested that the E3 ligase activity of Rnf2 may be dispensable for its function in suppressing antitumor immunity that we demonstrated with *Rnf2* KO.

We also performed ATACseq analysis of *Rnf2*$^{I53A/I53A}$ 4T1 tumor cells (n=2) isolated and enriched from tumors implanted into syngeneic BALB/c mice (Fig. 7f). We observed significant overlaps of both more and less accessible genes between *Rnf2* KO and *Rnf2*$^{I53A/I53A}$ 4T1 tumors (Fig. 7g). These overlap genes were enriched in the signatures of development and transcription, consistent with the well-established functions of PRC1 Complex/Rnf2 (Fig. 7h), and in the signature of response to estradiol consistent with the recently reported role of RNF2 in estrogen signaling that appeared to involve the E3 ligase activity of RNF2[22,23]. Although there were overlap genes related to inflammatory responses, cytokine production, chemotaxis, and myeloid leukocyte differentiation (Fig. 7h), the more accessible genes in *Rnf2*$^{I53A/I53A}$ tumors did not include those of MHCII and MHCII restricted antigen presentation which were enriched in *Rnf2* KO tumors (Fig. 7i). Moreover, genes that were more/less accessible in *Rnf2*$^{I53A/I53A}$ but not in *Rnf2* KO tumors were not directly related to immune process (Fig. 7j). These results suggested that transcriptional

regulation of MHCII and MHCII restricted antigen presentation by Rnf2 appeared not to require the E3 ligase activity.

Rnf2/Rsf1 KO induces durable anti-tumor memory

The findings that mice implanted with *Rnf2* KO or *Rsf1* KO tumors remained long-term tumor free post-rejection (Fig. 1f-g, Extended Data Fig. 3p-q) suggested that these mice potentially developed anti-tumor immune memory. To test this hypothesis, we re-challenged mice that initially cleared *Rnf2* KO or *Rsf1* KO tumors by injecting wildtype (WT) parental 4T1 tumor cells into the contralateral 4th mammary fat pads. Notably, these mice rejected WT tumors completely and efficiently in a short period and remained tumor free for a long period of time (> 300 days) (Fig. 8a, Extended Data Fig. 9a). The similar eradication of re-challenged WT EMT6 tumor was observed in immunocompetent mice that were previously exposed to and cleared *Rnf2* KO EMT6 tumors (Fig. 8b-d). In contrast, re-challenging mice that were previously exposed to *Rnf2* KO 4T1 tumors with TSA, another murine TNBC cell line that does not share antigens with 4T1[52], failed to induce rejection (Extended Data Fig. 9b). These results suggested that deletion of *Rnf2* or *Rsf1* programmed a specific anti-tumor recall response characteristic of immunological memory. Profiling immune cells of these WT 4T1 tumors prior to being cleared in mice that previously rejected *Rnf2* KO or *Rsf1* KO primary tumors consistently showed significantly more CD4$^+$ T-cells, NK cells and KLRG1$^+$ effector subsets among these cells than those of WT tumors in naïve mice (Fig. 8e, Extended Data Fig. 9c). Moreover, NK cells, but not CD4$^+$ or CD8$^+$ T-cells, expressed higher levels of granzyme B (Fig. 8e, Extended Data Fig. 9c).

We also determined which of these cells could potentially mediate the anti-tumor memory response by depleting each cell type using various neutralizing antibodies. Depletion of NK cells in mice that were previously exposed to *Rnf2* KO tumors rescued the tumor growth at the early time points (day 12). However, 4 out of 5 mice eventually cleared the tumors after day 48 (Extended Data Fig. 9d-e). Depletion of CD8$^+$ T-cells partially restored the tumor growth in 2 out of 5 mice (Extended Data Fig. 9f-h). In contrast, depleting CD4$^+$ T-cells fully rescued tumor growth in 5 out of 5 mice (Fig. 8f-g, Extended Data Fig. 9i), suggesting the central role of CD4$^+$ T-cells in the regulation of anti-tumor memory responses induced by ablation of *Rnf2*.

Discussion

The nature and effector status of tumor-infiltrating immune cells are predictors of clinical outcomes for many solid tumors, while factors expressed by the tumor itself influence immune profiles within the TME. It is critical to define the tumor-immune interactions for therapeutic strategies aiming at inducing optimal anti-tumor immunity[3,4]. Here we report an epigenetic reprogramming of tumor cells by depleting tumor-expressed *Rnf2/Bmi1/Rsf1*, which de-repressed tumor genes related to immune responses, including those involved in the MHCII-mediated antigen processing and presentation pathway. Mechanistically, the immune genes regulated by Rnf2/Rsf1 were rendered more accessible upon ablation of *Rnf2* or *Rsf1* in *in vivo* tumors. The subsequent remodeling of the TME not only promoted the recruitment of NK and CD4$^+$ T-cells into the tumor, but also reinvigorated their anti-tumor

activity. The resultant enhanced co-operative anti-tumor responses by these innate and adaptive immune cells led to immune memory and durable rejection of the tumor (please see the proposed model in Fig. 8h-i).

Our results support that the anticancer activity induced by *Rnf2* KO required an intact immune system, consistent with a recent report that human breast cancer cells T47D and MDA-MB-231 with *RNF2* knockdown do not exhibit apparent growth defects in immunocompromised mice[22]. $CD8^+$ T-cells are traditionally thought as the major immune cell type against cancer[36]. Unexpectedly, knocking out tumor *Rnf2/Rsf1* induced a preferential and concomitant activation of NK and $CD4^+$ T-cells, but not $CD8^+$ T-cells. Depletion of NK or $CD4^+$ T-cells but not $CD8^+$ T-cells rescued growth of *Rnf2/Rsf1* KO tumors in immunocompetent mice, supporting their anti-tumor activity in our system. Although the anticancer capacity of invariant T-cells are reported recently, the requirement of MHCII for anti-tumor responses upon *Rnf2* KO and the rescue of *Rnf2* KO tumor growth after the depletion of $CD4^+$ T-cells argue against the possible involvement of invariant T-cells in our models.

NK cells are one of the components of innate immunity mediating tumor killing, and their killing capacity does not require a prior sensitization, which may explain that depletion of NK cells in the immunocompetent host resulted in a quicker rescue of *Rnf2* KO tumors than that of deletion of $CD4^+$ T-cells. Most solid tumors present a barrier to NK cell infiltration, and intratumoral NK cells are often dysfunctional and exhausted. The influx and activation of NK cells induced by *Rnf2/Rsf1* KO may result from increased immune responses in these tumors that upregulate NKG2D on NK cells, and are further enhanced by $CD4^+$ T-cells.

Deficiencies in the activities and infiltration of $CD4^+$ T-cells within the TME can also promote tumorigenesis[36], emphasizing the critical role of these cells in the regulation of anti-cancer immunity. Provided with the CD28-mediated co-stimulatory signals, *Rnf2* KO tumor cells could directly activate $CD4^+$ T-cells *in vitro* that was abrogated by MHCII blockade/deletion, suggesting that deletion of tumor *Rnf2* reprogrammed tumor cells to acquire the potential capability of antigen presentation and activate $CD4^+$ T-cells in the absence of professional antigen-presenting cells (APCs). This $CD4^+$ T-cell activation appeared not to be a bystander effect considering the decreased activation of $CD4^+$ T cells and the rescue of *in vivo* growth of *Rnf2* KO tumor induced by additional KO of MHCII.

Although our system could not fully exclude the possible involvement of other cell types within the $CD45^-$ population in the activation of $CD4^+$ T-cells and NK/$CD4^+$ T-cells from mice bearing control tumors displayed basal activation in the coculture studies, our additional analysis of NK/$CD4^+$ T-cell activation using sorted GFP^+ tumor cells from *in vivo* tumors further support the capacity of *Rnf2* KO tumor cells to activate $CD4^+$ T-cells directly along with the CD28-CD80/CD86 co-stimulation. At least some of these activated $CD4^+$ T-cell subsets are reactive to tumor associated antigens as judged by the presence of CD4-dependent anti-tumor specific memory response, although the identity of antigens presented by MHCII in *Rnf2* KO tumors requires further investigation. Given the recently emerging appreciation of MHCII-restricted $CD4^+$ T-cell responses in anti-tumor immunity[53], our findings that the additional ablation of *MHCII* in *Rnf2* KO tumor rescued tumor growth *in*

vivo have revealed a previously unrecognized epigenetic mechanism controlling MHCII expression on tumor cells, thus leading to increased $CD4^+$ T-cell activation and the subsequent enhanced anti-tumor immunity.

The importance of $CD4^+$ T-cells in *Rnf2/Rsf1* KO-induced anti-tumor effects is further emphasized by the observation that deletion of tumoral *Rnf2/Rsf1* facilitated the generation of anti-tumor specific immunological memory that was abrogated by depletion of $CD4^+$ T-cells. This immune memory and prolonged tumor clearance could be leveraged to design more effective immunotherapy, considering the poor induction of sustained anti-tumor responses by current immunotherapies that focus on $CD8^+$ T-cells[54]. The observed activities of $CD4^+$ T-cells in enhancing NK cell function, in killing tumor cells[55] (albeit less potent than NK cells in our *in vitro* cytotoxicity assays), and in anticancer memory may explain why the extent of $CD4^+$ T-cells correlating to BRCA patient survival appeared greater than that of NK cells.

Perhaps one of the most intriguing findings in our study is the cooperative activation of innate NK and adaptive $CD4^+$ T-cells as a result of deletion of *Rnf2/Rsf1* in tumors. Although the interplay of NK and $CD4^+$ T-cells has been implicated in diverse settings[56,57], the activation of these two types of immune cells and their mutual dependence as a result of specific targeting of a single tumoral epigenetic regulator constitutes an unconventional mechanism for anti-tumor immunity. Despite that $CD4^+$ T-cells and NK cells may function with different tempos reflected by the different growth rates of the rescued *Rnf2* KO tumors upon depletion of NK and $CD4^+$ T-cells in immunocompetent mice, our data support a mutual activation of NK and $CD4^+$ T-cells in the context of *Rnf2* KO.

Although the mechanisms by which NK and $CD4^+$ T-cells cooperate against tumors require further analysis, our study has revealed that IFNγ may serve as one of the critical factors mediating their interplay to create an inflamed TME in *Rnf2/Rsf1* KO tumors. Further investigation is also required to precisely define how NK and $CD4^+$ T-cells communicate in real time during tumor progression. However, our results may suggest a sequential model in which NK cells as the first line of defense kill *Rnf2* KO tumors in a NKG2D-NKG2DL dependent pathway, followed by NK cell activation in the recognition of dead tumor cell-associated danger signals. Activated NK cells produce proinflammatory cytokines, like IFNγ, that function as the signal 3 for $CD4^+$ T-cell activation. The increased expression of IFNγ along with TNFα may also render $CD4^+$ T-cells to acquire the T-helper-1 (Th1) phenotype, in turn further enhancing NK cell function[36], including tumor killing activity. The resultant cooperative interactions by these two types of cells efficiently cleared *Rnf2/Rsf1* KO tumors and likely prevented them from constant exposure to the tumor cells/antigens and becoming exhausted. *Rnf2/Rsf1* KO also induced the generation of memory $CD4^+$ T-cells, which explains the long-term rejection of primary *Rnf2/Rsf1* KO tumors. Future characterization of memory $CD4^+$ T-cell subsets and the mechanisms by which IFNγ induces the cooperation between NK and $CD4^+$ T-cells leading to memory cells are expected to inform different strategies from current immunotherapies that have faced much resistance in cancer patients.

Given its plastic and druggable nature, the importance of epigenetic regulation in cancer immune evasion has been appreciated. Epigenetic regulators are reported to mediate silencing of endogenous retroviruses, chemokines, cancer testis antigens, IFN-responsive genes and MHCI to primarily dampen $CD8^+$ T-cell-mediated anti-tumor responses[10,11,13-17]. It is known that the PRC1 complex and the PRC2 complex regulate transcription cooperatively or independently[20]. Our results suggest that the mechanistic action of RNF2 in the regulation of tumor immunogenicity beyond its conventional roles in embryonic development and tumorigenesis appears distinct from and independent of the reported immune modulating functions of other epigenetic regulators, including EZH2. For example, analyzing the human invasive BRCA TCGA dataset revealed that the significant and negative correlations of *Rnf2/Rsf1* to most of the *MHCII* genes and chemokines were not observed for *EZH2*. The observed positive correlations of *EZH2* to chemokines in BRCA differ from a published report showing that EZH2 represses tumor production of CXCL9 and CXCL10 in ovarian cancer[14]. Although EZH2 is conventionally viewed as a transcription silencer, it has been recently reported to act as a contextual transcription activator[58]. The transition from transcription silencer to activator is thought to be driven by the changes in the posttranslational modifications, such as phosphorylation of the EZH2 protein. It is possible that in breast cancer these modifications may allow EZH2 to act as a transcription activator to express certain chemokines, which does not occur in ovarian cancer.

It remains controversial regarding the requirement of E3 ligase activity of RNF2 for its function[21,23,59,60]. Here, by employing an Rnf2 catalytic dead mutant knockin 4T1 cell line $Rnf2^{I53A/I53A}$, we demonstrated that its E3 ligase activity was dispensable for repressing immune gene transcription. RNF2 has been recently shown to directly compact chromatin independent of its E3 ligase activity[59]. This process is likely mediated by the canonical RNF2/PRC1 complex independent of histone H3K27me3 that is the substrate of PRC2 complex/EZH2/EZH1[59]. Further studies are warranted to explore whether the repression of immune related genes by RNF2 is related to its function to compact chromatin.

We previously identified Rsf1 as a ubiquitinated histone H2A binding protein from the ubiquitinated H2A containing nucleosome. Thus, it is expected to observe in *ex vivo*-isolated *Rnf2* KO and *Rsf1* KO tumor cells the overlaps of DEGs revealed by RNAseq and of a large number of genes with more/less accessible chromatin sites identified by ATACseq. It is also anticipated that *Rsf1* KO displayed similar phenotype as *Rnf2* KO to induce tumor rejection. Interestingly, $Rnf2^{I53A/I53A}$ tumor grew robustly in immunocompetent mice. H2A ubiquitination is catalyzed by PRC1 complex/Rnf2. It is possible that, in addition to ubiquitinated H2A, subunits of PRC1 complex or their interacting proteins recruit Rsf1 to certain immune related genes that are rendered open in *Rnf2* KO/*Rsf1* KO but not $Rnf2^{I53A/I53A}$ tumors to regulate their transcription. These immune genes may subsequently contribute to the different phenotypes of *Rnf2 KO/Rsf1* KO tumors versus $Rnf2^{I53A/I53A}$ tumors. The findings that additional KO of *MHCII* in *Rnf2* KO tumor abrogated the activation of NK, $CD4^+$ T-cells and their cooperativity *in vitro* as well as rescued *Rnf2* KO tumor *in vivo* may support this notion. Further dissection of the detailed molecular mechanisms by which Rsf1 is recruited to modulate the expression of these immune genes, including *MHCII*, is warranted.

In summary, we have identified a previously unrecognized epigenetic reprogramming of tumor cells by abrogating tumoral *Rnf2/Rsf1*. The resultant mobilization and cooperation of NK and $CD4^+$ T-cells, but not $CD8^+$ T-cells, constitutes unappreciated mechanisms regulating the tumor-immune interaction within the TME. These findings may suggest supplemental therapeutic approaches capable of complementing current immunotherapies that focus on boosting $CD8^+$ T-cell responses. Moreover, specific deletion of tumoral *Rnf2/Rsf1* induced durable tumor elimination without affecting systemic response may suggest additional advantages of targeting *RNF2/RSF1* over other epigenetic regulators. Importantly, the inverse correlation of *RNF2/RSF1* to immunogenicity and patient outcomes was observed in multiple human cancer types, indicating the potential general applicability for targeting these molecules in human cancers.

Methods

The research presented in this report complies with all relevant ethical regulations. All animal procedures were performed in compliance with federal laws and institutional guidelines as approved by the UAB's Animal Care and Use Committee. All reagents or resources are listed in Supplementary Table 1 and 2, if not specified in the text. Further information on research design is available in the Nature Research Reporting Summary linked to this article.

Cell Lines

Murine triple negative breast cancer cell lines TSA, luciferase-expressing 4T1[61] and EMT6 were kindly provided by Drs. Lizhong Wang and Runhua Liu, and Dr. Lalita Shevde-Samant, and Dr. Narendra Wajapeyee (all at University of Alabama at Birmingham), respectively. 4T1 cells were cultured in Dulbecco's Modified Eagle's Medium (DMEM)/ Hams F-12 50/50 Mix (Corning, Cat# 10-090-CV) supplemented with 10% Fetal Bovine Serum (FBS) (MilliporeSigma, Cat# 12306C), and 10 units of Penicillin and 10 μg/mL Streptomycin (GE, Cat# SV30010), and 50 μg/mL Geneticin (ThermoFisher Scientific, Cat# 10131035). TSA and EMT6 cells were cultured in DMEM (MilliporeSigma, Cat# D6429) supplemented with 10% FBS, and 10 units of Penicillin and 10 μg/mL Streptomycin. All the cell lines used were confirmed pathogens free, including Mycoplasma, by Charles River Research Animal Diagnostic Services.

Animal Studies

6-8 week old female BALB/c mice and immunodeficient NOD-Prkdc^{em26Cd52}Il2rg^{em26Cd22}/ NjuCrl (NCG) mice (Charles River Laboratories) were allowed to acclimatize for 1 week prior to experiments, except that age-matched 12-14 week old mice were used for the immune memory studies. In general, mice were randomly assigned to groups for each experiment in an unblinded fashion. The procedure to establish orthotopic 4T1 model was conducted as described previously[61]. Briefly, 4 x 10^5 control, or *Rnf2* KO, *Rsf1* KO 4T1 or doxycycline inducible *Rnf2* KO cells suspended in 100 μL HBSS (ThermoFisher Scientific, Cat# 14170112) were injected into the left 4th mammary fat pads of BALB/c or NCG mice using 28G 0.5 mL Insulin Syringes (BD Biosciences, Cat# 329461), and tumors were monitored weekly using the bioluminescence imaging system starting at day 0 after

injection. For immunological memory studies, 4 x 10^5 *Rnf2* KO or *Rsf1* KO 4T1/EMT6 cells were injected into BALB/c mice as described above. At day 45 when *Rnf2* KO or *Rsf1* KO 4T1/EMT6 cells were cleared, 4 x 10^5 wildtype 4T1/EMT6 or TSA cells were injected into the right 4th mammary fat pads. A group of age-matched naïve mice was included as controls. 4T1 tumors were monitored weekly using the bioluminescence imaging system starting at day 0 after injection. EMT6 or TSA tumors were measured using a caliper every 3 days starting at day 4 after injection.

For luciferase bioluminescence assay, animals were intraperitoneally administrated with 2.5 mg/100ul solution of XenoLight D-luciferin (PerkinElmer). The tumor images were captured using an IVIS 100 imaging system (PerkinElmer). In some experiments, antibodies to IFNγ, NK, $CD4^+$ or $CD8^+$ T cells (BioXcell) were intraperitoneally injected into mice at indicated time points, as described in the legends. To induce *Rnf2* KO in doxycycline inducible 4T1 cells in BALB/c mice, doxycycline (Dox) (MilliporeSigma, Cat# D9891) were injected intraperitoneally at 50 mg/kg suspended in saline with a concentration as 5 μg/μL as described in a published protocol[62]. Dox administration either started one day before tumor cells were injected or after the tumors were palpable. No obvious toxicity was noticed. For “abscopal” tumor models, 4 x 10^5 control and *Rnf2* KO 4T1 cells suspended in 100 μL HBSS were simultaneously injected into left and right 4th mammary pads of the BALB/c mice, respectively. These tumors were monitored weekly using the bioluminescence imaging system starting at day 0 after injection. The maximal tumor volume is permitted by UAB’s Animal Care and Use Committee Tumor burden is 10% of the normal body weight which was not exceeded in the animal studies. Once the tumor reaches this limit, the mouse bearing the tumor is sacrificed.

Generation of *Rnf2/Rsf1/Bmi1* knockdown/knockout and double/triple knockout cells

The establishment of stable 4T1 cells with shRNAs targeting *Rnf2* (MilliporeSigma) was performed as described previously[27]. Briefly, lentiviral particles were packaged in 293T cells (ATCC) and transduced into 4T1 cells in the presence of Hexadimethrine bromide (8 μg/mL) (MilliporeSigma). The positive transduced cells were selected by puromycin and the knockdown efficiency was verified by immunoblots. The process of knocking out (KO) *Rnf2*, *Rsf1* or *Bmi1* in 4T1/EMT6 cells was conducted as described previously[27]. Oligonucleotides encoding guide RNAs were synthesized from the Integrated DNA Technologies (IDT) and cloned into lentiviral vector lentiCRISPRv2 (Addgene) using BsmBI restriction sites. To knock out *MHCII I-A* and *I-E*, two separate oligonucleotides encoding guide RNAs targeting I-A and I-E, synthesized from IDT, were simultaneously cloned into pKLV2.2-h7SKgRNA5(SapI)-hU6gRNA5(BbsI)-PGKpuroBFP-W (Addgene) using SapI and BbsI restriction sites, respectively. Similar strategy was adopted for knocking out *IFNγR1* and *IFNγR2* in 4T1 *Rnf2* KO cells to establish double KO and triple KO cells. After verification of the plasmids by sequencing, *Rnf2* KO 4T1 cells were transduced and sorted into single cells that were BFP positive into 96-well plate with one cell in each well by FACS (UAB Flowcytometry Core Facility). The screening of positive clones were performed by Flowcytometry to analyze the MHCII or IFNγR1/IFNγR2 stained single cell populations. To establish doxycycline inducible *Rnf2* KO 4T1 cells, oligonucleotides encoding guide RNAs targeting *Rnf2* described above were cloned into lentiviral vector

TLCV2[32] (Addgene) that is an all-in-one dox inducible system using BsmBI restriction sites. After verification of the plasmids by sequencing, 4T1 cells were transduced, selected by puromycin and maintained in Tet System Approved FBS (TaKaRa, Cat#631106). The screening of dox-inducible clones were performed *in vitro* as we described.

Establishment of *Rnf2*$^{I53A/I53A}$ knockin 4T1cell by CRISPR/Cas9

To establish *Rnf2*$^{I53A/I53A}$ knockin 4T1 cells, our published protocol has been adopted[63]. Briefly, 10^6 cells were washed with Opti-MEM medium (ThermoFisher Scientific) and resuspended in 100 μl Nucleofector Solution (Lonza). 400 pmol of HiFi Cas9 (IDT) was mixed with 500 pmol sgRNA thoroughly. The mixture was incubated in room temperature for 10 minutes. 500 pmol ssODN was then mixed with the Cas9 RNP. The final mixture was added into Nucleofector Solution containing the cells and gently mixed before electroporation (program T-024, Lonza). Half of Electroporated cells were cultured for four days and then the genomic DNA was extracted. Gene targeting efficiency was examined by droplet digital PCR (ddPCR) as following composition: 11 μl 2X ddPCR Supermix for Probes (Bio-Rad), 1 μl mRnf2-f2 (5'-GTGGTTTCACCTAGAAGTCTACACA-3', 20 μM), 1μl mRnf2-r2 (5'-CCACTTCTAAGGGCTGTGATAA-3', 20 μM), 1μl mRnf2-I53A-FAM (5'-ATGTGCCCAGCCTGTTTGGATATG-3', 5 μM), 1 μl R381 (5'-GGCCACCTTGAGCTTCTCA-3', 20 μM), 1μl R382 (5'-CAAGATGATGACTTGATATAGGCA-3', 20 μM), 1μl R379-HEX (5'-CACAGGGCAGTAAGGGCAGC-3', 5 μM), 50 ng genomic DNA, add ddH2O to 22 μl of total volume). 20 μl of the PCR mix was transferred to DG8 Catridges (Bio-rad) and generated droplet with a QX200 Droplet Generator (Bio-rad). The droplets were transferred into a 96-well twin.tec PCR plate (Eppendorf), sealed with PX1 PCR Plate Sealer (Bio-rad) and perform PCR on a C1000 Touch Thermal Cycler (Bio-rad). The thermal cycling program conducted was: Step 1: 95°C 10 min; Step 2: 95°C 30s; Step 3: 56°C 1min; repeat steps 2-3 for 39 times; Step 4: 98°C 10min; Step 5: 8°C hold. After the PCR, the droplets were analyzed using a QX200 Droplet Reader (Bio-rad) with the "absolute quantification" option. Once I53A gene targeting was verified, the other half of the electroporated 4T1 cells were used for isolating single cell colonies with sib-selection as described[63].

Cell proliferation

Cell proliferation assays were performed as described previously. Briefly, cells were seeded in 24-well plates and harvested at the indicated times. Cells were washed with PBS, trypsinized, and diluted 1:20 in isotonic saline solution (RICCA Chemical) followed by counting on a Beckman Z1 Coulter particle counter.

Chromatin bound and unbound fractionation

Fractionation of chromatin bound and unbound cell lysates were performed following a modified published protocol[64]. Briefly, cells cultured in 10 cm dishes were fixed in culturing medium supplemented with 1% formaldehyde (ThermoFisher Scientific, Cat# 28908) for 15 min at room temperature followed by quench in 125 mM Glycine (MilliporeSigma) for 5 min at room temperature. After thoroughly washed in PBS for 3 times, cell were scraped in PBS and centrifuged at 2,000 rpm for 4 min at 4°C. Cell pellets were lysed by Dounce homogenizer on ice (50 times) after being incubated with lysis buffer A (5mM HEPES

pH7.9, 0.75mM MgCl2, 5mM KCl, 0.25mM dithiothreitol [DTT]) on ice for 30 min. After centrifuging for 15 min at 3,300g at 4 °C, supernatant (S1) was collected, and the pellet was resuspended in buffer B (buffer A supplemented with 0.34M sucrose, 10% glycerol, 10mM NaF and 1mM Na3VO4) plus 0.5% NP40. Next, samples were incubated on ice for another 30 min and centrifuged for 10 min at 3,300g at 4 °C. Supernatant (S2) was added to (S1) to make the “unbound” fraction. The pellet was the “bound” fraction that was used for subsequent immunoprecipitation.

Immunoprecipitation in chromatin bound proteins

The isolated chromatin bound protein pellets were dissolved in RIPA buffer (50 mM Tris.HCl, pH 8.0, 150 mM NaCl, 1% NP-40, 0.5% Sodium Deoxycholate, 0.1% SDS) by sonication multiple times in Sonic 60 Dismembrator on ice. The supernatants (after centrifuge at 13,300 rpm at 4 °C for 15 min) were diluted 1:1 with RIPA buffer without Sodium Deoxycholate, SDS and precleared with 1 μg IgG (Cell Signaling Technology, Cat# 2729) and 5 μL Protein A/G PLUS-Agarose (Santa Cruz Biotechnology, Cat# sc-2003), followed by incubation with agarose-crosslinked Rnf2 antibody (Cell Signaling Technology, Cat# 5694) or control rabbit IgG (Cell Signaling Technology, Cat# 2729) overnight at 4 °C. After extensive wash, twice with wash buffer (provided by Pierce™ Crosslink IP Kit (ThermoFisher Scientific, Cat# 26147)), once with high salt buffer (20 mM Tris.HCl, pH 7.9, 10% Glycerol, 0.5 M KCl, 0.2 mM EDTA), twice with wash buffer, the immunoprecipitation were eluted from agarose with Elution Buffer provided by Pierce™ Crosslink IP Kit. To minimalize the backgrounds, during each washing cycle, the beads were agitated on a vortex mixer. The elutes were immediately neutralized with Tris.HCl, pH 9.4 and boiled before being loaded on SDS-PAGE.

Phenotyping of blood cells

Blood from mouse tail vein was collected into 100 μl PBS/1% heparin solution and mixed immediately. After stained with the fixable viability dye (Biolegend), blood was incubated with an antibody cocktail for 30 min at 4°C followed by red blood cell lysis, wash and flow cytometry analysis.

Tumor cell isolation from mice

To isolate mouse breast cancer cells, each tumor was cut into small pieces (<3mm) and incubated in 3ml dissociation solution (PBS supplemented with 2% FBS, 1mg/ml collagenase/Dispase and 0.5 mg/ml DNase I) for 1 hour at 37°C with gentle shaking. Cell suspension was then passed through a 70 μm cell strainer and washed with DMEM/2% FBS followed by flow cytometry analysis.

Flow Cytometry and Sorting

Single cell suspension was first stained with the fixable viability dye (Biolegend) at 1:1000 in PBS for 10 min. After washed with FACS buffer (PBS/2% FBS), cells were then incubated with Fc block (anti-mouse CD16/32 antibody) at 1:100 for 10 min, followed by incubation with indicated antibody mixtures for 30 min before washing and flow cytometry analysis. For intracellular staining, cells were fixed and permeabilized using

the FoxP3 staining buffer set (ThermoFisher Scientific) according to the manufacturer's protocol, followed by incubation with Fc block and intracellular antibodies for 30 min prior to wash and flow cytometry analysis. All of steps were performed at 4°C. Cells were acquired on a BD LSRII using FACSDiva software (BD Biosciences) and analyzed with FlowJo v10 software (Treestar). For cell sorting, single-cell suspension of tumor cells was labeled with the fixable viability dye and antibodies to the surface antigens (CD45, CD3, NKp46, NK1.1), as described above, followed by sorting on a FACSAria II using FACSDiva software (BD Biosciences). $CD45^-$ live cells were collected as tumor cells and $CD45^+CD3^-NK1.1^+NKp46^+$ live cells were NK cells.

Microbead-based cell enrichment

Single-cell suspension isolated from mouse spleens or tumors was enriched for $CD4^+$ T cells, NK cells, or tumor cells using CD4, NK or CD45 microbeads (Miltenyi Biotec), respectively. $CD45^-$ cells in the effluent fluid after enrichment were collected as tumor cells.

In vitro tumor killing assay by activated $CD4^+$ T cells or NK cells

Enriched $CD4^+$ T cells were stimulated with plate-coated anti-CD3 antibody (5 μg/ml) and soluble anti-CD28 antibody (2 μg/ml) in the presence of recombinant human IL-2 (hIL-2) (50 U/ml) for 72 h. Enriched NK cells were incubated with hIL-2 (500 U/ml) for 72 h. Enriched tumor cells (Control or *Rnf2* KO) were labeled with CellTrace Violet (CTV) dye (5 μM) according to the manufacturer's protocol (ThermoFisher Scientific) followed by co-culture in triplicates without or with activated $CD4^+$ T cells, NK cells or $CD4^+$ T cells plus NK cells (the ratio of tumor: immune effector cells = 1:5) in the presence of hIL-2 (50 U/ml) for 16 h prior to staining with the fixable viability dye and flow cytometry analysis. In some cases, 30 μg/ml anti-NKG2D or rat IgG1 isotype antibody (Biolegend) was pre-incubated with NK cells or $CD4^+$ T cells for 15 min before addition to the co-culture. Cells positive for both CTV and fixable viability dye are defined as dead cells. The percent tumor killing is calculated using the following equation: [%dead cells (experimental group)-% dead cells (tumor alone)]/% dead cells (tumor alone).

In vitro activation of $CD4^+$ T cells or NK cells by tumor cells

NK and $CD4^+$ T cells were isolated from spleens of mice harboring control tumors and enriched as described above. Tumor cells (Control or *Rnf2* KO) were enriched as $CD45^-$ cells as described above, followed by co-culture in triplicates with $CD4^+$ T cells, NK cells or $CD4^+$ T cells plus NK cells (tumor: immune = 1:5) for 16 h in the presence of hIL-2 (50 U/ml) and soluble anti-CD28 (2 μg/ml, for groups with $CD4^+$ T cells). Cells were then incubated with the Golgi Plug (BD Biosciences) plus Golgi Stop (BD Biosciences) for 5 h prior to flow cytometry analysis of IFNγ production by $CD4^+$ T cells or NK cells. In some groups, 30 μg/ml anti-NKG2D or rat IgG1 isotype antibody (Biolegend) was pre-incubated with NK cells or $CD4^+$ T cells for 15 min before addition to the co-culture, and 10 μg/ml anti-IFNγR1 or rat IgG2a isotype antibody (Fisher) was pre-incubated with NK cells or $CD4^+$ T cells for 30 min before addition to the co-culture. 10 μg/mL anti-MHCII or rat IgG2b isotype antibody (BioXcell), or 10 μg/mL antibodies to IFNγ, IL-2 or recombinant mouse NKG2D Fc (blocking NKG2DL) were added into some groups. Groups with $CD4^+$ T cells or NK cell alone were also included for analysis.

RNA isolation and sequencing

Total RNA from sorted tumor cells and NK cells was extracted using a QIAshredder kit (QIAGEN) and an RNeasy Plus Micro Kit (QIAGEN) according to the manufacturer's protocol. RNA sequencing was performed at Genewiz (South Plainfield, NJ) using Ultra-Low Input RNA-Seq Service. Briefly, mRNA was specifically enriched from total RNA by removing rRNA and hydrolyzed into small pieces. The fragments were then reverse-transcribed into first-strand cDNA using random hexamer primers, followed by second strand synthesis. The short cDNA strands were ligated with 3′- and 5′-adapters for amplification and sequencing using the Illumina® platforms (HiSeq 2 x 150 bp, single index, per lane). The RNA-seq data have been deposited in the NCBI GEO under accession number GSE143352.

RNA-seq data analysis

Sequence reads were trimmed to remove possible adapter sequences and nucleotides with poor quality using Trimmomatic v.0.36. The trimmed reads were mapped to the Mus musculus GRCm38 reference genome available on ENSEMBL using the STAR aligner v.2.5.2b[65]. The STAR aligner is a splice aligner that detects splice junctions and incorporates them to help align the entire read sequences. BAM files were generated as a result of this step. Unique gene hit counts were calculated using feature Counts from the Subread package v.1.5.2. Only unique reads that fell within exon regions were counted. Since a strand-specific library preparation was performed, the reads were strand-specifically counted. After extraction of gene hit counts, the gene hit counts table was used for downstream differential expression analysis. Using DESeq2[66], a comparison of gene expression between the control groups and KO groups of samples was performed. The Wald test was used to generate p-values and log2 fold changes. Genes with an adjusted p-value < 0.05 and absolute log2 fold change > 1 were called as differentially expressed genes for each comparison. These differential gene expression data were uploaded into the published web tool NetworkAnalyst to generate the heatmap and the enriched gene sets[40].

Independently, Gene Set Enrichment Analysis (GSEA) was performed according to the previous protocols[67]. Gene set database "Mouse_GOBP_AllPathways_no_GO_iea_March_01_2019_symbol.gmt" was downloaded from http://baderlab.org/GeneSets. It contains only gene sets from GO biological process excluding annotations that have evidence code IEA (inferred from electronic annotation), ND (no biological data available), and RCA (inferred from reviewed computational analysis) and all pathway resources. Genes were ranked by fold change and subject to the analysis under the "GSEAPreranked" module. The method "classic" was used as the enrichment statistic method and pathways with the size 15 to 500 were used for analysis. The enriched pathways were defined as FDR value < 0.05.

ATACseq

Control, *Rnf2* KO, *Rsf1* KO, or *Rnf2*$^{I53A/I53A}$ tumor cells were isolated and enriched from *in vivo* tumors implanted into the 4th mammary fat pads at day 7 after tumor cell injection by FACS described above. Before being subjected to FACS, the cells were treated with 0.5 mg/ml DNase I for 1 hour at 37°C with gentle shaking to get rid of DNA released from

dead/damaged cells. The isolated cells were snap frozen in 70% DMEM, 20%FBS and 10%DMSO and delivered on dry ice to Active Motif Epigenetic Services who performed subsequent ATACseq using their standard procedure. Upon received, the cells were then thawed in a 37°C water bath, pelleted, washed with cold PBS, and tagmented as previously described, with some modifications based on a published protocol[68] to increase the signal-to-background ratio and remove the contamination of mitochondria genome. Briefly, cell pellets were resuspended in lysis buffer, pelleted, and tagmented using the enzyme and buffer provided in the Nextera Library Prep Kit (Illumina). Tagmented DNA was then purified using the MinElute PCR purification kit (Qiagen), amplified with 10 cycles of PCR, and purified using Agencourt AMPure SPRI beads (Beckman Coulter). Resulting material was quantified using the KAPA Library Quantification Kit for Illumina platforms (KAPA Biosystems), and sequenced with PE42 sequencing on the NextSeq 500 sequencer (Illumina).

ATACseq data analysis

Raw sequencing reads were aligned to the mouse reference genome (mm10) with BWA[69]. Only reads mapped uniquely to the nuclear genome (very few reads were mapped to mitochondria genome) and aligned with less than 3 mismatches were used for peak calling. Duplicate reads arose from PCR were also removed. Normalization was performed by randomly sampling reads of each sample to the number of reads present in the smallest sample. Peaks were identified by MACS2[70] with options "--nomodel -g 1.87e9 --bw 200". BigWig files were generated with BamCoverage from deepTools[71] and were used to visualize peaks in the genome browser. To compare peak metrics between samples, overlapping peak intervals were grouped into merged regions. Different accessible sites were identified by DESeq2[66] with input of read counts for all merged regions.

TCGA dataset analysis

For breast cancer samples, TCGA biolinks was implemented for data analysis[72]. RNA-seq data for each tumor sample was downloaded from GDC Data Portal (https://portal.gdc.cancer.gov/). Differential gene expression analysis was performed for the cancer samples compared to the normal samples. The program edgeR was employed to normalize gene expressions and perform differential expression analysis[73]. Quantile filtering was implemented to filtering low expressed genes. Differentially expressed genes (DEGs) were identified with at least two-fold change and FDR<=0.01. For pan-cancer analysis, the standardized, normalized, batch corrected and platform-corrected datasets were downloaded from the TCGA consortium (https://gdc.cancer.gov/about-data/publications/pancanatlas). Copy number variation was downloaded from Broad GDAC firehose (http://gdac.broadinstitute.org/runs/analyses__latest/data/). To analyze the correlation between RNF2 and other genes, linear regression model was used to calculate correlation coefficients and p value. To analyze immune cell cytolytic activity, immune cytolytic score was calculated by averaging log transformed transcript levels of two key cytolytic effectors, granzyme A (GZMA) and perforin (PRF1)[29]. To analyze ICPi responsive gene signature, the gene expression profile score was calculated by averaging log transformed transcript levels of 18 genes.

For survival analysis, clinical information of each patient was downloaded by TCGA biolinks. The survival time was calculated based on their live status. Survival time was chosen as “days to death” or “days to last follow up” based on patient alive status. “Surv” function in “Survival” package of R was used to build the standard survival object. The variable time records survival time, and the status indicates whether the patient’s death was observed (status = 1) or that survival time was censored (status = 0). A survival curve was computed for the censored data using the Kaplan-Meier method. To investigate whether the gene expression level can influence a patient’s survival, the median gene expression was calculated, and patient samples were grouped into high expression or low expression group based on their expression levels. Then survival curves were computed for the patient with each group. The log rank test was used to define whether patients with different gene expressions have significantly different survival time ($p < 0.05$).

ChIPSeq and ChIPSeq analysis

Control 4T1 cells were snap frozen and delivered on dry ice to Active Motif Epigenetic Services who performed subsequent CHIPseq using their standard procedure. ChIP-Seq data were aligned to the mouse reference genome (mm10) using BWA[69]. Samples were normalized by randomly sampling reads to the same number. Peaks were identified with MACS2[70] with input as control sample and “-g 1.87e9 -f BAM --nomodel -p 1.00e-07 --extsize 200”. Peaks were annotated by comparing to the Ensembl gene annotation (release 99 for GRCm38) with custom Python script. Read depth was computed by DeepTools bamCoverage[71] at bin width of 50bp. The bigWig files were displayed in the UCSC genome browser.

ChIP-seq analysis of Published Data

The samples, GSM2862178 (control) and GSM2862179 (RNF2), from the published ChIP-seq data (GSE107176)[22] of MDA-MB-231 cell line were downloaded from the NCBI Gene Expression Omnibus (GEO) database. Trimmomatic (v0.36) were implemented to remove low-quality reads. Then the raw reads were aligned to the human genome hg19 using Bowtie2 (v2.3.5.1)[74]. Duplicate reads were removed using Samblaster (v0.1.24)[75].

Peaks were called using MACS2.1 (v2.1.2) with default parameters with 0.05 q value as a cutoff [70]. Peaks with fold change > 4 were used for downstream analysis. The resulted bedgraph files were visualized by IGV (v2.6)[76]. The RNF2 bound genes were uploaded to the published web tool GSEA[28] to generate the enriched gene sets by overlapping with Reactome gene sets[77].

Cut&Run-qPCR

Cut&Run assay was performed using kit purchased from Cell Signaling Technology (Cat# #86652) according its standard protocol. The pulled-down chromatin DNA was amplified as described previously[27].

Public IHC Data

The images of IHC of RNF2 and RSF1 were downloaded from Human Protein Atlas (http://www.proteinatlas.org)[78].

Statistical analysis and Reproducibility

Statistical analyses were performed using two-tailed, unpaired Student's t test, one-way or two-way ANNOVA with GraphPad Prism V8 software, as indicated. A p value of < 0.05 was considered to be statistically significant (*p < 0.05, **p < 0.01, ***p < 0.001, ****p < 0.0001). No exclusion of data points was used. Sample size was not specifically predetermined, but the number of mice used was consistent with previous experience with similar experiments. The experiments were not randomized and the Investigators were not blinded to allocation during experiments and outcome assessment. Most studies were either exactly independently repeated or confirmed independently with different models/systems.

Data availability

ChIP-seq, RNA–seq and ATAC-seq data that support the findings of this study have been deposited in the Gene Expression Omnibus (GEO) under accession codes GSE143352. Previously published ChIP-seq data that were re-analyzed here are available under accession code GSE10573[47], GSE34520[45] and GSE107176[22].

The human pan-cancer and breast cancer data were derived from the TCGA Research Network: https://portal.gdc.cancer.gov/. For pan-cancer analysis, the standardized, normalized, batch corrected and platform-corrected datasets were downloaded from the TCGA consortium (https://gdc.cancer.gov/about-data/publications/pancanatlas). Copy number variation was downloaded from Broad GDAC firehose (http://gdac.broadinstitute.org/runs/analyses__latest/data/). Source data have been provided as Source Data files. All other data supporting the findings of this study are available from the corresponding author on reasonable request.

Code availability

The software and methods to generate the results have been described in detail in the Method part. No additional code needs to be deposited.

Extended Data

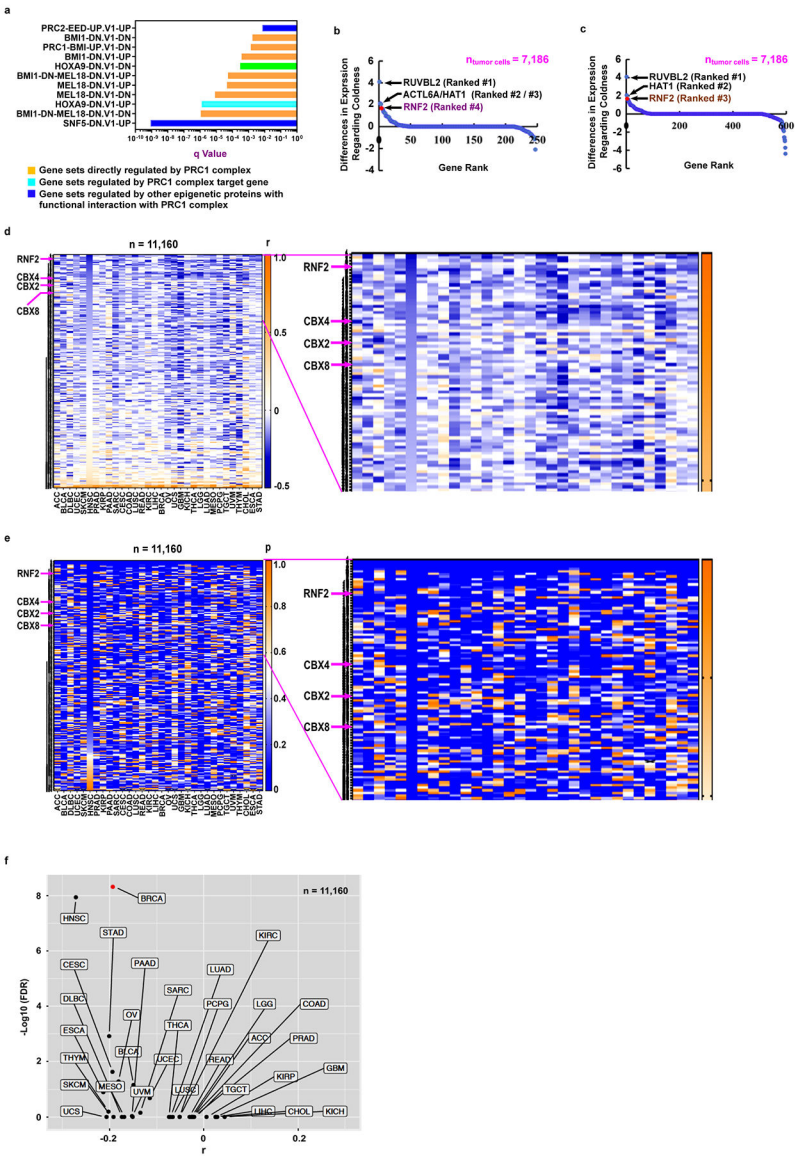

Extended Data Fig. 1. *RNF2* marks the signature of immunologically cold tumors and is negatively associated with cytotoxicity of immune cells.

a. GSEA analysis of the gene signature of cold tumor (noted as T cell exclusion) revealed in single cell RNAseq of tumor cells from melanoma patients using oncogenic gene sets (C6). Gene sets related to epigenetic pathways are shown. n = 7,186 single tumor cells from 33 human melanoma tumors (from 31 patients).

b-c. The ranking of 248 (**b**) or 524 (**c**) epigenetic regulators based on their median expression levels in relation to the high and low expression of “cold” gene signature, extracted from the dataset in panel **a** via the Single Cell Portal. Each value at the y-axis for each gene is defined as its median expression level in the single tumor cells with high expression of cold gene signature minus that in the tumor cells with low expression of cold gene signature. These values were used to sort and plot corresponding genes on a

two-dimensional plane. The x-axis denotes the rank of these genes. *RNF2* is ranked as the top 4th/3rd gene. The number (n) of single tumor cells included in this single cell RNAseq is noted.

d-f. Analysis of genes extracted from TCGA datasets. Heatmaps (**Left**) with the top parts zoomed in (**Right**) show correlations between expression levels of 248 epigenetic genes with the immune cell cytotoxicity gene signature, *GZMA* and *PRF1*, in diverse human cancers. The expression levels of these genes are extracted from TCGA. The coefficients (r) (**d**), and p values of these correlations (**e**) are shown. The zoomed in images of the top parts of the graph are shown in the right. **f**. The volcano plot shows the correlation of *RNF2* to *GZMA* and *PRF1* in human cancers. The y-axis and x-axis denote Log10(FDR) and coefficients (r) of correlations, respectively. The case numbers (n) are noted. n = 11,160 patients.

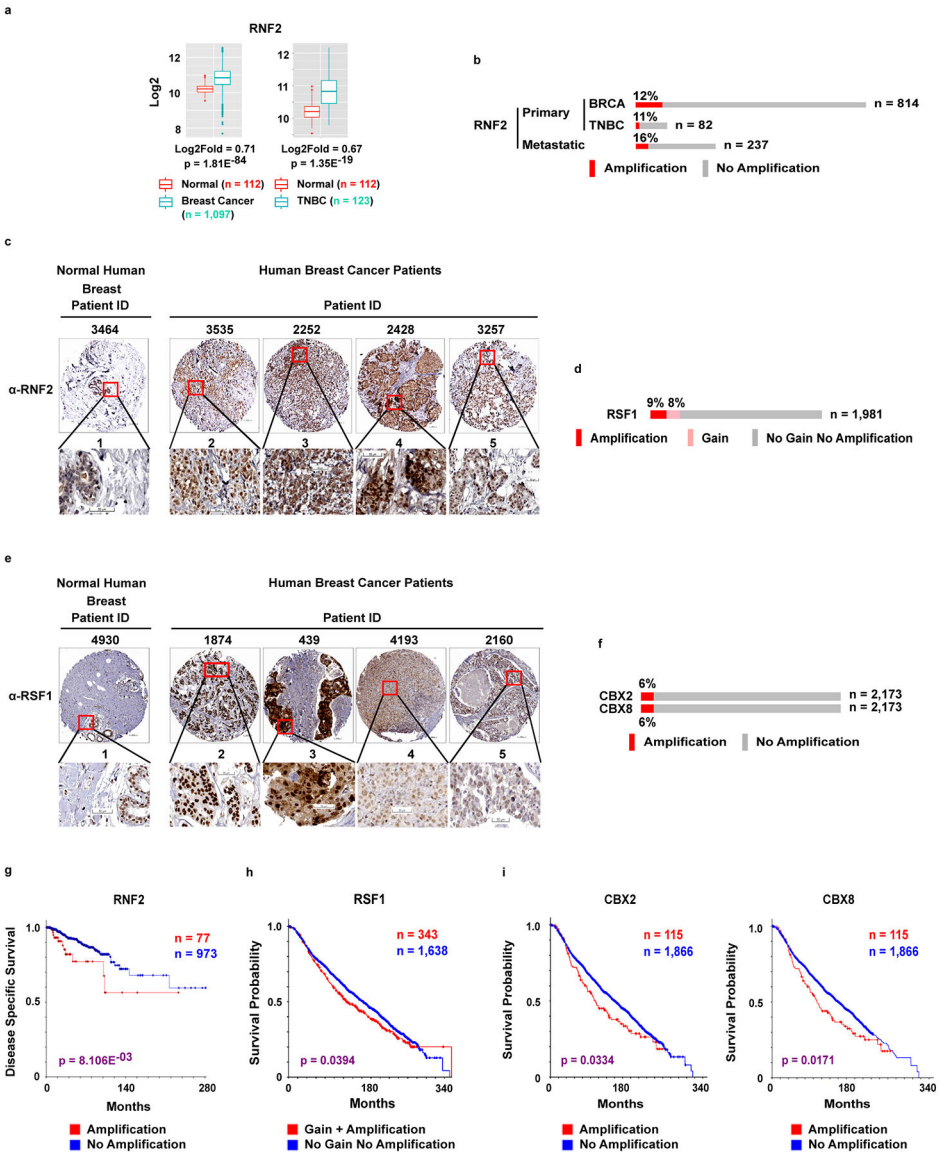

Extended Data Fig. 2. RNF2/CBX2/CBX8/RSF1 is amplified/overexpressed in human breast cancer patients, and associated with shorter survival time.

a. The box plot shows the expression levels of *RNF2* in human normal breast tissue, invasive breast cancer tissues (**Left**) and triple negative breast cancer (TNBC) tissues (**Right**). Log2 fold change (Log2Fold) of cancer tissues relative to normal tissues and significance (p) of the correlations are displayed. The lower and upper bound of box plot represent the first quartile (Q1, 25% of data) and third quartile (Q3, 75% of data) of the data. Center line within the box represents the median value (also the second quartile). The whisker marks 1.5*IQR (Inter Quartile Range, the distance between Q1 and Q3) at both side of the box. Dots are the outliers, which are the values outside the whiskers (> Q3 + 1.5*IQR or < Q1 - 1.5*IQR). Normal controls for breast cancer patients: n = 125; breast cancer patients: n = 1,097; normal controls for TNBC patients: n = 112; TNBC patients: n = 123.

b. The percentages of primary invasive breast cancer (BRCA), primary TNBC and metastatic breast cancer patients with *RNF2* amplification. The numbers of patients (n) are indicated.

c. Images with patient IDs from The Human Protein Atlas (http://www.proteinatlas.org) display the expression of RNF2 protein in normal breast tissues and human breast cancer tissues by immunohistochemistry staining. Scale bars: 100 (Upper)/50 (Bottom) μm. The website link for each image is provided in the Resources Table.

d. The percentages of invasive breast cancer patients (n = 1,981) with the gain and amplification of *RSF1*, obtained from the METABRIC dataset via cBioPortal.

e. Images with patient IDs from The Human Protein Atlas (http://www.proteinatlas.org) display the expression of RSF1 protein in normal breast tissues and human breast cancer tissues by immunohistochemistry staining. Scale bars: 100 (Upper)/50 (Bottom) μm. The website link for each image is provided in the Resources Table.

f. The percentages of breast cancer patients with the amplification of *CBX2* and *CBX8* obtained from METABRIC dataset via cBioPortal. The numbers of patients (n) are indicated.

g-i. The correlations of amplification of *RNF2* (**g**) or *Rsf1* (**h**) or *CBX2*/*CBX8* (**i**) to the survival of invasive breast cancer patients (PanCancer Atlas) (**g**), or breast cancer patients (METABRIC dataset) (**h**, **i**) obtained from cBioPortal. P values are generated using two-tailed LogRank Test. The numbers of BRCA patients (n) with (**red** color) or without (**blue** color) amplification/amplification + gain of indicated gene are shown.

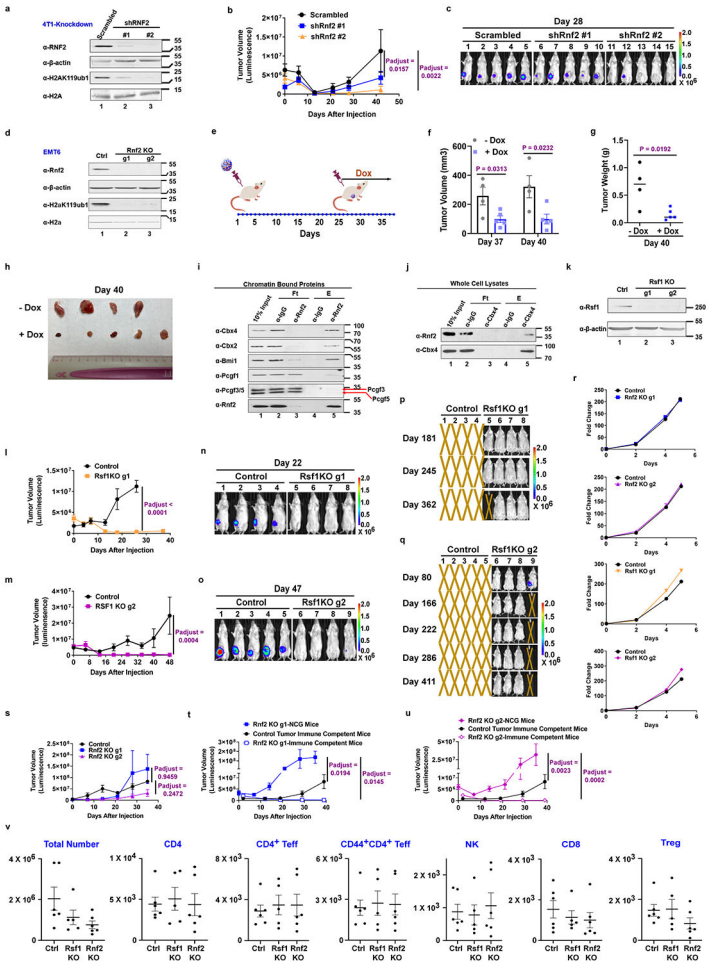

Extended Data Fig. 3. Targeting *Rnf2/Rsf1* results in tumor rejection in syngeneic murine breast cancer models.

a-c. **a**. Immunoblots of indicated proteins in 4T1 cells transduced with the scrambled shRNA or two independent shRNAs targeting *Rnf2* gene, which represents two independent experiments with similar results. The knockdown efficiency has been independently confirmed. **b-c**. The volumes (**b**) and representative BLIs at day 28 after inoculation (**c**) of tumors transduced with shRNAs as described in panel **a** (mean ± SEM, n = 5 mice/group, each mouse harboring one tumor) in mice.

d. Immunoblots of indicated proteins in Ctrl and *Rnf2* KO (two independent gRNAs, g1 and g2) EMT6 cells. The knockout efficiency was independently confirmed at least twice.

e-h. **e**. Treating regimen. **f**. Tumor volumes of doxycycline inducible *Rnf2* KO tumors at the indicated days after implantation in BALB/c mice. Tumor volumes were calculated by length X width^2/2. **g**, **h**. The weights (**g**) and images (**h**) of the tumors at the end of the study. n = 4 mice for - Dox, n = 5 mice for + Dox, each mouse harboring one tumor.

i-j. Immunoblots show the selective subunits of PRC1 complex interacting with Rnf2 that was immunoprecipitated from chromatin of 4T1 cells (**i**) or Rnf2 interacting with Cbx4 that was immunoprecipitated from whole cell lysates of 4T1 cells (**j**). Ft, Flowthrough, E, Elute, which represents two independent experiments with similar results.

k. Immunoblots of Rsf1/β-actin in Ctrl and *Rsf1* KO (two independent gRNAs, g1 and g2) 4T1 cells. The knockout efficiency was independently confirmed at least twice.

l-q. **l**, **m**. The tumor volumes (mean ± SEM) in mice implanted with control or *Rsf1* KO 4T1 tumor cells (guide 1 (n = 4 mice/group) (**l**) or guide 2 (n = 5 mice in control group, n = 4 mice in Rsf1 KO group) (each mouse harboring one tumor). (**m**). n-q. Representative tumor BLIs of tumors at day 22/47 after inoculation (**n**, **o**) or at longer time points (**p**, **q**). X, mice were sacrificed because of the big tumor burdens at the day when images were taken.

r. The proliferation (mean of quadruplicates, n = 4 for technical replicates), (fold changes in cell numbers), of control or *Rnf2* KO (g1 and g2) or *Rsf1* KO (g1 and g2) 4T1 cells *in vitro*. Cell numbers at day 0 are set as 1.

s-**u**. s. The volumes of control or *Rnf2* KO 4T1 tumors (g1 and g2) implanted into the 4th mammary pads of the immuno-compromised NOD-Prkdcem26Cd52Il2rgem26Cd22/NjuCrl (NCG) mice. Mean ± SEM (n = 5 mice/group, each mouse harboring one tumor). **t-u**. The volumes of control tumors or *Rnf2* KO 4T1 tumors ((g1) (**t**) or (g2) (**u**)) implanted into the immuno-compromised NCG mice (as in panel s) or immune competent BALB/c mice (as in Fig. 1b-c). Mean ± SEM (n = 5 mice/group, each mouse harboring one tumor).

v. Numbers of total cells and of intratumoral immune cells of 4T1 tumors (Ctrl, *Rnf2* KO and *Rsf1* KO) displayed in Fig. 2a-b. n = 6 mice for Ctrl /*Rnf2* KO; n = 5 mice for *Rsf1* KO, each mouse harboring one tumor. Symbols, individual mouse (bars, mean ± SEM).

Two-way ANOVA with Tukey's test in b, s, t, u; unpaired two tailed Student's t test in f, g, r; two-way ANOVA with Sidak's test in l, m.

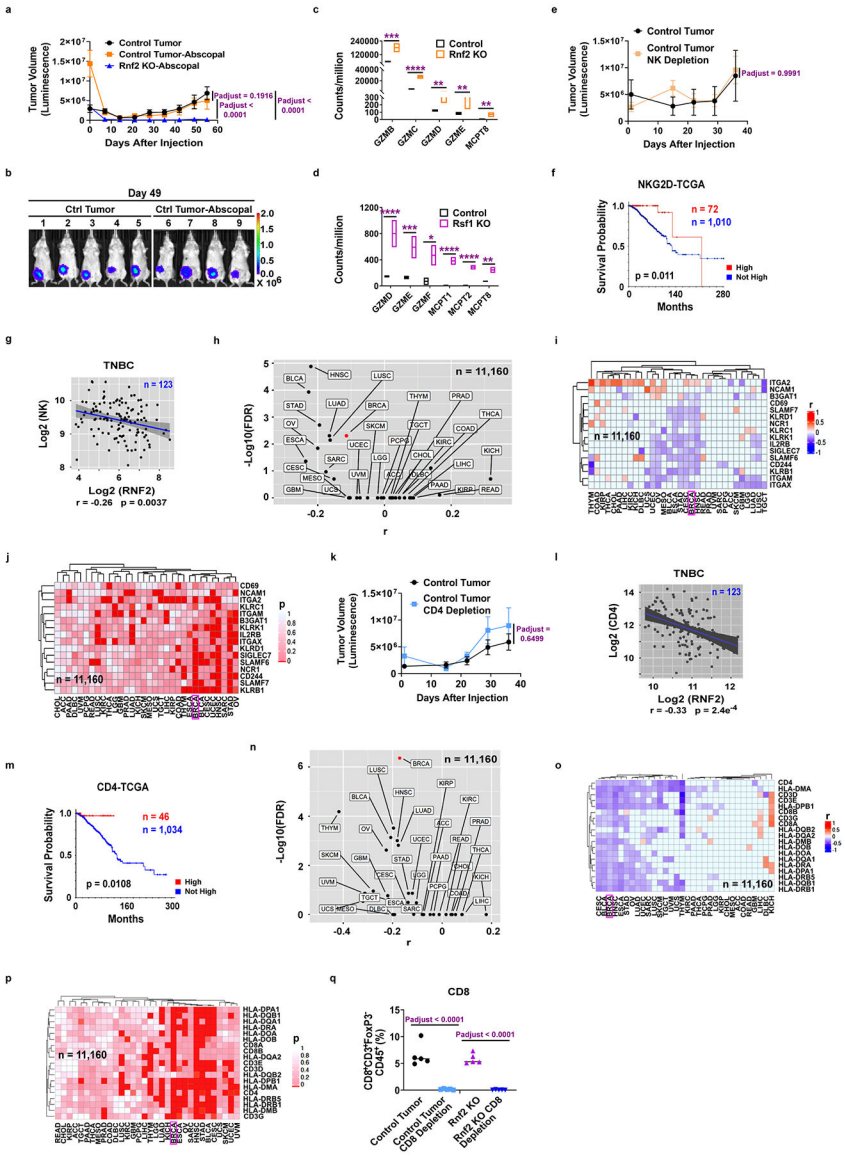

Extended Data Fig. 4. *Rnf2/Rsf1* is negatively correlated to infiltration/activation of NK and CD4+ T-cells.

a-b. BALB/c mice were inoculated with control 4T1 tumor into the left 4th mammary fat pads or simultaneously with control tumor into the left 4th mammary fat pads and *Rnf2* KO 4T1 tumors (*Rnf2* KO g2) into the right 4th mammary pads. **a**. Tumor volumes (mean ± SEM, n = 5 mice in the group of 4T1 tumor injected into the left 4th mammary fat pads (Control Tumor), each mouse harboring one tumor; n = 4 mice in the group of simultaneously injected with control tumor into the left 4th mammary fat pads (Control Tumor-Abscopal) and *Rnf2* KO 4T1 tumors into the right 4th mammary pads (*Rnf2* KO-Abscopal)), each mouse harboring two tumors: one is control tumor injected in the left mammary fat pad, the other one is *Rnf2* KO tumor injected into the right mammary fat pad. $p < 0.0001$ (control tumors injected alone (Control Tumor) vs. *Rnf2* KO tumors injected into the right mammary pads of the mice in which control tumors were injected simultaneously into the left mammary pads (*Rnf2* KO-Abscopal)); $p<0.0001$ (control tumor injected into the

left mammary pads of the mice in which *Rnf2* KO tumors were injected simultaneously into the right mammary pads (Control Tumor-Abscopal) vs. *Rnf2* KO tumors injected into the right mammary pads of the mice in which control tumors were injected simultaneously into the left mammary pads (*Rnf2* KO-Abscopal)); not statistically significant (control tumors injected alone (Control Tumor) vs. Control tumor injected into the left mammary pads of the mice in which *Rnf2* KO tumors were injected simultaneously into the right mammary pads (Control Tumor-Abscopal)) (two-way ANOVA with Tukey's test). **b**. Representative BLIs of tumors at indicated days.

c-d. The counts of genes encoding granzymes (GZMB, GZMC, GZMD, GZME, GZMF) and mast cell proteases (MCPT1, MCP2, MCPT8), revealed in RNAseq of FACS-sorted NK cells from control 4T1 tumors compared to those in *Rnf2* KO tumors (Upper) or *Rsf1* KO tumors (Bottom), at day 7 after implantation. The RNAseq was performed in control tumors (n = 2, two groups of cells, each group of cells pooled from 25 mice, each mouse harboring one tumor), *Rnf2* KO tumors (n = 2, two groups of cells, one group of cells pooled from 25 mice, each mouse harboring one tumor of *Rnf2* KO g1, the other group of cells pooled from another 25 mice, each mouse harboring one tumor of *Rnf2* KO g2), *Rsf1* KO tumors (n = 2, two groups of cells, one group of cells pooled from 25 mice, each mouse harboring one tumor of *Rsf1* KO g1, the other group of cells pooled from another 25 mice, each mouse harboring one tumor of *Rsf1* KOg2). The full list of p values can be found in the source data for this figure (two-tailed Wald test).

e. The volumes of 4T1 control tumors in BALB/c mice treated with/without α-asialo GM1 at days 2, 5, 10 post-implantation. Mean ± SEM (n = 5 mice/group, each mouse harboring one tumor. Two-way ANOVA with Sidak's test.

f. The correlation of expression of *NKG2D* with the overall survival of invasive breast cancer patients (TCGA dataset) via cBioPortal. High, expression level > 1.5 SD above the mean. P value is generated using two-tailed LogRank test. Numbers of BRCA patients (n) with (**red** color)/without (**blue** color) high expression of *NKG2D* are indicated.

g. The correlation of *RNF2* expression to the published NK cell signature in TNBC was analyzed by Pearson correlation (two-tailed, no adjustment for multiple comparisons because of one correlation test for a gene pair). The expression levels of these genes are extracted from the TCGA dataset. The values of the coefficients (r) and significance (p) are indicated. Shaded area, 95% confidential interval. n = TNBC patient numbers.

h-j. The expression levels of *RNF2* and indicated genes from the published NK cell gene signature are extracted from TCGA RNAseq datasets of various cancer types (n = 11,160 patients). The correlations of *RNF2* expression to the levels of these genes as a whole (**h**), or individually (r in **i**; p values in **j**) are shown.

k. The volumes of control 4T1 tumors in BALB/c mice treated with α-CD4 (GK1.5) or its isotype control antibody at days 2, 5 post-implantation. Mean ± SEM (n = 5 mice/group, each mouse harboring one tumor.). Two-way ANOVA with Sidak's test.

l. The correlation of *RNF2* to CD4 expression level in TNBC was analyzed by Pearson correlation (two-tailed, no adjustment for multiple comparisons because of one correlation test for a gene pair). The expression levels of these genes are extracted from the TCGA dataset. The values of the coefficients (r) and significance (p) of the correlations are displayed. Shaded area, 95% confidential interval. n = TNBC patient numbers.

m.The correlation of *CD4* expression with the overall survival of invasive breast cancer patients (TCGA dataset) via cBioPortal. P value is generated using LogRank test. High, the expression level > 2 SD above the mean. P value is generated using two-tailed LogRank test. Numbers of BRCA patients (n) with (**red** color)/without (**blue** color) high expression of *CD4* are indicated.

n-p. The expression levels of *RNF2* and genes encoding T cell markers and MHCII are extracted from TCGA RNAseq datasets of various cancer types (n = 11,160 patients). The correlations of *RNF2* expression to the levels of these genes as a whole (**n**) or individually (r in **o**; p values in **p**) are shown.

q. Frequencies of peripheral blood $CD8^+$ T-cells in mice bearing control or *Rnf2* KO tumors at day 10 after injection of anti-CD8 (2.43) or control antibody. Symbols depict individual mouse (bars, mean ± SEM). n = 5 mice/group, each mouse harboring one tumor. One-way ANOVA with Tukey's test.

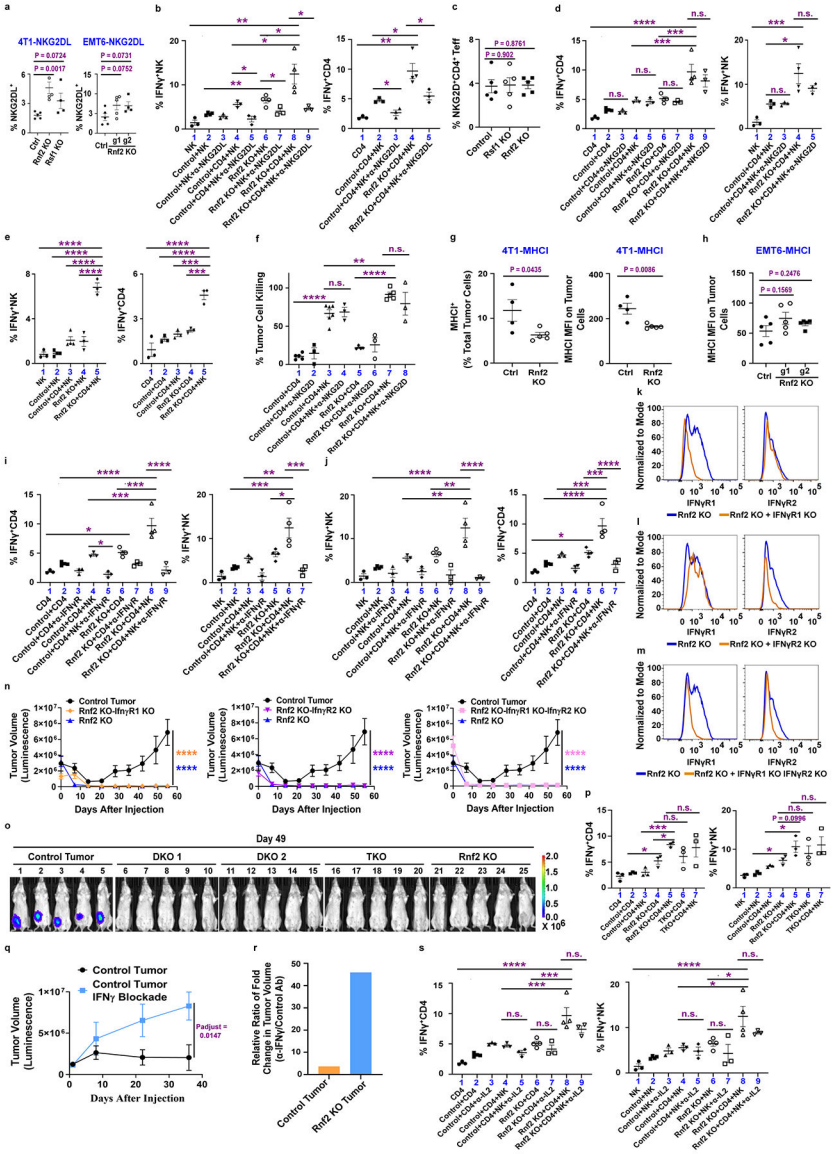

Extended Data Fig. 5. Tumoral NKG2DL and NK/CD4+ T cell-expressed IFNγR are required for the activation of these immune cells by *Rnf2* KO tumors.

a. The frequencies of NKG2DL^{+}CD45^{-} tumor cells isolated from Ctrl/*Rnf2* KO/*Rsf1* KO 4T1 tumors (Left, n = 5 mice for Ctrl, n = 4 mice for *Rnf2* KO and *Rsf1* KO, each mouse harboring one tumor) or EMT6 tumors (Right, n = 5 mice for Ctrl and *Rnf2* KO g1, n = 4 mice for *Rnf2* KO g2, each mouse harboring one tumor) at day 7 post-implantation. Symbols, individual mouse (bars, mean ± SEM).

b. Tumor cells (CD45^{-}) were isolated and enriched from indicated tumors, co-cultured with NK/CD4^{+} T-cells/both. The coculture setup is similar to that described in Fig. 3c. Anti-NKG2DL/control antibody was added into the co-culture. Each group has 3/4 replicates of co-culture. Tumor cells (Ctrl/*Rnf2* KO) in each replicate of co-culture were pooled from 2-3 tumors from 2-3 mice (each mouse harboring one tumor). Frequencies of IFNγ^{+}NK cells (**Left**) or IFNγ^{+}CD4^{+} T-cells (**Right**) are shown as mean ± SEM of triplicates.

c. Frequencies of intratumoral NKG2D$^+$ cells of CD4$^+$ T effector cells of control, *Rnf2* KO and *Rsf1* KO 4T1 tumors at day 7 post-implantation. Symbols, individual mouse (bars, mean ± SEM). n = 5 mice/group, each mouse harboring one tumor.

d. *In vitro* co-culture experiment was set up as that shown in panel **b**, except the addition of anti-NKG2DL antibody. Instead, CD4$^+$ T-cells were pre-incubated with anti-NKG2D antibody for 30 min before being added into the co-culture. Each group has 3/4 replicates of co-culture. Tumor cells (Ctrl/*Rnf2* KO) in each replicate of co-culture were pooled from 2-3 tumors from 2-3 mice (each mouse harboring one tumor). Frequencies of IFNγ^+CD4$^+$ T-cells (**Left**) or IFNγ^+NK cells (**Right**) are shown as mean ± SEM of triplicates.

e. Tumor cells (GFP$^+$) were isolated and enriched by FACS for GFP positive populations from indicated 4T1 tumors in mice. They were co-cultured with NK/CD4$^+$ T cells/both. The coculture setup is similar to that described in Fig. 3c. Each group has 3/4 replicates of co-culture. Tumor cells (Ctrl/Rnf2 KO) in each replicate of co-culture were pooled from 2-3 tumors from 2-3 mice (each mouse harboring one tumor). Frequencies of IFNγ^+NK cells (**Left**) or IFNγ^+CD4$^+$ T cells (**Right**) are shown as mean ± SEM of triplicates.

f. Tumor cells (CD45$^-$) were enriched from indicated 4T1 tumors in mice and co-cultured with pre-activated NK/CD4$^+$ T-cells/both. CD4$^+$ T-cells were pre-incubated with anti-NKG2D antibody for 30 min before being added into the co-culture. The coculture setup is similar to that described in Fig. 3e. Each group has 3/4/5/6 replicates of co-culture. Tumor cells (Ctrl/Rnf2 KO) in each replicate of co-culture were pooled from 2-3 tumors from 2-3 mice (each mouse harboring one tumor). The percent tumor killing is shown as mean ± SEM of triplicates.

g-h. The frequencies of MHCI$^+$CD45$^-$ tumor cells and/or the MFI of MHCI expression on CD45$^-$ tumor cells isolated from control (Ctrl)/*Rnf2* KO cells of 4T1 tumors (**g**, n = 4 mice for Ctrl, n = 5 mice for *Rnf2* KO, each mouse harboring one tumor) or EMT6 tumors (**h**, n = 5/group, each mouse harboring one tumor) at day 7 post-implantation. Symbols depict individual mouse (bars, mean ± SEM).

i-j. Tumor cells (CD45$^-$) were enriched from indicated 4T1 tumors in mice, co-cultured with NK/CD4$^+$ T-cells/both. The coculture setup is similar to that described in Fig. 3c. CD4$^+$ T-cells (**i**) or NK cells (**j**) were pre-incubated with anti-IFNγ receptor (IFNγR) antibody (GR-20) for 30 min before being added into the co-culture. Each group has 3/4 replicates of co-culture. Tumor cells (Ctrl/*Rnf2* KO) in each replicate of co-culture were pooled from 2-3 tumors from 2-3 mice (each mouse harboring one tumor). Frequencies of IFNγ^+CD4$^+$ T-cells or IFNγ^+NK cells are shown as mean ± SEM of triplicates.

k-m. Expression levels of *IFNγR1* and *IFNγR2* in *Rnf2* KO plus *IFNγR1* KO (DKO1) (k), *Rnf2* KO plus *IFNγR2* KO (DKO2) (l), and *Rnf2* KO plus *IFNγR1* KO and *IFNγR2* KO (TKO) (m) 4T1 cells, measured by Flowcytometry (Histogram), which represents two independent experiments.

n-o. n. The volumes (**n**) and representative BLIs at day 49 (**o**) of indicated 4T1 tumors in BALB/c mice. Mean ± SEM (n = 5 mice/group, each mouse harboring one tumor). DKO 1: *Rnf2* KO + *IFNγR1* KO; DKO 2: *Rnf2* KO + *IFNγR2* KO. TKO: *Rnf2* KO + *IFNγR1* KO + *IFNγR2* KO. ****, control tumor vs. *Rnf2* KO + *IFNγR1* KO tumor; ****, control tumor vs. *Rnf2* KO + *IFNγR2* KO tumor; ****, control tumor vs. *Rnf2* KO + *IFNγR1* KO + *IFNγR2* KO tumor; ****, control tumor vs. *Rnf2* KO tumor.

p. Tumor cells ($CD45^-$) were enriched from indicated tumors in mice, co-cultured with NK/$CD4^+$ T-cells/both. The coculture setup is similar to that described in Fig. 3c. Each group has 3 replicates of co-culture. Tumor cells (Ctrl/*Rnf2* KO) in each replicate of co-culture were pooled from 2-3 tumors from 2-3 mice (each mouse harboring one tumor). Frequencies of IFNγ^+CD4^+ T-cells (**Left**) or IFNγ^+NK cells (**Right**) are shown as mean ± SEM of triplicates.

q-r. q. The volumes of control 4T1 tumors in BALB/c mice treated with control/anti-IFNγ antibody at day 2, 5 post-implantation. Mean ± SEM (n = 5 mice/group, each mouse harboring one tumor).

r. The relative ratio of the fold changes in the tumor volumes (=Average of Fold Changes in tumor volumes of the group of anti-IFNγ divided by Average of Fold Changes in tumor volumes of the group of Control antibody) in control 4T1 tumors (panel **q**) or *Rnf2* KO tumors (shown in Fig. 3h) at the end of the study. n = 5 mice for Ctrl Tumor treated with Ctrl Antibody; n = 4 mice for Ctrl Tumor treated with IFNγ Antibody; n = 4 mice for *Rnf2* KO treated with Ctrl Antibody; n = 5 mice for *Rnf2* KO treated with IFNγ Antibody. Each mouse harbored one tumor.

s. Tumor cells ($CD45^-$) were enriched from indicated 4T1 tumors in mice, co-cultured with NK/$CD4^+$ T-cells/both. The coculture setup is similar to that described in Fig. 3c. Control/anti-IL-2 antibody (JES6-1A12) was supplemented in the co-culture. Each group has 3/4 replicates of co-culture. Tumor cells (Ctrl/*Rnf2* KO) in each replicate of co-culture were pooled from 2-3 tumors from 2-3 mice (each mouse harboring one tumor). Frequencies of IFNγ^+CD4^+ T-cells (**Left**) or IFNγ^+NK cells (**Right**) are shown as mean ± SEM of triplicates.

*p<0.05, **p<0.01, ***p<0.001,****p<0.0001, n.s., not statistically significant (unpaired two-tailed Student's t test in a, b, c, f, g, h, p; one-way ANOVA with Tukey's test in d, e, i, j, s; two-way ANOVA with Tukey's test in n; two-way ANOVA with Sidak's test in q). The full list of p values can be found in the source data for this figure.

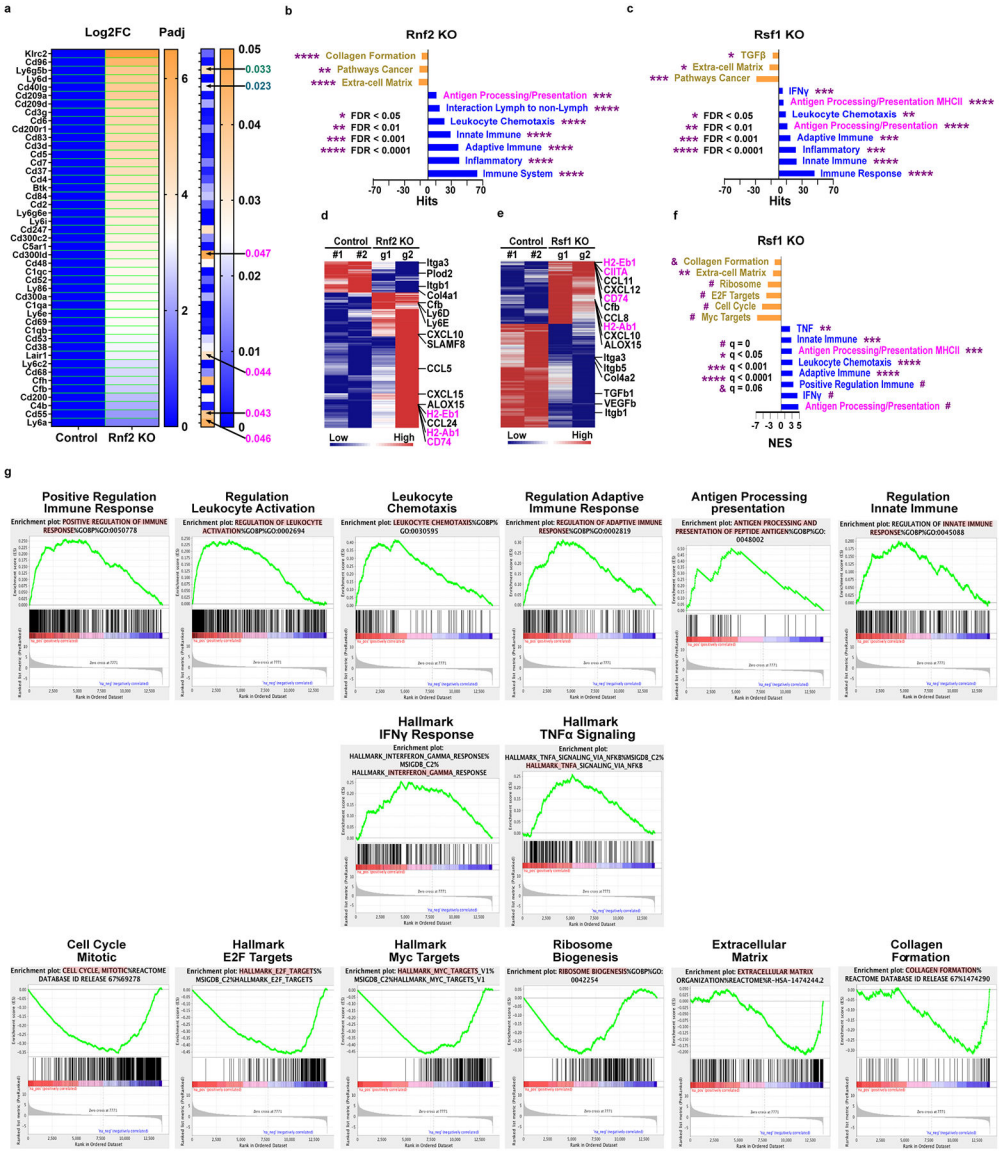

Extended Data Fig. 6. *Rnf2/Rsf1* KO tumors upregulate genes related to immunity.

a. Log2FC (fold change) (**Left**) and adjusted p values (padj) (**Right**) of the upregulated immune cell markers expressed in *Rnf2* KO 4T1 tumor cells (n = 2, two groups of tumor cells, one group of cells was from *Rnf2* KO g1, the other group was from *Rnf2* KO g2, each group of cells were pooled from 25 mice, each mouse harboring one tumor) compared to those in control tumor cells (n = 2, two groups of cells, each group of cells pooled from 25 mice, each mouse harboring one tumor) isolated and sorted from *in vivo* tumors at day 7 post-implantation followed by RNAseq analysis, as in Fig. 4a.

b-e. Analysis of differentially expressed genes revealed in RNAseq of FACS-sorted *Rnf2* KO 4T1 tumor cells (as described in panel **a**) (n = 2, two groups of cells, one group of cells was from *Rnf2* KO g1, the other group was from *Rnf2* KO g2, each group of cells pooled from 25 mice) (**b**), or *Rsf1* KO 4T1 tumor cells (similar to that described in panel **a**) (n = 2, two groups of cells, one group of cells was from *Rsf1* KO g1, the other group was from

Rsf1 KO g2, each group of cells pooled from 25 mice) (**c**) compared to control 4T1 tumors cells (n = 2, two groups of cells, each group of cells pooled from 25 mice, each mouse harboring one tumor) isolated from *in vivo* tumors at day 7 post-tumor implantation, using Network Analyst. The representative enriched gene sets with FDR q values are shown (**b**, **c**). Heatmaps display these DEGs and representative genes related to immunity are noted (**d**, **e**).
f. GSEA analysis of differentially expressed genes (DEGs) revealed in RNAseq of FACS-sorted *Rsf1* KO 4T1 tumor cells (as described in panel **c**) (n = 2, *Rsf1* KO g1 and g2, two groups of cells, each group of cells pooled from 25 mice) compared to control 4T1 tumors cells (n = 2, two groups of cells, each group of cells pooled from 25 mice)isolated from corresponding tumors implanted in mice at day 7 post-tumor implantation. The representative enriched gene sets with FDR q values are shown.
g. Representative GSEA Enrichment plots (score curves) of DEGs determined by RNAseq in *Rnf2* KO compared to control tumors. GSEA analysis of DEGs revealed in RNAseq of 4T1 tumors is performed as in Fig. 4a. The representative Enrichment plots of positively or negatively regulated genes in *Rnf2* KO tumor cells compared to control tumor cells are shown.

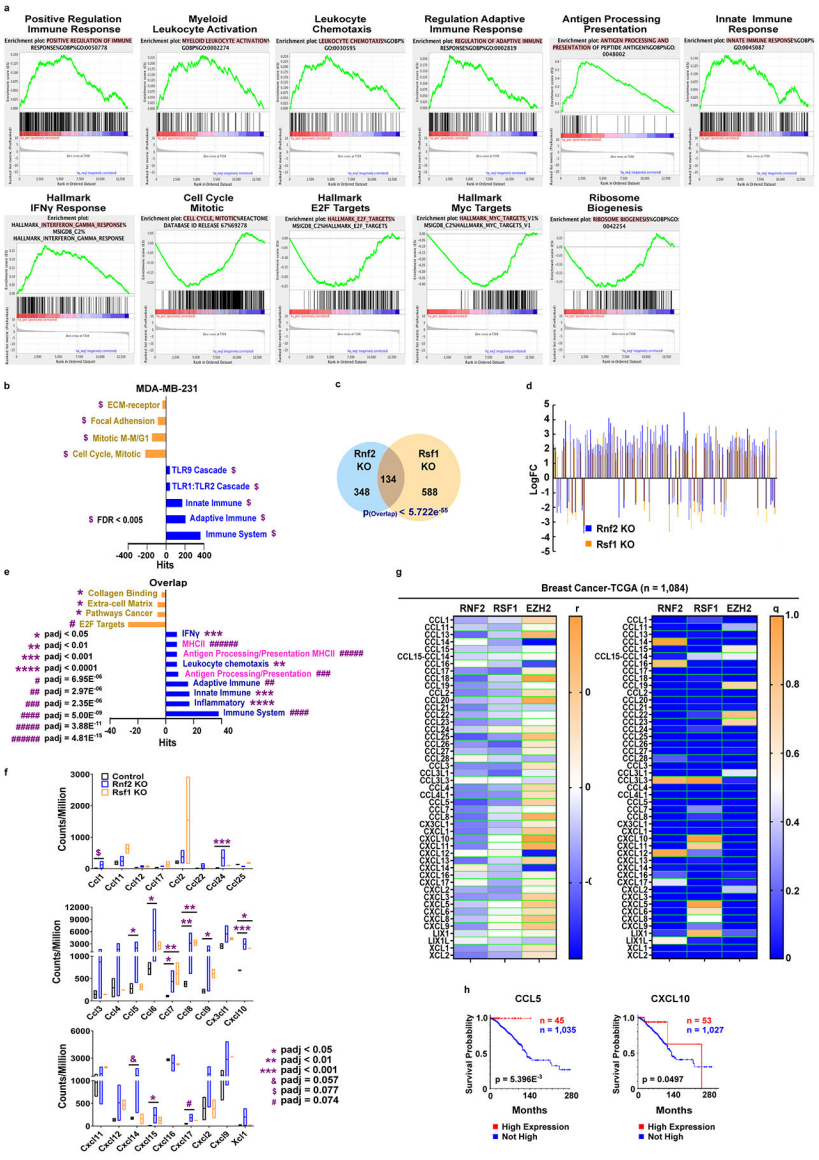

Extended Data Fig. 7. Rsf1 regulates expression of an overlapping group of immune-related genes with Rnf2.

a. Representative GSEA Enrichment plots (score curves) of DEGs in *Rsf1* KO compared to control tumors. GSEA analysis of DEGs revealed in RNAseq of 4T1 tumors is performed as in Extended-Fig. 6f. The representative Enrichment plots are shown.

b. Analysis of DEGs revealed in a published RNAseq of control siRNA- compared to *RNF2* siRNA-treated human TNBC cell line MDA-MB-231 (log2FC≥ 1 and log2FC≤ −1) using Network Analyst. The representative enriched gene sets with FDR q values are shown.

c. The overlap of DEGs in *Rnf2* KO and *Rsf1* KO 4T1 tumor cells compared to control 4T1 tumors cells, which were isolated by FACS from *in vivo* tumors. DEGs are determined and described in Fig. 4a and Extended-Fig. 6f. P value of overlap is calculated using web tool SSOTGNB (http://nemates.org/MA/progs/overlap_stats.html), similar to that described in Fig. 5c.

d. The log2FC (Fold Change) of overlapping DEGs in *Rnf2* KO tumors and *Rsf1* KO tumors. DEGs are determined and described in Fig. 4a and Extended-Fig. 6f.
e. g:Profiler analysis of the 134 overlapped DEGs in panel c. The adjust p value (padj) is indicated (one-tailed hypergeometric test with adjustment for multiple comparisons).
f. A floating bars graph (min, max and line at mean) depicts the counts of genes encoding chemokines revealed in RNAseq of FACS-sorted tumors cells, as in Fig. 4a and Extended Fig. 6f. These *Rnf2* KO (n = 2, two groups of cells, one group was from *Rnf2* KO g1, the other group was from *Rnf2* KO g2, each group of cells pooled from 25 mice, each mouse harboring one tumor), *Rsf1* KO (n = 2, two groups of cells, one group was from *Rsf1* KO g1, the other group was from *Rsf1* KO g2, each group of cells pooled from 25 mice, each mouse harboring one tumor) and control (n = 2, two groups of cells, each group of cells pooled from 25 mice, each mouse harboring one tumor) 4T1 tumors cells were isolated by FACS from corresponding *in vivo* tumors. The adjust p values (padj) are determined by the two-tailed Wald test and can be found in the source data for this figure.
g. The correlations of expressions of *RNF2*, *RSF1* or *EZH2* to the levels of human chemokine genes were analyzed using the RNAseq data extracted from invasive breast cancer TCGA dataset. Heatmaps show the correlation coefficients (**Left**) and q values of each correlation (**Right**). n = 1,084 BRCA patients.
h. The correlations of the chemokine gene *CCL5* or *CXCL10* to the overall survival of invasive breast cancer patients, extracted from the TCGA dataset via cBioPortal. High expression is defined as the expression levels greater than 2 SD above the mean. P values are generated using two-tailed LogRank test. Numbers (n) of BRCA patients with (**red** color)/without (**blue** color) high expression of CCL5 (**left**)/CXCL10 (**right**) are indicated.

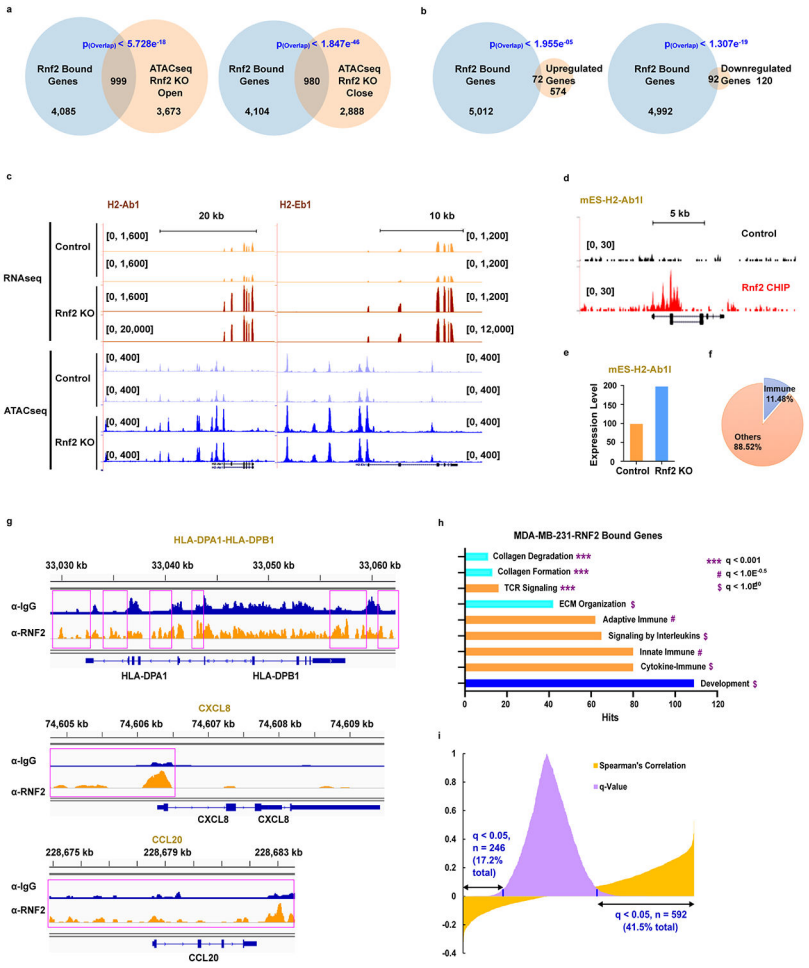

Extended Data Fig. 8. Rnf2 binds to immune related genes in mouse and human breast cancer cells.

a-b. The overlap of Rnf2 target genes in cultured 4T1 cells determined by Rnf2 CHIPseq with genes displaying significantly more/less accessible chromatin sites in *Rnf2* KO 4T1 tumors determined by ATACseq as in Fig. 5a (**a**) or with DEGs (determined by RNAseq shown in Fig. 4a) in *Rnf2* KO 4T1 tumors (compared to control 4T1 tumors) (**b**). P values of the overlap are calculated using web tool SSOTGNB (http://nemates.org/MA/progs/overlap_stats.html), similar to that described in Fig. 5c.

c-d. Screenshots of genes *H2-Ab1* and *H2-Eb1* in both control and *Rnf2* KO 4T1 tumor cells obtained from RNAseq (determined and described in Fig. 4a) and ATACseq (determined and described in Fig. 5a) (**c**) or of gene H2-Ab1 in mouse embryonic stem cells (mES) obtained by reanalyzing published datasets of Rnf2 CHIPseq (GSE34520) (**d**).

e. Expression level of gene *H2-Ab1* in control and *Rnf2* KO mES cells obtained by reanalyzing published dataset of RNA microarray (GSE10573).

f. Genes occupied by RNF2 were identified by CHIPseq analysis of human TNBC cell line MDA-MB-231 using anti-RNF2 antibody compared to Input (GSE107176).

g. Integrative genomics viewer (IGV) screenshots of Input or RNF2 ChIPseq (as in panel **f**) tracks (scale bar, 40) of *HLA-DPA1*, *HLA-DPB1*, *CCL20* and *CXCL8*.

h. GSEA analysis (REACTOME) of genes occupied by RNF2 revealed in published CHIPseq of human TNBC cell line MDA-MB-231 using anti-RNF2 antibody compared to Input (as in panel **f**). The representative enriched pathways with FDR q values are shown. The full list of q values is provided in the Source Data File associated with this panel.
i. The correlations of *RNF2* expression in BRCA patients to the levels of its bound genes that were determined as in panel **f**. The correlation analyses were performed similar to that described in Fig. 5h. The expression levels of these RNF2 bound genes and of *RNF2* were extracted from the invasive breast cancer TCGA dataset. The coefficient (yellow) and q value (purple) of each correlation are indicated at the y-axis (two-tailed Spearman correlation analysis). The number (n) of RNF2 bound genes with FDR q values (indicative of the significance of the correlations of these genes to *RNF2* expression) < 0.05, and the percentages of these genes (q < 0.05) among the total RNF2 bound genes are noted in blue. The blue vertical bars mark the q value at 0.05. Totally 1,070 BRCA patient samples were included.

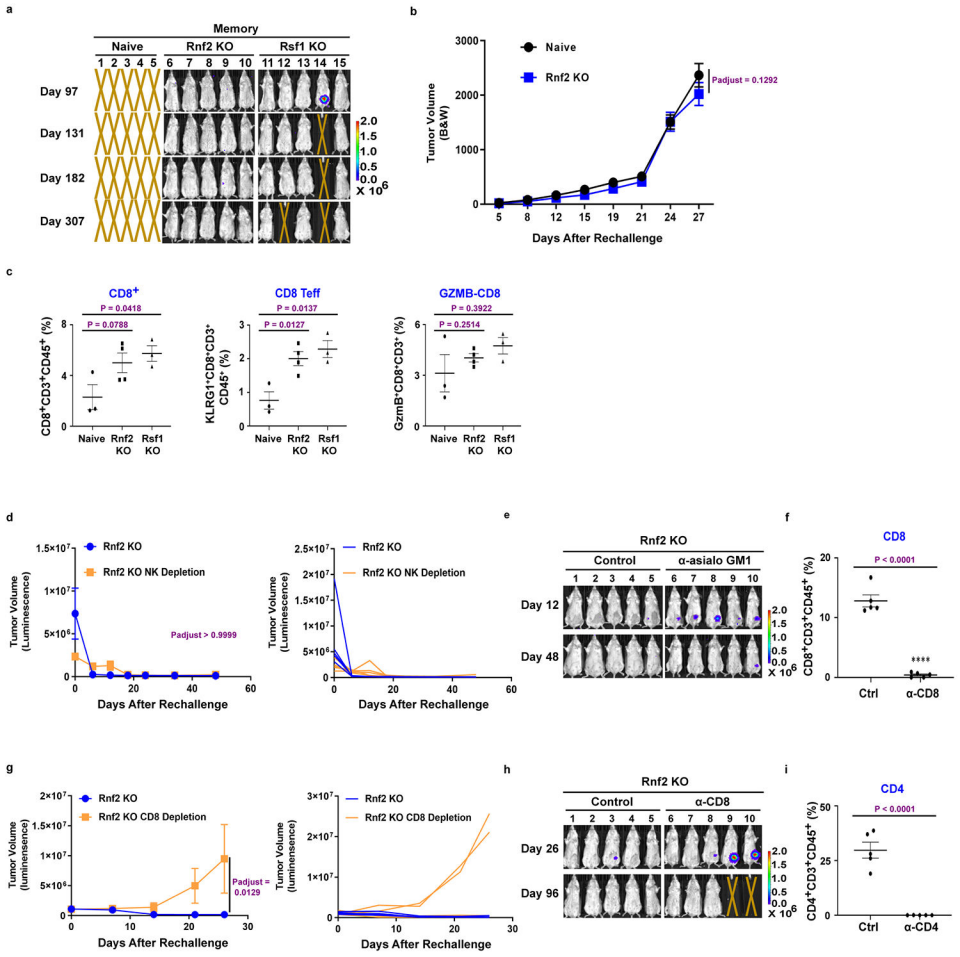

Extended Data Fig. 9. Ablation of Rnf2/Rsf1 induces anti-tumor memory response.
a. BALB/c mice were inoculated with *Rnf2* KO 4T1 tumors (*Rnf2* KO g2) or *Rsf1* KO 4T1 tumors (*Rsf1* KO g1) in the left 4th mammary pads. At day 45 after the primary tumors were rejected, wildtype 4T1 tumors were implanted into the right 4th mammary pads or naïve

mice. n = 5 mice /group, each mouse harboring one tumor. Representative BLIs of wildtype 4T1 tumors at days 97, 131, 182 and 307 after the 2nd challenge are shown. X, mice were sacrificed because of the big tumor burdens at the day when images were taken.

b. BALB/c mice were inoculated with *Rnf2* KO 4T1 tumors (*Rnf2* KO g2) in the left 4th mammary pads. At day 45 after the *Rnf2* KO tumors were rejected, TSA tumors were implanted into the right 4th mammary pads or naïve mice. The tumor volumes were measured by caliper (mean ± SEM, n = 5 mice for naïve, n=4 mice for *Rnf2* KO, each mouse harboring one tumor).

c. Frequencies of intratumoral indicated immune cells in wildtype 4T1 tumors at day 7 after the 2nd challenge, measured similar to that described in Fig. 8e. Symbols, individual mouse (bars, mean ± SEM). n = 3 mice for naïve and *Rsf1* KO, n = 4 mice for *Rnf2* KO, each mouse harboring one tumor.

d-e. Mice were inoculated with *Rnf2* KO 4T1 tumors and re-challenged with wildtype 4T1 tumors on the contralateral, as in panel **a** and Fig. 8a. α-asialo GM1 antibody was injected at days −1, +1, +4 relative to the 2nd challenge. **d**. Volumes (**Left**, luminescence intensities, mean ± SEM, n = 5 mice/group, each mouse harboring one tumor; **Right**, individual mouse) of wildtype 4T1 tumors. **e**. Representative BLIs of wildtype 4T1 tumors at indicated days after the 2nd challenge.

f. Frequencies of peripheral blood CD8^{+} T-cells in *Rnf2* KO mice at day 10 after injection of anti-CD8 (2.43) or control antibody. Symbols, individual mouse (bars, mean ± SEM). n = 5 mice/group, each mouse harboring one tumor.

g-h. **g**. Mice were inoculated with *Rnf2* KO 4T1 tumors (*Rnf2* KO g2) and re-challenged with wildtype 4T1 tumors on the contralateral, as in panel **a** and Fig. 8a. Anti-CD8 or control antibody was injected at days −1 and +1 relative to the 2nd challenge. **g**. Volumes (**Left**, luminescence intensities, mean ± SEM, n = 5 mice/group, each mouse harboring one tumor; **Right**, individual mouse) of wildtype 4T1 tumors. **h**. Representative BLIs of wildtype 4T1 tumors at day 26 or day 96 after the 2nd challenge.

i. Frequencies of peripheral blood CD4^{+} T-cells in *Rnf2* KO mice at day 10 after injection of anti-CD4 (GK1.5) or control antibody. Symbols, anti-tumor memory response. individual mouse (bars, mean ± SEM). n = 5 mice/group, each mouse harboring one tumor.

Unpaired two-tailed Student’s t test in c, f, i; two-way ANOVA with Sidak’s test in b, d, g.

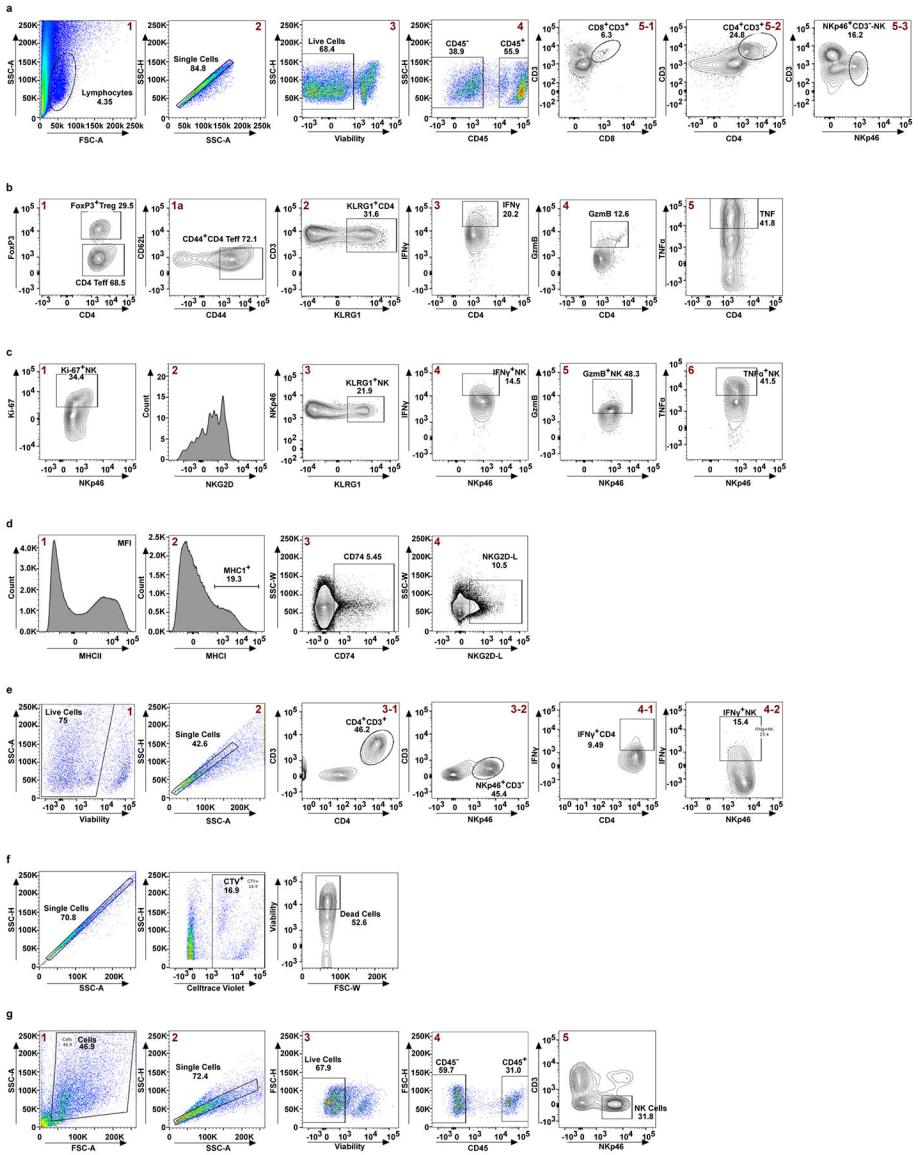

Extended Data Fig. 10. Gating Strategy used for flow cytometry.

a. Gating Strategy used for analysis of immune cells from tumors isolated from tumor-bearing mice presented on Fig. 2a-e, Fig. 3a-b, Fig. 4c, Fig. 7e, Fig. 8e, Extended Fig. 3v, Extended Fig. 5a,c,g-h, Extended Fig. 9c.

b. Gating Strategy used for analysis of each subset of CD4+ T-cells in a (5-2).

c. Gating Strategy used for analysis of each subset or marker of NK cells in a (5-3).

d. Gating Strategy used for analysis of each subset or marker of CD45–tumor cells in a.

e. Gating Strategy used for analysis of CD4+ T-cells or NK cells from the in vitro co-culture assays presented on Fig. 3c-d, f-g, Fig. 4j-k, Extended Fig. 5b, d-e, Extended Fig. 5i-j, p, s.

f. Gating Strategy used for analysis of dead tumors in the in vitro killing assays presented on Fig. 3e, Fig 4l, Extended Fig. 5f.

g. Gating Strategy used for sorting of tumor cells (CD45–) and NK cells (CD45+NKp46+CD3−) for RNA-Seq and ATAC-Seq presented on Fig. 4a-b, Fig. 5a-f, Fig. 6, Fig. 7f-j, Extended Fig. 4c-d, Extended Fig. 6, Extended Fig. 7a, c-f, Extended Fig. 8a-c.

Supplementary Material

Refer to Web version on PubMed Central for supplementary material.

Acknowledgments

We thank Drs. Lewis Zhichang Shi, and Hengbin Wang for helpful discussion on this project. We are grateful to Drs. Hongxing Shen and Suresh Bugide for the technical assistance. We also thank Vidya Sagar Hanumanthu and the UAB Comprehensive Flow Cytometry Core for their assistance with FACS analysis and cell sorting. Eddy S Yang is a ROAR Southeast Cancer Foundation Endowed Chair. This work was supported by grants from Autotech LLC (to E.S.Y.), from Breast Cancer Research Foundation of Alabama (to E.S.Y.), from American Association for Cancer Research/Triple Negative Breast Cancer Foundation (15-20-43-YANG) (to E.S.Y.), from the Start-up funds from the University of Alabama at Birmingham (to J.W.L.). J.W.L. is also supported by the DoD PRCRP Career Award (W81XWH-18-1-0315) and NIH R01AI148711. N.W. is supported by the DoD grant W81XWH-19-1-0084.

References

1. Leach DR, Krummel MF & Allison JP Enhancement of antitumor immunity by CTLA-4 blockade. Science 271, 1734–1736, doi:10.1126/science.271.5256.1734 (1996). [PubMed: 8596936]
2. Patel SA & Minn AJ Combination Cancer Therapy with Immune Checkpoint Blockade: Mechanisms and Strategies. Immunity 48, 417–433, doi:10.1016/j.immuni.2018.03.007 (2018). [PubMed: 29562193]
3. Frankel T, Lanfranca MP & Zou W The Role of Tumor Microenvironment in Cancer Immunotherapy. Adv Exp Med Biol 1036, 51–64, doi:10.1007/978-3-319-67577-0_4 (2017). [PubMed: 29275464]
4. Benci JL et al. Opposing Functions of Interferon Coordinate Adaptive and Innate Immune Responses to Cancer Immune Checkpoint Blockade. Cell 178, 933–948 e914, doi:10.1016/j.cell.2019.07.019 (2019). [PubMed: 31398344]
5. Hegde PS & Chen DS Top 10 Challenges in Cancer Immunotherapy. Immunity 52, 17–35, doi:10.1016/j.immuni.2019.12.011 (2020). [PubMed: 31940268]
6. Yu J et al. Liver metastasis restrains immunotherapy efficacy via macrophage-mediated T cell elimination. Nat Med, doi:10.1038/s41591-020-1131-x (2021).
7. Kalbasi A & Ribas A Tumour-intrinsic resistance to immune checkpoint blockade. Nat Rev Immunol 20, 25–39, doi:10.1038/s41577-019-0218-4 (2020). [PubMed: 31570880]
8. Bian Y et al. Cancer SLC43A2 alters T cell methionine metabolism and histone methylation. Nature 585, 277–282, doi:10.1038/s41586-020-2682-1 (2020). [PubMed: 32879489]
9. Sanmamed MF & Chen L A Paradigm Shift in Cancer Immunotherapy: From Enhancement to Normalization. Cell 175, 313–326, doi:10.1016/j.cell.2018.09.035 (2018). [PubMed: 30290139]
10. Sheng W et al. LSD1 Ablation Stimulates Anti-tumor Immunity and Enables Checkpoint Blockade. Cell 174, 549–563 e519, doi:10.1016/j.cell.2018.05.052 (2018). [PubMed: 29937226]
11. Pan D et al. A major chromatin regulator determines resistance of tumor cells to T cell-mediated killing. Science 359, 770–775, doi:10.1126/science.aao1710 (2018). [PubMed: 29301958]
12. Adeegbe DO et al. Synergistic Immunostimulatory Effects and Therapeutic Benefit of Combined Histone Deacetylase and Bromodomain Inhibition in Non-Small Cell Lung Cancer. Cancer Discov 7, 852–867, doi:10.1158/2159-8290.CD-16-1020 (2017). [PubMed: 28408401]
13. Li F et al. In Vivo Epigenetic CRISPR Screen Identifies Asf1a as an Immunotherapeutic Target in Kras-Mutant Lung Adenocarcinoma. Cancer Discov 10, 270–287, doi:10.1158/2159-8290.CD-19-0780 (2020). [PubMed: 31744829]
14. Peng D et al. Epigenetic silencing of TH1-type chemokines shapes tumour immunity and immunotherapy. Nature 527, 249–253, doi:10.1038/nature15520 (2015). [PubMed: 26503055]

15. Li J et al. Epigenetic driver mutations in ARID1A shape cancer immune phenotype and immunotherapy. J Clin Invest 130, 2712–2726, doi:10.1172/JCI134402 (2020). [PubMed: 32027624]
16. Burr ML et al. An Evolutionarily Conserved Function of Polycomb Silences the MHC Class I Antigen Presentation Pathway and Enables Immune Evasion in Cancer. Cancer Cell 36, 385–401 e388, doi:10.1016/j.ccell.2019.08.008 (2019). [PubMed: 31564637]
17. Su W et al. The Polycomb Repressor Complex 1 Drives Double-Negative Prostate Cancer Metastasis by Coordinating Stemness and Immune Suppression. Cancer Cell 36, 139–155 e110, doi:10.1016/j.ccell.2019.06.009 (2019). [PubMed: 31327655]
18. Connolly RM et al. Combination Epigenetic Therapy in Advanced Breast Cancer with 5-Azacitidine and Entinostat: A Phase II National Cancer Institute/Stand Up to Cancer Study. Clin Cancer Res 23, 2691–2701, doi:10.1158/1078-0432.CCR-16-1729 (2017). [PubMed: 27979916]
19. Jerby-Arnon L et al. A Cancer Cell Program Promotes T Cell Exclusion and Resistance to Checkpoint Blockade. Cell 175, 984–997 e924, doi:10.1016/j.cell.2018.09.006 (2018). [PubMed: 30388455]
20. Piunti A & Shilatifard A Epigenetic balance of gene expression by Polycomb and COMPASS families. Science 352, aad9780, doi:10.1126/science.aad9780 (2016). [PubMed: 27257261]
21. Rai K et al. Dual Roles of RNF2 in Melanoma Progression. Cancer Discov 5, 1314–1327, doi:10.1158/2159-8290.CD-15-0493 (2015). [PubMed: 26450788]
22. Chan HL et al. Polycomb complexes associate with enhancers and promote oncogenic transcriptional programs in cancer through multiple mechanisms. Nat Commun 9, 3377, doi:10.1038/s41467-018-05728-x (2018). [PubMed: 30139998]
23. Zhang Y et al. Estrogen induces dynamic ERalpha and RING1B recruitment to control gene and enhancer activities in luminal breast cancer. Sci Adv 6, eaaz7249, doi:10.1126/sciadv.aaz7249 (2020). [PubMed: 32548262]
24. Laugesen A & Helin K Chromatin repressive complexes in stem cells, development, and cancer. Cell Stem Cell 14, 735–751, doi:10.1016/j.stem.2014.05.006 (2014). [PubMed: 24905164]
25. Piunti A & Shilatifard A The roles of Polycomb repressive complexes in mammalian development and cancer. Nat Rev Mol Cell Biol 22, 326–345, doi:10.1038/s41580-021-00341-1 (2021). [PubMed: 33723438]
26. Adams S et al. Current Landscape of Immunotherapy in Breast Cancer: A Review. JAMA Oncol, doi:10.1001/jamaoncol.2018.7147 (2019).
27. Zhang Z et al. Role of remodeling and spacing factor 1 in histone H2A ubiquitination-mediated gene silencing. Proc Natl Acad Sci U S A 114, E7949–E7958, doi:10.1073/pnas.1711158114 (2017). [PubMed: 28855339]
28. Mootha VK et al. PGC-1alpha-responsive genes involved in oxidative phosphorylation are coordinately downregulated in human diabetes. Nat Genet 34, 267–273, doi:10.1038/ng1180 (2003). [PubMed: 12808457]
29. Rooney MS, Shukla SA, Wu CJ, Getz G & Hacohen N Molecular and genetic properties of tumors associated with local immune cytolytic activity. Cell 160, 48–61, doi:10.1016/j.cell.2014.12.033 (2015). [PubMed: 25594174]
30. Cai G, Yang Q & Sun W RSF1 in cancer: interactions and functions. Cancer Cell Int 21, 315, doi:10.1186/s12935-021-02012-9 (2021). [PubMed: 34147108]
31. Wu J et al. The oncogenic impact of RNF2 on cell proliferation, invasion and migration through EMT on mammary carcinoma. Pathol Res Pract 215, 152523, doi:10.1016/j.prp.2019.152523 (2019). [PubMed: 31300294]
32. Barger CJ, Branick C, Chee L & Karpf AR Pan-Cancer Analyses Reveal Genomic Features of FOXM1 Overexpression in Cancer. Cancers (Basel) 11, doi:10.3390/cancers11020251 (2019).
33. Shabason JE & Minn AJ Radiation and Immune Checkpoint Blockade: From Bench to Clinic. Semin Radiat Oncol 27, 289–298, doi:10.1016/j.semradonc.2017.03.002 (2017). [PubMed: 28577836]
34. Wang W et al. CD8(+) T cells regulate tumour ferroptosis during cancer immunotherapy. Nature 569, 270–274, doi:10.1038/s41586-019-1170-y (2019). [PubMed: 31043744]

35. Babic M et al. NK cell receptor NKG2D enforces proinflammatory features and pathogenicity of Th1 and Th17 cells. J Exp Med 217, doi:10.1084/jem.20190133 (2020).
36. Borst J, Ahrends T, Babala N, Melief CJM & Kastenmuller W CD4(+) T cell help in cancer immunology and immunotherapy. Nat Rev Immunol 18, 635–647, doi:10.1038/s41577-018-0044-0 (2018). [PubMed: 30057419]
37. Minn AJ Interferons and the Immunogenic Effects of Cancer Therapy. Trends Immunol 36, 725–737, doi:10.1016/j.it.2015.09.007 (2015). [PubMed: 26604042]
38. Feng M et al. Phagocytosis checkpoints as new targets for cancer immunotherapy. Nat Rev Cancer 19, 568–586, doi:10.1038/s41568-019-0183-z (2019). [PubMed: 31462760]
39. Ross SH & Cantrell DA Signaling and Function of Interleukin-2 in T Lymphocytes. Annu Rev Immunol 36, 411–433, doi:10.1146/annurev-immunol-042617-053352 (2018). [PubMed: 29677473]
40. Xia J, Gill EE & Hancock RE NetworkAnalyst for statistical, visual and network-based meta-analysis of gene expression data. Nature protocols 10, 823–844, doi:10.1038/nprot.2015.052 (2015). [PubMed: 25950236]
41. Klusmann I et al. Chromatin modifiers Mdm2 and RNF2 prevent RNA:DNA hybrids that impair DNA replication. Proc Natl Acad Sci U S A 115, E11311–E11320, doi:10.1073/pnas.1809592115 (2018). [PubMed: 30413623]
42. Lee HS et al. The chromatin remodeler RSF1 controls centromeric histone modifications to coordinate chromosome segregation. Nat Commun 9, 3848, doi:10.1038/s41467-018-06377-w (2018). [PubMed: 30242288]
43. Forero A et al. Expression of the MHC Class II Pathway in Triple-Negative Breast Cancer Tumor Cells Is Associated with a Good Prognosis and Infiltrating Lymphocytes. Cancer Immunol Res 4, 390–399, doi:10.1158/2326-6066.CIR-15-0243 (2016). [PubMed: 26980599]
44. Morey L & Helin K Polycomb group protein-mediated repression of transcription. Trends Biochem Sci 35, 323–332, doi:10.1016/j.tibs.2010.02.009 (2010). [PubMed: 20346678]
45. Brookes E et al. Polycomb associates genome-wide with a specific RNA polymerase II variant, and regulates metabolic genes in ESCs. Cell Stem Cell 10, 157–170, doi:10.1016/j.stem.2011.12.017 (2012). [PubMed: 22305566]
46. Cohen I et al. PRC1 preserves epidermal tissue integrity independently of PRC2. Genes Dev 33, 55–60, doi:10.1101/gad.319939.118 (2019). [PubMed: 30567998]
47. Endoh M et al. Polycomb group proteins Ring1A/B are functionally linked to the core transcriptional regulatory circuitry to maintain ES cell identity. Development 135, 1513–1524, doi:10.1242/dev.014340 (2008). [PubMed: 18339675]
48. Wang H et al. Role of histone H2A ubiquitination in Polycomb silencing. Nature 431, 873–878, doi:10.1038/nature02985 (2004). [PubMed: 15386022]
49. Yasinska IM et al. The Tim-3-Galectin-9 Pathway and Its Regulatory Mechanisms in Human Breast Cancer. Front Immunol 10, 1594, doi:10.3389/fimmu.2019.01594 (2019). [PubMed: 31354733]
50. Li X et al. Immune profiling of pre- and post-treatment breast cancer tissues from the SWOG S0800 neoadjuvant trial. J Immunother Cancer 7, 88, doi:10.1186/s40425-019-0563-7 (2019). [PubMed: 30967156]
51. Toniolo PA et al. Deregulation of SOCS5 suppresses dendritic cell function in chronic lymphocytic leukemia. Oncotarget 7, 46301–46314, doi:10.18632/oncotarget.10093 (2016). [PubMed: 27317770]
52. Li Q et al. Adoptive transfer of tumor reactive B cells confers host T-cell immunity and tumor regression. Clin Cancer Res 17, 4987–4995, doi:10.1158/1078-0432.CCR-11-0207 (2011). [PubMed: 21690573]
53. Alspach E et al. MHC-II neoantigens shape tumour immunity and response to immunotherapy. Nature 574, 696–701, doi:10.1038/s41586-019-1671-8 (2019). [PubMed: 31645760]
54. Ribas A et al. Association of Pembrolizumab With Tumor Response and Survival Among Patients With Advanced Melanoma. JAMA 315, 1600–1609, doi:10.1001/jama.2016.4059 (2016). [PubMed: 27092830]

55. Hirschhorn-Cymerman D et al. Induction of tumoricidal function in CD4+ T cells is associated with concomitant memory and terminally differentiated phenotype. J Exp Med 209, 2113–2126, doi:10.1084/jem.20120532 (2012). [PubMed: 23008334]

56. Kerdiles Y, Ugolini S & Vivier E T cell regulation of natural killer cells. J Exp Med 210, 1065–1068, doi:10.1084/jem.20130960 (2013). [PubMed: 23733834]

57. Waggoner SN, Cornberg M, Selin LK & Welsh RM Natural killer cells act as rheostats modulating antiviral T cells. Nature 481, 394–398, doi:10.1038/nature10624 (2011). [PubMed: 22101430]

58. Jiao L et al. A partially disordered region connects gene repression and activation functions of EZH2. Proc Natl Acad Sci U S A 117, 16992–17002, doi:10.1073/pnas.1914866117 (2020). [PubMed: 32631994]

59. Boyle S et al. A central role for canonical PRC1 in shaping the 3D nuclear landscape. Genes Dev 34, 931–949, doi:10.1101/gad.336487.120 (2020). [PubMed: 32439634]

60. Illingworth RS et al. The E3 ubiquitin ligase activity of RING1B is not essential for early mouse development. Genes Dev 29, 1897–1902, doi:10.1101/gad.268151.115 (2015). [PubMed: 26385961]

Methods-only references

61. Hanna A et al. Inhibition of Hedgehog signaling reprograms the dysfunctional immune microenvironment in breast cancer. Oncoimmunology 8, 1548241, doi:10.1080/2162402X.2018.1548241 (2019). [PubMed: 30723576]

62. Zabala M et al. Optimization of the Tet-on system to regulate interleukin 12 expression in the liver for the treatment of hepatic tumors. Cancer Res 64, 2799–2804, doi:10.1158/0008-5472.can-03-3061 (2004). [PubMed: 15087396]

63. Li C et al. Novel HDAd/EBV Reprogramming Vector and Highly Efficient Ad/CRISPR-Cas Sickle Cell Disease Gene Correction. Sci Rep 6, 30422, doi:10.1038/srep30422 (2016). [PubMed: 27460639]

64. Zhang Z et al. USP49 deubiquitinates histone H2B and regulates cotranscriptional pre-mRNA splicing. Genes Dev 27, 1581–1595, doi:10.1101/gad.211037.112 (2013). [PubMed: 23824326]

65. Dobin A et al. STAR: ultrafast universal RNA-seq aligner. Bioinformatics 29, 15–21, doi:10.1093/bioinformatics/bts635 (2013). [PubMed: 23104886]

66. Love MI, Huber W & Anders S Moderated estimation of fold change and dispersion for RNA-seq data with DESeq2. Genome Biol 15, 550, doi:10.1186/s13059-014-0550-8 (2014). [PubMed: 25516281]

67. Reimand J et al. Pathway enrichment analysis and visualization of omics data using g:Profiler, GSEA, Cytoscape and EnrichmentMap. Nat Protoc 14, 482–517, doi:10.1038/s41596-018-0103-9 (2019). [PubMed: 30664679]

68. Corces MR et al. An improved ATAC-seq protocol reduces background and enables interrogation of frozen tissues. Nat Methods 14, 959–962, doi:10.1038/nmeth.4396 (2017). [PubMed: 28846090]

69. Li H Aligning sequence reads, clone sequences and assembly contigs with BWA-MEM. arXiv. , 1303.3997 (2013).

70. Zhang Y et al. Model-based analysis of ChIP-Seq (MACS). Genome Biol 9, R137, doi:10.1186/gb-2008-9-9-r137 (2008). [PubMed: 18798982]

71. Ramirez F et al. deepTools2: a next generation web server for deep-sequencing data analysis. Nucleic Acids Res 44, W160–165, doi:10.1093/nar/gkw257 (2016). [PubMed: 27079975]

72. Colaprico A et al. TCGAbiolinks: an R/Bioconductor package for integrative analysis of TCGA data. Nucleic Acids Res 44, e71, doi:10.1093/nar/gkv1507 (2016). [PubMed: 26704973]

73. Robinson MD, McCarthy DJ & Smyth GK edgeR: a Bioconductor package for differential expression analysis of digital gene expression data. Bioinformatics 26, 139–140, doi:10.1093/bioinformatics/btp616 (2010). [PubMed: 19910308]

74. Langmead B & Salzberg SL Fast gapped-read alignment with Bowtie 2. Nat Methods 9, 357–359, doi:10.1038/nmeth.1923 (2012). [PubMed: 22388286]

75. Faust GG & Hall IM SAMBLASTER: fast duplicate marking and structural variant read extraction. Bioinformatics 30, 2503–2505, doi:10.1093/bioinformatics/btu314 (2014). [PubMed: 24812344]

76. Robinson JT et al. Integrative genomics viewer. Nat Biotechnol 29, 24–26, doi:10.1038/nbt.1754 (2011). [PubMed: 21221095]

77. Fabregat A et al. The Reactome Pathway Knowledgebase. Nucleic Acids Res 46, D649–D655, doi:10.1093/nar/gkx1132 (2018). [PubMed: 29145629]

78. Uhlen M et al. Proteomics. Tissue-based map of the human proteome. Science 347, 1260419, doi:10.1126/science.1260419 (2015). [PubMed: 25613900]

79. Ashburner M et al. Gene ontology: tool for the unification of biology. The Gene Ontology Consortium. Nat Genet 25, 25–29, doi:10.1038/75556 (2000). [PubMed: 10802651]

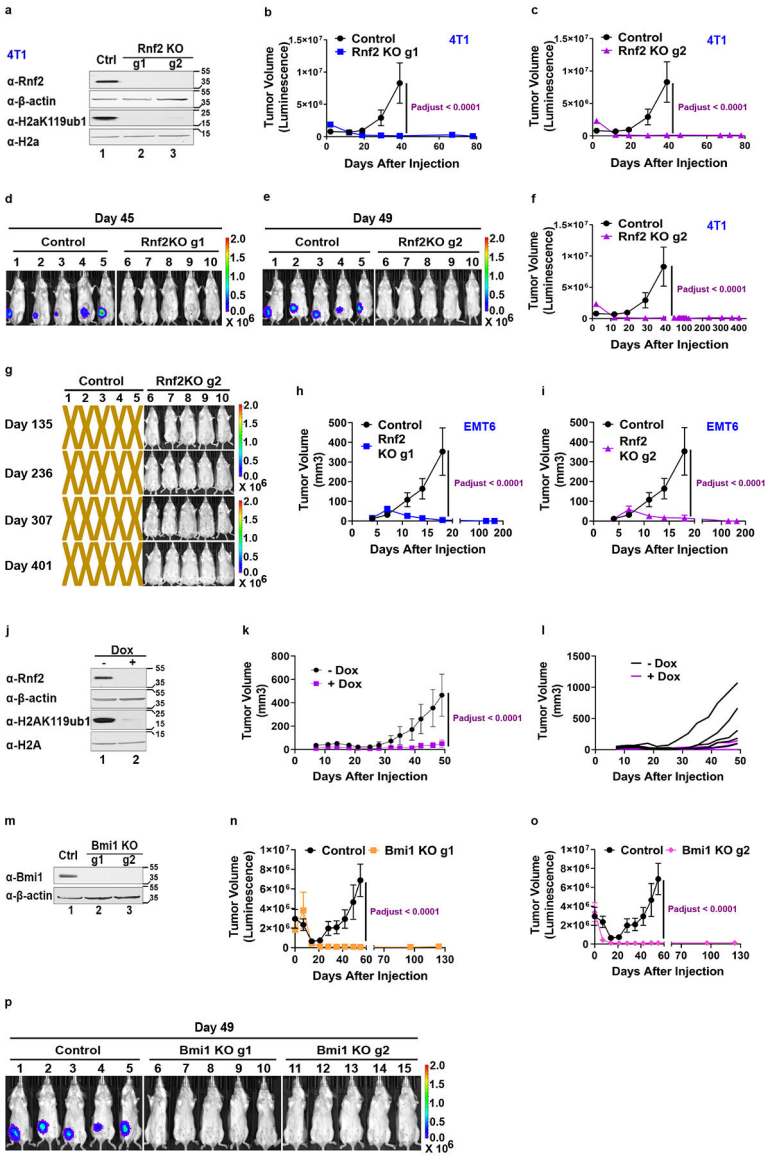

Figure 1. *Rnf2/Bmi1* KO induces durable tumor rejection in syngeneic murine models of breast cancer.

a. Immunoblots show the levels of selected proteins in control (Ctrl) and *Rnf2* KO (two independent guide RNAs (gRNAs), g1 and g2) 4T1 cells, which represents at least 3 independent experiments.

b-e. The volumes (luminescence intensities) of control or *Rnf2* KO 4T1 tumors (two independent gRNAs, g1 (**b**) and g2 (**c**)) implanted into the 4th mammary pads of the syngeneic BALB/c mice. **d, e.** Representative tumor bioluminescence images (BLIs) at indicated days after inoculation. *Rnf2* KO tumor phenotypes were repeated at least three times. Mean ± SEM (n = 5 mice [for Ctrl, *Rnf2* KO g1 and g2 groups, each mouse harbored one tumor).

f-g. The volumes (**f**) (luminescence intensities) and representative tumor BLIs (**g**) at longer time points of panel **c**. Mean ± SEM. n= 5 mice/group, each mouse harbored one tumor. X,

control mice were sacrificed because of the big tumor burdens at the day when images were taken.

h-i. Tumor growth of control and *Rnf2* KO EMT6 tumors (two independent gRNAs, g1 (**h**) and g2 (**i**)) implanted into the 4th mammary pads of the BALB/c mice. Tumor volumes = length X width^2/2. Mean ± SEM (n = 5 mice/group, each mouse harbored one tumor).

j-l. **j**. Immunoblots show the levels of selected proteins in vehicle or doxycycline treated doxycycline inducible *Rnf2* KO 4T1 cells, which represents 2 independent experiments.

k-l. Tumor growth (**k**) of doxycycline inducible *Rnf2* KO 4T1 tumors in immunocompetent BALB/c mice treated with doxycycline or vehicle (treatment started 1 day before tumor cells were injected). Tumor volumes = length X width^2/2. Mean ± SEM (n = 5 mice/group, each mouse harbored one tumor). **i.** Tumor volumes shown in **panel k** were displayed in individual mice.

m-p. **m**. Immunoblots show the levels of selected proteins in Ctrl and *Bmi1* KO (two independent gRNAs, g1 and g2) 4T1 cells, which represents 2 independent experiments with similar results. **n-p.** The volumes (luminescence intensities) of control or *Bmi1* KO 4T1 tumors (induced by two independent gRNAs, g1 (**n**) and g2 (**o**)) implanted into the 4th mammary pads of BALB/c mice. **p.** Representative tumor BLIs at indicated days after inoculation. Mean ± SEM (n = 5 mice/group, each mouse harbored one tumor). Two-way ANOVA with Sidak's test, in b, c, f, h, i, k, n, o.

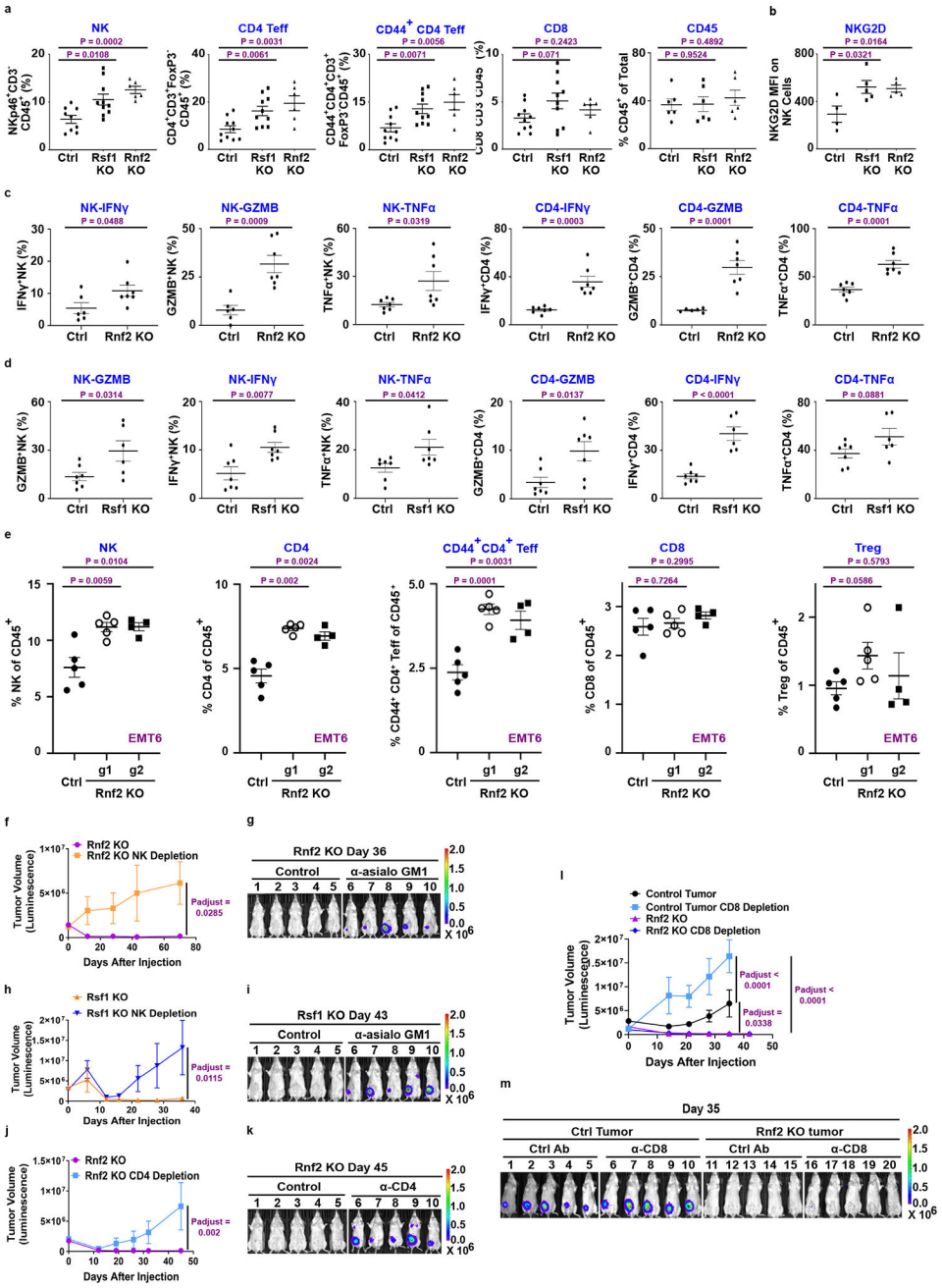

Figure 2. *Rnf2/Rsf1* KO mobilizes NK and CD4$^+$ T-cells.

a. Frequencies of indicated intratumoral immune cells in Ctrl, *Rnf2* KO or *Rsf1* KO 4T1 tumors at day 7 post-implantation. n = 10 mice for ctrl and *Rsf1* KO for the first 4 panels, n=6 mice for *Rsf1* KO in the fifth panel, n = 6 mice for *Rnf2* KO. Each mouse harbored one tumor, bars, mean ± SEM. Symbols depict individual mouse.

b. The mean fluorescence intensity (MFI) of NKG2D expression on NK cells in Ctrl, *Rnf2* KO or *Rsf1* KO 4T1 tumors at day 7 post-implantation. n = 4 mice for Ctrl, n = 5 mice for *Rnf2* KO/*Rsf1* KO. Each mouse harbored one tumor, bars, mean ± SEM. Symbols depict individual mouse.

c-d. Frequencies of IFNγ^+, GzmB$^+$, TNFα^+ -NK or -CD4$^+$ T-cells in Ctrl, *Rnf2* KO (**c**) or *Rsf1* KO (**d**) 4T1 tumors at day 7 post-implantation. n = 6/7 mice for Ctrl, n = 7 mice for *Rnf2* KO, n = 6/7 mice for *Rsf1* KO. Each mouse harbored one tumor, bars, mean ± SEM. Symbols depict individual mouse.

e. Frequencies of indicated intratumoral immune cells in Ctrl, *Rnf2* KO (two independent gRNAs, g1 and g2) EMT6 tumors at day 7 post-implantation. n= 5 mice for Ctrl or *Rnf2* KO g1, n = 4 mice for *Rnf2* KO g2. Each mouse harbored one tumor, bars, mean ± SEM. Symbols depict individual mouse.

f-i. The volumes (**f, h**) of 4T1 *Rnf2* KO tumors (*Rnf2* KO g2) (**f**) or *Rsf1* KO tumors (*Rsf1* KO g1) (**h**) in BALB/c mice treated with/without α-asialo GM1 at days 2, 5, 10 post-implantation. Mean ± SEM (n = 5 mice/group, each mouse harbored one tumor.). **g, i.** Representative tumor BLIs at the indicated day.

j-k. The volumes (**j**) of 4T1 *Rnf2* KO tumors (*Rnf2* KO g2) in BALB/c mice treated with α-CD4 (GK1.5) or control antibody at days 2, 5 post-implantation. Mean ± SEM (n = 5 mice/group, each mouse harbored one tumor.). **k.** Representative BLIs of tumors at day 45.

l-m. The volumes (**l**) of control or 4T1 *Rnf2* KO tumors (*Rnf2* KO g2) in BALB/c mice treated with α-CD8 antibody (Ab) or control Ab at days 2, 5 after tumor implantation. Mean ± SEM (n = 5 mice/group, each mouse harbored one tumor.). **m.** Representative tumor bioluminescence images (BLIs) at indicated day after inoculation.

Unpaired two-tailed Student's t test in a, b, c, d, e, two-way ANOVA with Sidak's test in f, h, j, l.

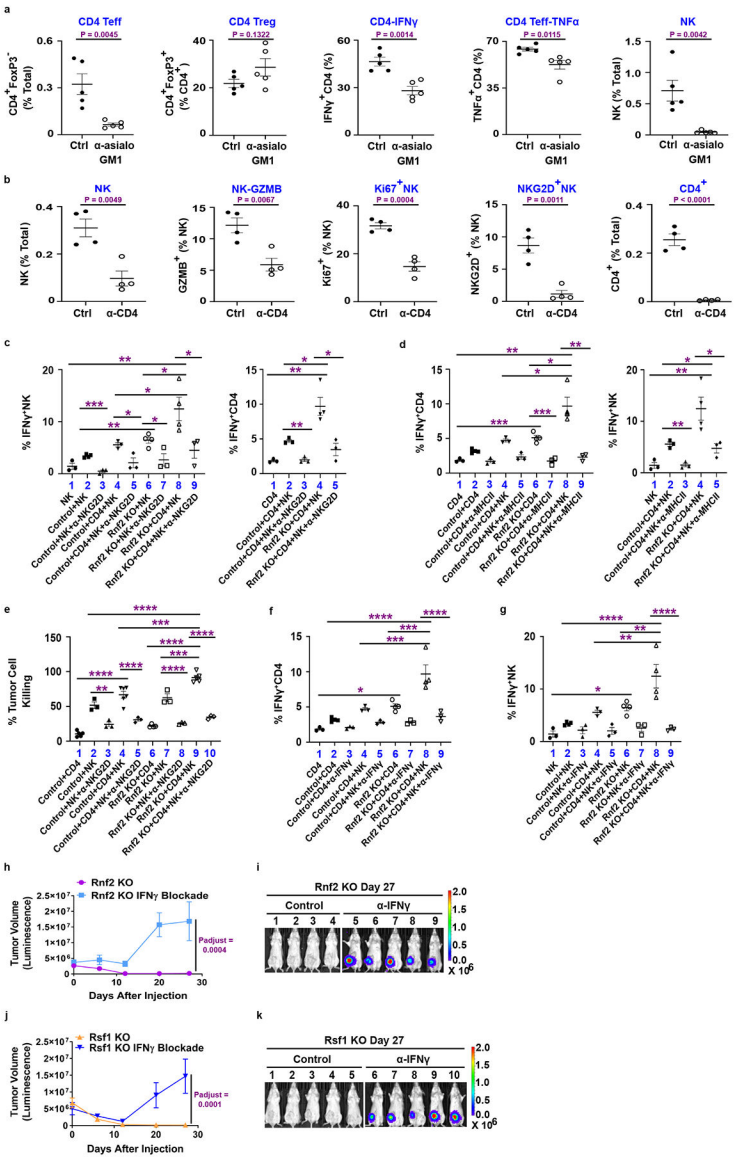

Figure 3. *Rnf2* KO/*Rsf1* KO induces cooperation between NK and CD4$^+$ T-cells.

a-b. Frequencies of indicated immune cell subsets in 4T1 *Rnf2* KO tumors (*Rnf2* KO g2) in mice treated with/ without α-asialo GM1 (**a**) (n = 5 mice/group, each mouse harbored one tumor.) or α-CD4 (GK1.5) (**b**) (n = 4 mice/group, each mouse harbored one tumor.) at day 7 post-inoculation. Symbols depict individual mouse (bars, mean ± SEM).

c-d. Tumor cells (CD45$^-$) were isolated and enriched from control/*Rnf2* KO 4T1 tumors, co-cultured with CD4$^+$ T-cells, or NK cells or both. The anti-NKG2D/control antibody (30 μg/ml) was pre-incubated with NK cells (**c**) or anti-MHCII/control antibody was added to the co-cultures with CD4$^+$ T-cells (**d**). Frequencies of IFNγ$^+$CD4$^+$ T-cells or IFNγ$^+$NK cells are shown as mean ± SEM of triplicates. Each group has 3/4 replicates of co-culture. Tumor cells (Ctrl/*Rnf2* KO) in each replicate of co-culture were pooled from 2-3 tumors from 2-3 mice (each mouse harboring one tumor). Data represent one of two independent experiments.

e. Tumor cells (CD45$^-$) were isolated and enriched from control/*Rnf2* KO 4T1 tumors, co-cultured with pre-activated CD4$^+$ T-cells, or NK cells or both. The anti-NKG2D/control antibody (30 μg/ml) was pre-incubated with NK cells for 15 min before co-culture. The percent tumor killing is shown as mean ± SEM of triplicates. Each group has 3/4/5/6 replicates of co-culture. Tumor cells (Ctrl/*Rnf2* KO) in each replicate of co-culture were pooled from 2-3 tumors from 2-3 mice (each mouse harboring one tumor).

f-g. Tumor cells (CD45$^-$) were isolated and enriched from control or *Rnf2* KO 4T1 tumors, and co-cultured with CD4$^+$ T-cells, or NK cells or both. Anti-IFNγ (XMG1.2)/control antibody was added to the co-cultures. Frequencies of IFNγ$^+$CD4$^+$ T-cells (**f**) or IFNγ$^+$NK cells (**g**) are shown as mean ± SEM of triplicates. Each group has 3/4 replicates of co-culture. Tumor cells (Ctrl/*Rnf2* KO) in each replicate of co-culture were pooled from 2-3 tumors from 2-3 mice (each mouse harboring one tumor). Data represent one of two independent experiments.

h-k. The volumes of *Rnf2* KO tumors (*Rnf2* KO g2) (**h**) or *Rsf1* KO tumors (*Rsf1* KO g1) (**j**) in BALB/c mice treated with control/anti-IFNγ antibody (Ab) at day 2, 5 post-implantation. Mean ± SEM (n = 4 mice for control Ab treated *Rnf2* KO tumors; n = 5 mice for control Ab treated*Rsf1* KO tumors; n = 5 mice for *Rnf2* KO or *Rsf1* KO tumors treated with anti-IFNγ Ab, each mouse harbored one tumor). **i, k,** representative tumor BLIs at day 27 after inoculation.

*p < 0.05, **p < 0.01, ***p < 0.001, and ****p < 0.0001 (unpaired two-tailed Student's t test in a, b, c, d; one-way ANOVA with Tukey's test in e, f, g; two-way ANOVA with Sidak's test in h, j). The full list of p values can be found in the source data for this figure.

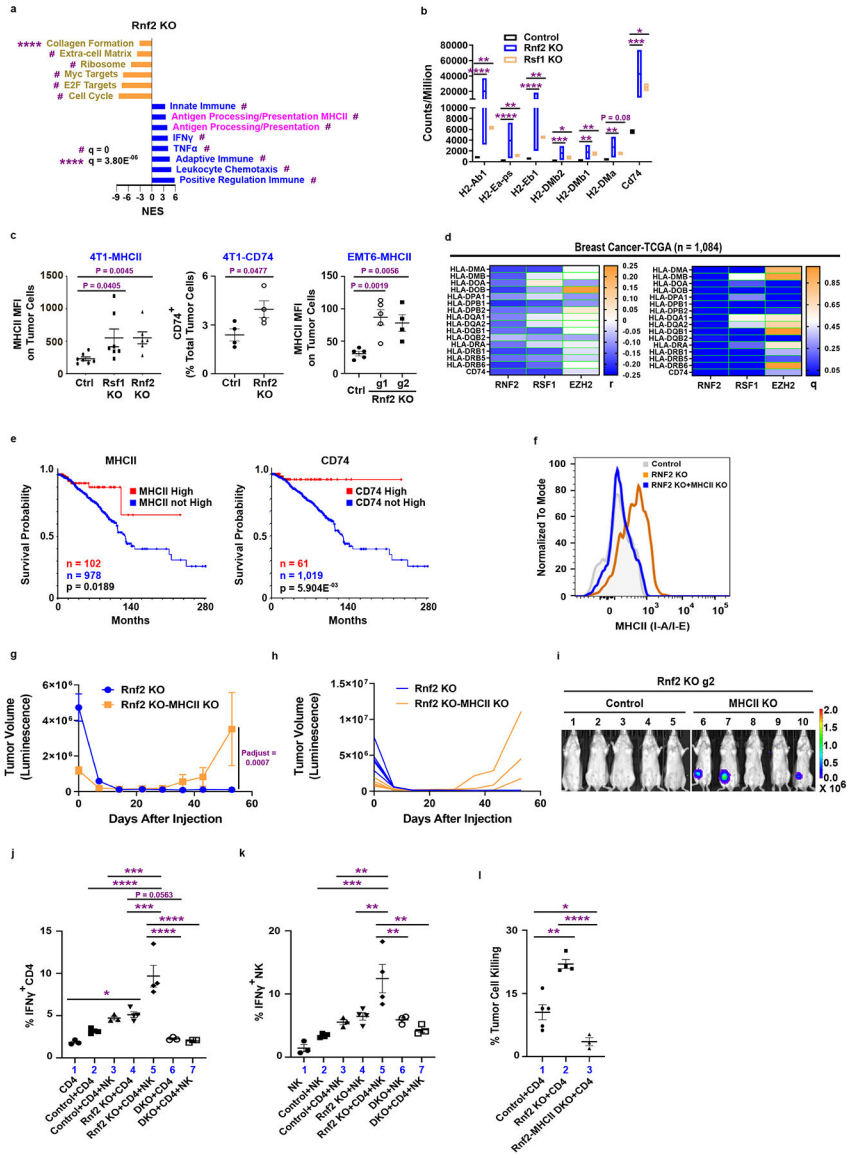

Figure 4. *Rnf2/Rsf1* KO tumors upregulate *MHCII/CD74*.

a. GSEA of DEGs revealed in RNAseq of *Rnf2* KO (two groups of cells, *Rnf2* KO g1 and *Rnf2* KO g2, each group of cells pooled from 25 mice) compared to control 4T1 cells (two groups of cells, each group cells pooled from 25 mice) enriched from tumors in mice (each mouse harbored one tumor) at day-7 post-implantation. The representative enriched gene sets with q values are shown.

b. A floating bars graph (min, max and line at mean) of the counts of *MHCII* isoforms and *Cd74*, revealed in RNAseq as in **panel a**. *Rnf2* KO (two groups of cells, each group of cells pooled from 25 mice)/control 4T1 cells (two groups, each group of cells pooled from 25 mice) were enriched from tumors in mice, each mouse harbored one tumor.

c. The MFI of MHCII on $CD45^-$ tumor cells and frequencies of $CD74^+CD45^-$ tumor cells isolated from indicated 4T1 (n = 7/4 mice for Ctrl (7 for Left panel, 4 for Middle panel) , n = 7 mice for *Rsf1* KO, n = 6/4 mice for *Rnf2* KO (6 for Left panel, 4 for Middle

panel)) or EMT6 (n = 5 mice for Ctrl/*Rnf2* KO g1, n =4 for *Rnf2* KO g2) tumors at day 7 post-implantation. Symbols, individual mouse (bars, mean ± SEM).

d-e. The correlations of *RNF2/RSF1/EZH2* to the *MHCII* isoforms/*CD74* (**d**) or the correlations of *MHCII* isoforms/*CD74* to the survival of invasive breast cancer patients (**e**), derived from invasive breast cancer TCGA dataset through cBioportal. High expression, mRNA > 2 SD above the mean. n = 1084 (**d**)/1080 (**e**) patients total.

f-i. f. Histogram overlays of MHCII expression on Ctrl, *Rnf2* KO and *Rnf2* KO with additional deletion of *MHCII* (*Rnf2* KO g2-*MHCII* KO, DKO) 4T1 cells, which represents two independent experiments. **g-h.** The volumes of indicated tumors in BALB/c mice. **g**. Mean ± SEM (n = 5 mice/group, each mouse harboring one tumor). **h.** Individual mouse. **i.** Representative tumor BLIs at day 53.

j-l. Tumor cells ($CD45^-$) were isolated from indicated 4T1 tumors and co-cultured with $CD4^+$ T-cells/NK cells/both (**j**, **k**) or pre-activated $CD4^+$ T-cells (**l**). Frequencies of $IFN\gamma^+CD4^+$ T (**j**)/$IFN\gamma^+$NK cells (**k**)/percent dead tumor cells (CTV^+FVD^+) (**l**) are shown as mean ± SEM of triplicates. Each group has 3/4/5 replicates of co-culture. Tumor cells (Ctrl/*Rnf2* KO) in each replicate of co-culture were pooled from 2-3 tumors from 2-3 mice (each mouse harboring one tumor).

*p < 0.05 **p < 0.01, ***p < 0.001 and ****p < 0.0001 (padj in b). Two-tailed Wald test in b, unpaired two-tailed Student's t test in c, l, two-tailed LogRank test in e, two-way ANOVA with Sidak's test in g, one-way ANOVA with Tukey's test in j, k. Exact p values for b, j-l are listed in the source data.

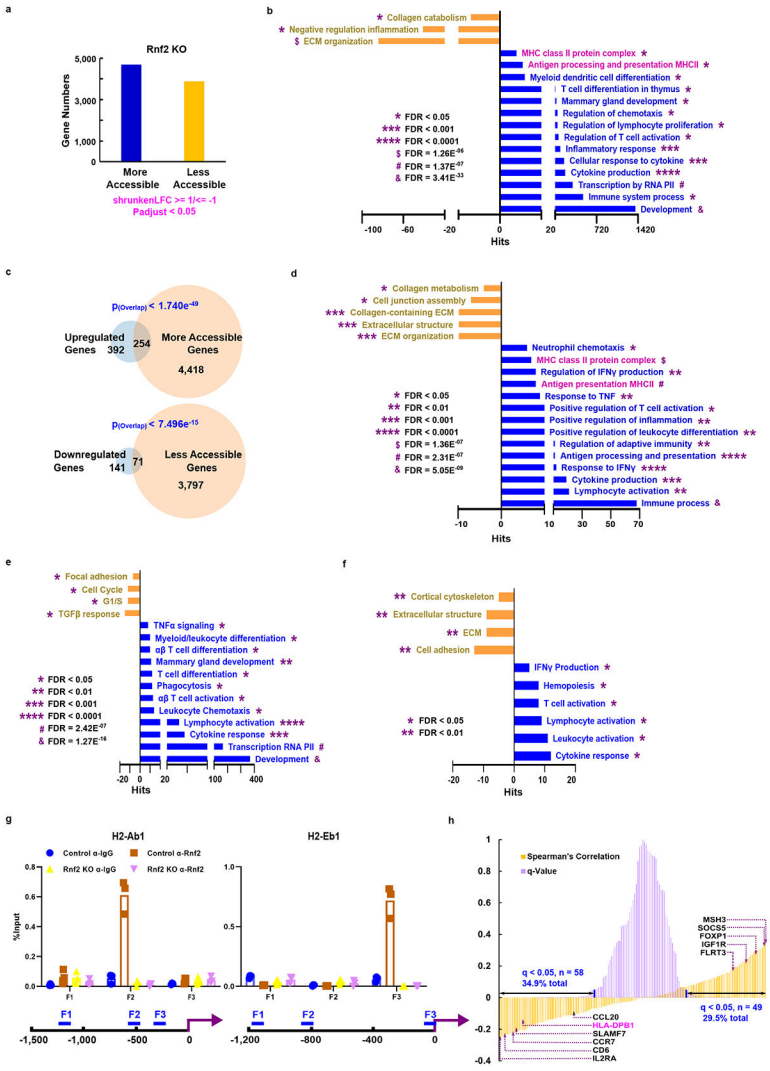

Figure 5. Rnf2 modulates accessibilities of immune-related genes.

a. The numbers of genes with significantly more/less accessible chromatin sites in *Rnf2* KO (n = 2, two groups of cells, each group of cells pooled from 25 mice, each mouse harboring one tumor) compared to control 4T1 tumor cells (n = 2, two groups of cells, each group of cells pooled from 25 mice, each mouse harboring one tumor), enriched from the corresponding tumors in mice at day 7 after implantation, were determined by ATACseq.

b. Gene ontology analyses of genes determined in **panel a** were performed through online tool THE GENE ONTOLOGY RESOURCE[79]. The representative enriched gene sets with FDR q values are shown (Fisher Test, one-tailed hypergeometric test).

c. The overlap of DEGs (determined by RNAseq in Figure 4a) in *Rnf2* KO 4T1 tumors with genes significantly more/less open in *Rnf2* KO 4T1 tumors determined in **panel a**. P values of the overlap are calculated using the web tool Statistical significance of overlap of two groups of genes from Nematode Bioinformatics (SSOTGNB) (http://nemates.org/MA/progs/overlap_stats.html).

d-f. Gene ontology analyses of overlapping genes determined in **panel c** (**d**) or in Extended-Figure 8a (**e**) or in Extended-Figure 8b (**f**) were performed through online tool THE GENE

ONTOLOGY RESOURCE[79]. The representative enriched gene sets with FDR q values are shown (Fisher Test, one-tailed hypergeometric test).

g. Cut&Run-qPCR analysis of chromatin DNA pulled down by control IgG, or Rnf2 antibody from control or *Rnf2* KO 4T1 tumor cell lines. The amplicons are indicated. Data are shown as the percentage of input, n = 3 technical replicates. Fn, Fragment n of the 5'-untranscribed region.

h. The correlations of *RNF2* to the levels of its bound immune-related genes that were determined as in Extended-Figure 8f in BRCA patients. The expression levels of these RNF2 bound genes and of *RNF2* were extracted from the invasive breast cancer TCGA dataset via cBioportal. The coefficient (*yellow*) and q value (*pink*) of each correlation are indicated at the y-axis. The number (n) of RNF2 bound immune-related genes with FDR q values < 0.05, and the percentages of these genes (q < 0.05) among the total RNF2 bound immune-related genes are noted in blue. The blue vertical bars mark the q value at 0.05. Representative immune-related genes with coefficients < 0 or > 0 and q < 0.05 are indicated. Totally 1,070 BRCA patient samples were included.

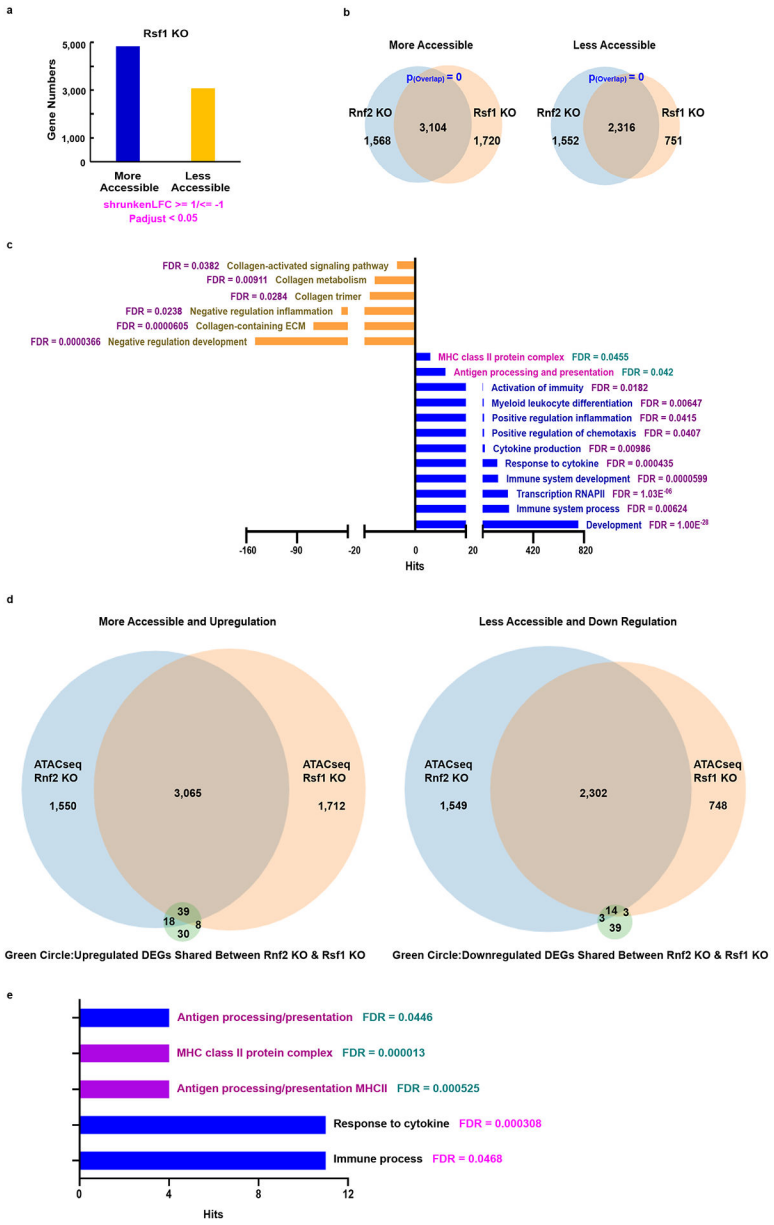

Figure 6. Rsf1 modulates accessibilities of an overlapping group of immune-related genes with Rnf2.

a. The numbers of genes with significantly more/less accessible chromatin sites in *Rsf1* KO (n = 2, two groups of cells, each group of cells pooled from 25 mice, each mouse harboring one tumor) compared to control 4T1 tumor cells (n = 2, two groups of cells, each group cells pooled from 25 mice, each mouse harboring one tumor), enriched from the corresponding tumors in mice at day 7 after implantation, were determined by ATACseq similar to that described in Figure 5a.

b. Overlap of genes with significantly more/less accessible chromatin sites in *Rnf2* KO and *Rsf1* KO 4T1 tumors measured by ATACseq determined in **panel a** and Figure 5a, respectively. P values of the overlap were calculated using the web tool SSOTGNB (http://nemates.org/MA/progs/overlap_stats.html) similar to that described in Figure 5c.

c. Gene ontology analyses of overlapping genes determined in **panel b** were performed through online tool THE GENE ONTOLOGY RESOURCE, similar to that described in Figure 5b. The representative enriched gene sets with FDR q values are shown (Fisher Test, one-tailed hypergeometric test).

d-e. d. The overlap of shared significantly upregulated (**Left**)/downregulated (**Right**) DEGs of *Rnf2* KO and *Rsf1* KO 4T1 tumors (determined by comparing to control 4T1 tumors shown in Extended-Figure 7c) with genes showing significantly more (**Left**)/less (**Right**) accessible chromatin sites in *Rnf2* KO and *Rsf1* KO 4T1 tumors (determined by ATACseq by comparing to control 4T1 tumors shown in **panel a** and Figure 5a, respectively). **e.** Gene ontology analyses of overlapping significantly upregulated and more accessible genes determined in **panel d** were performed through online tool THE GENE ONTOLOGY RESOURCE. The representative enriched gene sets with FDR q values are shown (Fisher Test, one-tailed hypergeometric test), similar to that in Figure 5b.

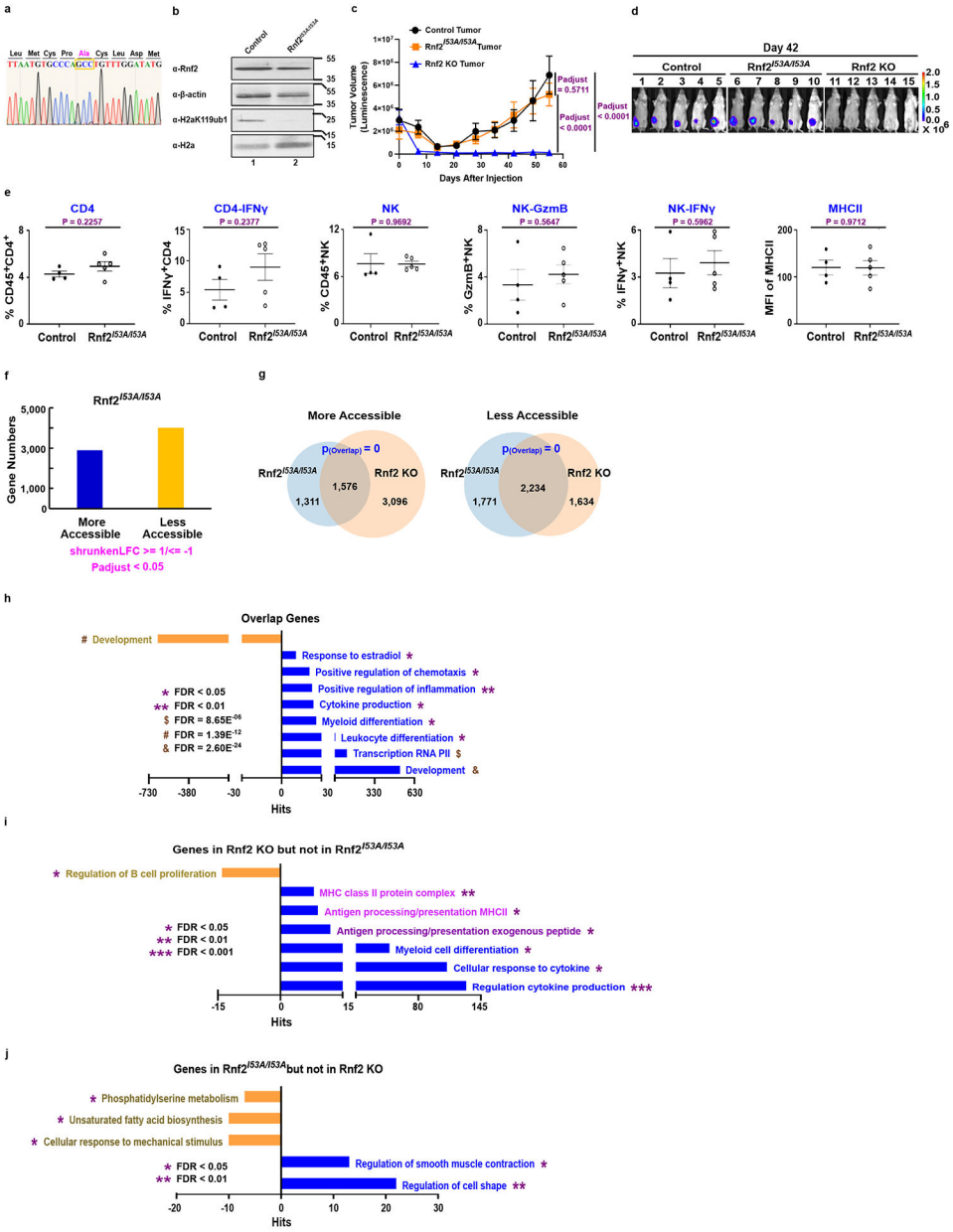

Figure 7. The E3 ligase activity of Rnf2 is dispensable for its regulation of anti-tumor immunity.

a. The sequencing result of the I53A knockin mutant. The mutated genomic sequence encoding Alanine is highlighted.

b. Immunoblots show the protein levels of H2AK119ub1 in control and *Rnf2*$^{I53A/I53A}$ knockin 4T1 tumor cells. The reduction of H2aK119ub1 level has been independently confirmed twice.

c-d. The volumes (**c**) (luminescence intensities) of control 4T1 tumors or *Rnf2*$^{I53A/I53A}$ 4T1 tumors implanted into the 4th mammary pads of the syngeneic BALB/c mice and representative tumor bioluminescence images (BLIs) (**d**) at indicated days after inoculation. Mean ± SEM (n = 5 mice/group, each mouse harbored one tumor, two-way ANOVA

with Tukey's test). The *in vivo* growing phenotype of *Rnf2*$^{I53A/I53A}$ 4T1 tumor has been independently confirmed.

e. Frequencies of indicated immune cell subsets in 4T1 control and *Rnf2*$^{I53A/I53A}$ tumors injected into the 4th mammary fat pads of syngeneic BALB/c mice at day 7 after tumor inoculation. Symbols, individual mouse (bars, mean ± SEM, n = 4 mice for Ctrl, n = 5 mice for *Rnf2*$^{I53A/I53A}$, each mouse harboring one tumor, unpaired two-tailed Student's t test).

f. The numbers of genes with significantly more/less accessible chromatin sites in 4T1 *Rnf2*$^{I53A/I53A}$ tumor cells (n = 2, two groups of cells, each group of cells pooled from 25 mice, each mouse harboring one tumor) compared to 4T1 control tumor cells (n = 2, two groups of cells, each group of cells pooled from 25 mice, each mouse harboring one tumor) were determined by ATACseq, similar to that described in Figure 5a. These tumor cells were enriched by FACS from the corresponding tumors implanted into the 4th mammary fat pads of syngeneic BALB/c mice. The tumors were removed at day 7 after implantation.

g. Overlap of genes with more/less accessible chromatin sites in *Rnf2* KO (determined in Figure 5a) and *Rnf2*$^{I53A/I53A}$ (**panel f**) 4T1 tumors, which were measured by ATACseq and determined by compared to control 4T1 tumors. These tumor cells were enriched by FACS from corresponding tumors implanted in BALB/c mice. Both *Rnf2* KO and *Rnf2*$^{I53A/I53A}$ had two group of tumor cells with each group of cells pooled from 25 mice (each mouse harboring one tumor). P values of the overlap were calculated using the web tool SSOTGNB (http://nemates.org/MA/progs/overlap_stats.html), similar to that described in Figure 5c.

h-j. Gene ontology analyses of overlap (**h**) and not overlap genes (**I, j**) determined in **panel g** were performed through online tool THE GENE ONTOLOGY RESOURCE. The representative enriched gene sets with FDR q values are shown (Fisher Test, one-tailed hypergeometric test), similar to that described in Figure 5b.

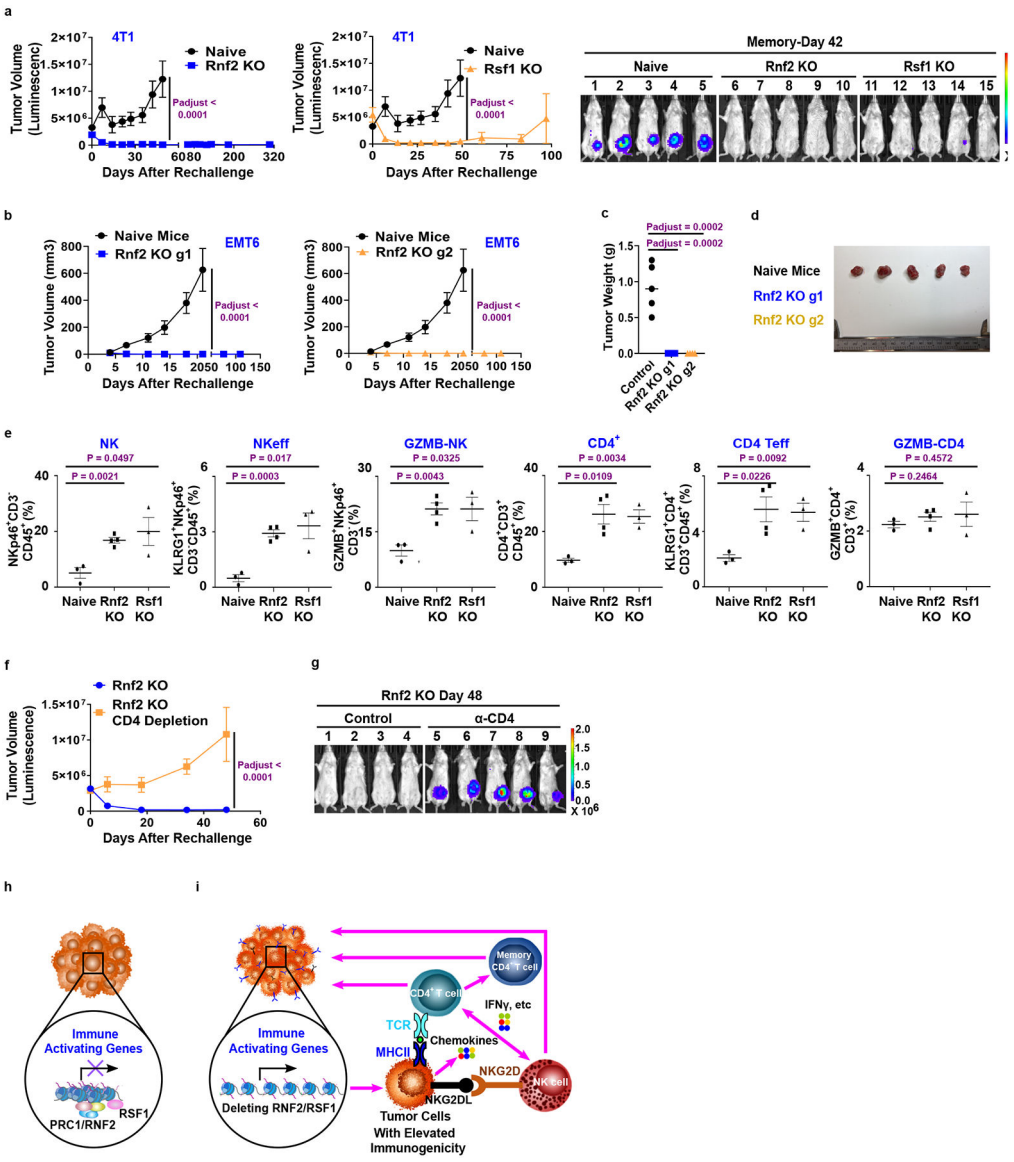

Figure 8. Ablation of *Rnf2/Rsf1* induces anti-tumor memory response that is dependent of CD4$^+$ T-cells.

a. BALB/c mice were inoculated with *Rnf2* KO- (*Rnf2* KO g2) (**Left**) or *Rsf1* KO-4T1 tumors (*Rsf1* KO g1) (**middle**) in the left 4th mammary pads. At day 45 after the primary tumors were rejected, wildtype 4T1 tumors were implanted into the right 4th mammary pads of these mice or of naïve mice. n = 5 mice/group, each mouse harboring one tumor. **Left**/**middle**, Volumes (luminescence intensities) (mean ± SEM). **Right**, Representative BLIs of wildtype 4T1 tumors at day 42 after the 2nd challenge.

b-d. BALB/c mice were inoculated with *Rnf2* KO EMT6 tumors (*Rnf2* KO g1 and g2) in the left 4th mammary pads. At day 45 after the primary tumors were rejected, wildtype EMT6 tumors were implanted into the right 4th mammary pads of these mice or of naïve mice. Tumor volumes (**b**) were calculated by length X width^2/2. Mean ± SEM (n = 5 mice in naïve mice group, n = 4 mice for *Rnf2* KO g1 or g2 group, each mouse harboring one tumor). The weights (**c**) and image (**d**) of the tumors at the end of the study.

e. Frequencies of indicated immune cells in wildtype 4T1 tumors at day 7 after the 2nd challenge, as in **panel a**. Symbols, individual mouse (bars, mean ± SEM). n = 3 mice for naïve and *Rsf1* KO, n = 4 mice for *Rnf2* KO, each mouse harboring one tumor.
f-g. Mice were inoculated with *Rnf2* KO 4T1 tumors and re-challenged with wildtype 4T1 tumors on the contralateral, as in **panel a**. Anti-CD4 (GK1.5) or control antibody was injected at days −1 and +1 relative to tumor implantation. **f.** Volumes (luminescence intensities) of wildtype 4T1 tumors. Mean ± SEM (n = 4 mice for control antibody, n = 5 mice for GK1.5, each mouse harboring one tumor). **g.** Representative tumor BLIs at day 48 after the 2nd challenge.
h-i. Working models.
Two-way ANOVA with Sidak's test in a, b, f; one-way ANOVA with Tukey's test in c; unpaired two-tailed Student's t test in e.